SEMPACT

USDOT Region 2 University Transportation Center

New Jersey | New York | Puerto Rico | US Virgin Islands

FINAL REPORT

Predicting urban stormwater flooding using geomorphic information

Prepared by:

New Jersey Institute of Technology

August 31, 2024

Prepared for:

University Transportation Research Center

Sponsor: SEMPACT (USDOT Region 2 UTC under BIL)

Disclaimer

The contents of this report reflect the views of the authors, who are responsible for the facts and the accuracy of the information presented herein. The contents do not necessarily reflect the official views or policies of the UTRC, SEMPACT, or the Federal Highway Administration. This report does not constitute a standard, specification or regulation. This document is disseminated under the sponsorship of the Department of Transportation, University Transportation Centers Program, in the interest of information exchange. The U.S. Government assumes no liability for the contents or use thereof.

TECHNICAL PROJECT COVER SHEET

PROJECT TITLE:
Predicting urban stormwater flooding using geomorphic information

PRINCIPAL INVESTIGATOR:
Michel C. Boufadel, PhD, PE
Director, Center for Natural Resources
Distinguished Professor, Department of Civil and Environmental Engineering
New Jersey Institute of Technology
University Heights, Newark, NJ, 07102, USA
http://cnr.njit.edu
Tel: 973-596-5657; Email: boufadel@njit.edu

CO-PRINCIPAL INVESTIGATORS:
Viravid Na Nagara, PhD
Postdoctoral Researcher, Center for Natural Resources
New Jersey Institute of Technology
University Heights, Newark, NJ, 07102, USA
http://cnr.njit.edu
Tel: 973-596-6067; Email: vn274@njit.edu

SPONSOR:
- U.S. Department of Transportation
- SEMPACT (*Center for Social and Economic Mobility for People and Communities through Transportation* – USDOT Region 2 UTC under Bipartisan Infrastructure Law)

SEMPACT RESEARCH PRIORITY AREA:
- Inclusive advanced technology applications

RESEARCH PROJECT MANAGER:
Jerry He

PROJECT DURATION: 12 months (September 1, 2023 to August 31, 2024)

DATE SUBMITTED: August 31, 2024

TECHNICAL REPORT STANDARD TITLE PAGE

1. Report No.	2.Government Accession No.	3. Recipient's Catalog No.

4. Title and Subtitle	5. Report Date
Predicting urban stormwater flooding using geomorphic information	August 31, 2024
	6. Performing Organization Code

7. Author(s)	8. Performing Organization Report No.
Michel C. Boufadel and Viravid Na Nagara	RF# 49426-01-01

9. Performing Organization Name and Address	10. Work Unit No.
New Jersey Institute of Technology University Heights, Newark, NJ, 07102, USA	11. Contract or Grant No. 69A3552348302

12. Sponsoring Agency Name and Address	13. Type of Report and Period Covered
Center for Social and Economic Mobility for People and Communities Through Transportation (SEMPACT) Region 2 University Transportation Center New York, New Jersey, Puerto Rico, and U.S. Virgin Islands Marshak Hall, Room 910, The City College of NY, New York, NY 10031	14. Sponsoring Agency Code

15. Supplementary Notes

16. Abstract

Stormwater flooding presents substantial challenges in urban settings, impacting transportation networks, economic activities, and public safety. Conventional flood prediction relies heavily on hydrologic and hydraulic (H&H) simulations, which are computationally intensive and require specialized expertise, rendering them costly and resource demanding. This project seeks to address these challenges by developing empirical models to predict flooding at specific locations using easily obtainable parameters such as specific catchment area, slope, and flow path length. The goal is to offer a more accessible and cost-effective alternative to complex hydraulic modeling. Hydraulic simulations were performed using the Hydrologic Engineering Center's River Analysis System (HEC-RAS) for 20 representative sites in Newark, New Jersey. The simulation results, in conjunction with geomorphic data from these sites, were utilized to formulate empirical flood prediction models. This approach transitions from resource-intensive hydraulic simulations to streamlined empirical models using readily available data, enhancing urban flood risk assessment and management. The proposed methodology offers practical benefits for cities facing stormwater flooding, facilitating more informed decision-making and enhancing resilience in transportation and urban planning.

17. Key Words	18. Distribution Statement
Flooding, modeling, geomorphic information	

19. Security Classif (of this report)	20. Security Classif. (of this page)	21. No of Pages	22. Price
Unclassified	Unclassified		

Form DOT F 1700.7 (8-69)

Abstract

Stormwater flooding presents substantial challenges in urban settings, impacting transportation networks, economic activities, and public safety. Conventional flood prediction relies heavily on hydrologic and hydraulic (H&H) simulations, which are computationally intensive and require specialized expertise, rendering them costly and resource demanding. This project seeks to address these challenges by developing empirical models to predict flooding at specific locations using easily obtainable parameters such as specific catchment area, slope, and flow path length. The goal is to offer a more accessible and cost-effective alternative to complex hydraulic modeling. Hydraulic simulations were performed using the Hydrologic Engineering Center's River Analysis System (HEC-RAS) for 20 representative sites in Newark, New Jersey. The simulation results, in conjunction with geomorphic data from these sites, were utilized to formulate empirical flood prediction models. This approach transitions from resource-intensive hydraulic simulations to streamlined empirical models using readily available data, enhancing urban flood risk assessment and management. The proposed methodology offers practical benefits for cities facing stormwater flooding, facilitating more informed decision-making and enhancing resilience in transportation and urban planning.

Key words: Flooding, modeling, geomorphic information

1. Introduction

Urban areas are increasingly vulnerable to stormwater flooding, a phenomenon that not only disrupts transportation networks but also hampers economic activities and endangers public safety. The rapid pace of urbanization, coupled with climate change, has exacerbated the frequency and intensity of flood events in cities worldwide (Le et al., 2024). The impervious surfaces characteristic of urban environments, such as roads, buildings, and parking lots, prevent natural infiltration of rainwater into the ground, leading to higher volumes of runoff during storm events (Li et al., 2024). This runoff, if not properly managed, can overwhelm drainage systems, leading to widespread flooding that poses significant risks to infrastructure and human life (Chen et al., 2024).

Flooding is categorized into three primary types based on its source: coastal, fluvial, and pluvial (Bates et al., 2021). Coastal flooding arises from extreme high tides or storm surges (Muthusamy et al., 2021), affecting coastal and estuarine areas. Fluvial flooding happens when rivers overflow their banks due to excess water volume, leading to the inundation of adjacent floodplains. Pluvial flooding, often referred to as stormwater flooding, occurs when heavy rainfall generates overland flow and ponding, particularly when drainage systems are overwhelmed. (Coles et al., 2017). Unlike fluvial and coastal events, pluvial flooding lacks comprehensive national guidelines, even though it occurs more frequently and can result in substantial cumulative impacts on communities, economies, and the environment (Azizi et al., 2022). Consequently, there is an urgent need to develop precise and detailed flood maps that account for the intricacies of pluvial flooding, particularly within urban environments.

To improve flood preparedness and risk management, it is imperative to develop pluvial flood maps that incorporate key factors such as flood depth and velocity. These parameters are critical for assessing flood impacts and ensuring public safety. For example, flow velocities

between 1.5 and 2 m/s at depths below 0.2 m pose significant hazards to pedestrians, potentially leading to loss of stability and the risk of being swept away (Martínez-Gomariz et al., 2016; Russo et al., 2013). Additionally, as flood depth increases from 0 to 0.2 m, vehicle speeds can drastically reduce from 80 km/h to 15 km/h, causing substantial traffic disruptions (Choo et al., 2020). Consequently, precise identification and mapping of these factors are essential for robust flood risk assessment and mitigation strategies.

Traditionally, the prediction and management of flooding have relied on hydrologic and hydraulic (H&H) models, which simulate the movement of water through the landscape and drainage networks. These models are invaluable for understanding the dynamics of flood events and for designing mitigation strategies (Boufadel, 1998; Boufadel, 2000; Luo et al., 2022). However, they are also highly complex, requiring detailed input data, specialized software, and a significant level of expertise to operate and interpret. The computational demands of these models can be substantial, particularly when modeling large areas or when simulating the impacts of various storm scenarios. As a result, the application of H&H models can be both time-consuming and expensive, limiting their use in situations where resources are constrained or where rapid decision-making is required.

Empirical models have several advantages that address the gaps left by traditional H&H approaches. First, they are less data-intensive, relying on parameters that are typically easier to obtain or already available from existing geographic information systems (GIS) databases. This reduces the need for costly data collection efforts, making it possible for empirical models to effectively predict urban flooding using commonly available data. Second, empirical models are generally less complex, which means they require less computational power and can be run more quickly, making them ideal for use in emergency response scenarios where time is of the essence.

2. Problem Statement

Given the limitations of traditional H&H modeling, there is a growing need for alternative approaches that can provide reliable flood predictions with fewer resources. One such approach is the development of empirical models, which use statistical relationships between easily measurable parameters—such as elevation, slope, and catchment area—and observed flood characteristics. Empirical models, while simpler than their H&H counterparts, can offer a more accessible and cost-effective means of predicting flooding, particularly in urban settings where data availability and timeliness are critical. This study aims to develop empirical models that can predict flooding at specific locations using parameters that are readily obtainable from existing geographic and land-use data. The ultimate goal is to provide an alternative to traditional hydraulic modeling that is both more practical for routine use and capable of delivering timely information to support decision-making in urban flood management.

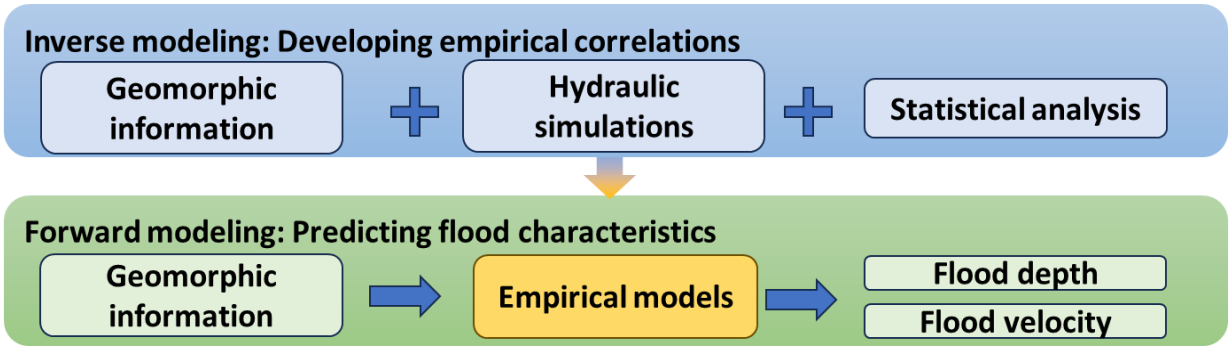

Figure 1 Diagram showing the objective and overall approach

3. Methodology

3.1. Study area

Newark, New Jersey, a densely populated urban center, has faced significant challenges related to flooding over the years, particularly due to its location and infrastructure. Situated in the northeastern part of the state, Newark lies in a low-lying area near the confluence of the Passaic River and Newark Bay. This geographic positioning, combined with aging infrastructure and the effects of climate change, has made the city increasingly vulnerable to flooding. One of the primary causes of flooding in Newark is heavy rainfall, which can overwhelm the city's drainage systems, leading to pluvial flooding. The city's extensive impervious surfaces—such as roads, parking lots, and buildings—exacerbate the problem by preventing natural infiltration of rainwater into the ground. Instead, water quickly accumulates on the surface, leading to flash floods, particularly in areas with poor drainage. Climate change is expected to exacerbate Newark's flooding problems in the coming years. Rising sea levels and more frequent and intense storms are likely to increase the frequency and severity of flooding events.

Twenty representative sites in Newark, New Jersey (Table 1) were selected for empirical model development. A map showing the locations of the selected site is presented in Figure 2. These sites were selected based on their flood history and ongoing efforts in mitigating flooding. Various sites were included in this study to represent a range of urban conditions, including variations in elevation, slope, catchment area, and land use.

3.2 Data collection and preparation

The geomorphic parameters for the study sites were processed using QGIS software. High-resolution 1-meter digital elevation models (DEMs) were sourced from the U.S. Geological Survey (USGS) National Elevation Dataset (NED). All GIS layers were reprojected to align with the New Jersey State Plane Coordinate System, NAD83, ensuring consistency with local standards. Land use and land cover data were acquired from the 2020 NJ Statewide Land Use/Land Cover dataset provided by the New Jersey Department of Environmental Protection (NJDEP). Soil data were obtained from the Soil Survey Geographic Database (SSURGO) by the U.S. Department of Agriculture - Natural Resources Conservation Service (USDA-NRCS). The specific catchment area (SCA) and slope layers for the study sites were then generated using

the Flow Width and Specific Catchment Area tool and Slope, Aspect, Curvature tool from the System for Automated Geoscientific Analyses (SAGA) GIS package within the QGIS software. The SCA was generated with the Multiple Flow Direction method (Quinn et al., 1991), whereas the slope was generated with the Least Squares method (Costa-Cabral and Burges, 1994; Horn, 1981). The literature showed that flow path length, also known as slope length or drainage length, was one of the key parameters for predicting water depth (Han et al., 2021; Xiao et al., 2023). Therefore, flow path length data were also processed using the Slope Length tool within the QGIS software.

Table 1 Selected sites in Newark, New Jersey

Site ID	Site Name	Approximate Site Address
1	Newark Police Station 3rd Precinct	649 Market Street Newark, NJ 07105
2	Nasto's Ice Cream	236 Jefferson Street Newark, NJ 07105
3	Art of Survival Garden	367 Seymour Avenue Newark, NJ 07112
4	Hawthorne Hawks Healthy Harvest Farm	446 Hawthorne Avenue Newark, NJ 07112
5	HOV Healthy Haven Garden	1068 18th Avenue Newark, NJ 07106
6	Harriet Tubman Elementary School Living Laboratory Garden	South 10th St & Blum St Newark, NJ 07103
7	Down Bottom Farms Traffic Triangle	706 Market Street Newark, NJ 07105
8	Branch Brook Alliance	115 Clifton Ave, Newark, NJ 07104
9	Wanda Upshaw Meditation Garden	454 South 13th Street, Newark, NJ 07103
10	Newark Educators Community Charter School	9-11 Hill Street, Newark, NJ 07102
11	Bergen Street Community Garden	616 Bergen Street, Newark, NJ 07108
12	14th Avenue Community Garden	316 14th Avenue, Newark, NJ 07103
13	Urban League of Essex County	508 Central Ave, Newark, NJ 07107
14	Astor Street Community Garden	40 Astor Street, Newark, NJ 07114
15	South Street Academy	151 South Street, Newark, NJ 07114
16	St. Ann's Church	103 16th Avenue, Newark, NJ 07103
17	James C. White Manor Senior Housing Community Garden	517 Bergen Street, Newark, NJ 07108
18	Court Street Urban Farm	138 Court Street, Newark, NJ 07103
19	Rutgers School of Health Professions Vacant Lot	115 12th Avenue, Newark, NJ 07103
20	Robert Treat Academy Charter School	443 Clifton Avenue Newark, NJ 07104

3.3 Hydraulic modeling

Hydraulic modeling was performed for the selected sites using the Hydrologic Engineering Center's River Analysis System (HEC-RAS) based on the obtained GIS data. Two-dimension unsteady flow simulations were conducted based on the NJDEP Water Quality Design Storm (WQDS) which is 1.25 inches of rainfall in 2 hours. The SCS Curve Number infiltration method was used in the simulations. The Manning's Roughness Coefficients were referred from the HEC-RAS 2D User's Manual (Brunner, 2022).

3.4 Empirical model development

3.4.1 Selection of flood predictors

Water depth and velocity data were extracted from HEC-RAS and imported into QGIS. Within QGIS, a 2-meter grid was created to extract values from both the simulation results and the associated geomorphic parameters. The extracted data from these grid points were then exported to the JMP statistical software for principal component analysis (PCA) and multivariate analysis. Along with the geomorphic parameters exported from QGIS, three indices frequently utilized in geomorphology and hydrology—namely the Topographic Wetness Index (TWI), Sediment Transport Index (STI), and Stream Power Index (SPI)—were computed and incorporated into the empirical model development. The TWI, for instance, is a topographic index derived from runoff accumulation and slope, and can be represented as follows (Beven and Kirkby, 1979):

$$TWI = \ln\left(\frac{SCA}{\tan(\beta)}\right) \quad \text{(Equation 1)}$$

where SCA is specific catchment area and β is slope in radius.

STI is a parameter used in geomorphology and hydrology to assess the potential for sediment movement within a landscape based on topographic characteristics which can be expressed as (Moore and Burch, 1986):

$$STI = 1.4\left(\frac{SCA}{22.13}\right)^{0.4}\left(\frac{\sin(B)}{0.0896}\right)^{1.3} \quad \text{(Equation 3)}$$

B is slope in degree.

SPI is generally used to describe the flow and erosion potential which can be expressed as (Moore et al., 1988):

$$SPI = \ln(SCA \times \tan(\beta)) \quad \text{(Equation 4)}$$

3.4.2 Model fitting

Before fitting the model, data cleaning was performed to remove any data points with missing values and to eliminate outliers or anomalies that could distort the results. Data points with a catchment area of less than 200 m² and a flow path length of less than 20 m were excluded to reduce noise, as these small areas are unlikely to exhibit significant water depth. For water depth prediction, TWI was selected for developing water depth models due to its relatively high correlation with water depth based on the findings from parameter screening. Therefore, three empirical models developed based on the TWI (Equations 5 to 7) as shown below were considered for depth model fitting. Upstream flow path length, often referred to as slope length

or drainage length, was also considered in the evaluation, as it is identified in the literature as a key parameter for predicting water depth (Han et al., 2021; Xiao et al., 2023).

Modified TWI 1: $$Depth = \ln\left(\frac{SCA^{c_1}}{S^{c_2}}\right)$$ (Equation 5)

Modified TWI 2: $$Depth = c_1 \cdot \ln\left(\frac{SCA^{c_2}}{S^{c_3}}\right)$$ (Equation 6)

Modified TWI 3: $$Depth = c_1 \cdot \ln\left(\frac{SCA^{c_2}}{S^{c_3}} \cdot F^{c_4}\right)$$ (Equation 7)

where F is flow path length in m, whereas c_1, c_2, c_3, and c_4 are fitting coefficients. The Nonlinear Regression tool in the JMP statistical software package was used to fit the models.

For water velocity prediction, four models (Equations 8 to 11) were developed based on the STI and SPI. The following equations were considered:

Modified SPI 1: $$Velocity = \ln(SCA^{v_1} \cdot S^{v_2})$$ (Equation 8)

Modified SPI 2: $$Velocity = v_1 \cdot \ln(SCA^{v_2} \cdot S^{v_3}) + v_4$$ (Equation 9)

Modified STI 1: $$Velocity = v_1\left(\frac{SCA}{v_2}\right)^{v_3}\left(\frac{S}{v_4}\right)^{v_5}$$ (Equation 10)

Modified STI 2: $$Velocity = v_1\left(\frac{SCA}{v_2}\right)^{v_3}\left(\frac{S}{v_4}\right)^{v_5} + v_6$$ (Equation 11)

Additionally, the literature suggested that free surface flow is influenced by slope, with the general form expressed as follows (Machiels et al., 2009; Maidment et al., 1996):

$$Velocity = v_1 S^{v_2} R_h^{v_3}$$ (Equation 12)

Where S is slope, R_h is hydraulic radius, and v_i are model coefficients. One of the most widely recognized empirical models in this category is Manning's equation, which can be expressed as follows (Manning, 1891):

$$Velocity = \frac{1}{n} S^{1/2} R_h^{2/3}$$ (Equation 13)

Therefore, in addition to Equations 8 to 11, variations of Manning's equation, as outlined in Equations 14 to 16, were also tested to identify the most suitable empirical model for predicting

water velocity. In the context of stormwater runoff, which is typically wide and shallow, the hydraulic radius is equivalent to the water depth (h).

Modified Manning 1 $$Velocity = \frac{1}{v_1 \cdot n} h^{v_2} S^{v_3}$$ (Equation 14)

Modified Manning 2 $$Velocity = \frac{1}{v_1 \cdot n} h^{v_2} S^{v_3} \cdot \ln(v_4 \cdot SCA)$$ (Equation 15)

Modified Manning 3 $$Velocity = \frac{1}{v_1 \cdot n} h^{v_2} S^{v_3} \cdot \ln(v_4 \cdot SCA \cdot S)$$ (Equation 16)

3.5 Model validation and stormwater flood map generation

Hydraulic modeling was conducted for five additional locations to serve as a new data set for model validation. Water depth and velocity data from HEC-RAS simulations were extracted from five additional locations, as detailed in Table 2. The modeled water depth and velocity were calculated using the optimal models which were Modified TWI 3 (Equation 7) and Modified Manning 2 (Equation 15) models, respectively. The data extraction and analysis followed the same methodology used during the model development phase, utilizing a 1-meter spatial interval for data extraction. Subsequently, the empirical models were used to generate stormwater flood maps for the selected sites listed in Table 1.

Table 2 Selected sites for model evaluation and validation in Newark, New Jersey

Site ID	Approximate Site Address
V1	Walnut St. and Jefferson St., NJ 07105
V2	Avon Ave. and Farley Ave., Newark, NJ 07108
V3	Victoria Ave. and Garside St., Newark, NJ 07104
V4	S 8 St. and 11th Ave. W, Newark, NJ 07107
V5	Emmet St. and Pennsylvania Ave., Newark, NJ 07114

4. Results

4.1 Hydraulic modeling

Two-dimension unsteady flow simulations were conducted using the NJDEP Water Quality Design Storm (WQDS) which is 1.25 inches of rainfall in 2 hours. Time series plots of flow rate, water depth, and water speed at Sites 1 to 20 are presented in Figures 7 to 26.

4.2 Empirical model development

The PCA results for all 20 sites are presented in Figure 27. The relationships between individual parameters were analyzed by observing the angles between their loading vectors in the PCA loading plot. A smaller angle indicated a stronger correlation, while an angle of 180 degrees signified an inverse correlation. Water velocity showed a strong positive correlation with slope,

with catchment area also playing a significant role in the observed variations. Water depth was primarily influenced by Manning's n value, followed by the curve number and catchment area. Additionally, a negative correlation between elevation and water depth was identified, indicating that higher elevations were associated with lower water depths across the sites studied. Based on the multivariate analysis, water depth showed relatively high correlations with curve number and TWI whereas velocity was highly associated with SPI and STI (Table 3).

Table 3 Correlation matrix from the multivariate analysis.

	Slope	Elevation	Depth	Velocity	Catchment area	Manning's n value	Curve number	TWI	SPI	STI
Slope	1.000									
Elevation	0.101	1.000								
Depth	-0.045	-0.092	1.000							
Velocity	0.276	0.201	0.063	1.000						
Catchment area	0.066	0.063	0.086	0.222	1.000					
Manning's n value	0.003*	-0.050	0.017	-0.056	0.002*	1.000				
Curve number	-0.031	-0.330	0.138	-0.087	0.012*	0.293	1.000			
TWI	-0.202	0.096	0.110	0.125	0.527	0.004*	-0.016	1.000		
SPI	0.533	0.147	0.083	0.337	0.510	-0.007*	-0.036	0.617	1.000	
STI	0.491	0.119	0.026	0.355	0.661	0.002*	-0.008*	0.503	0.837	1.000

Note: All correlations reported in the table are statistically significant at the 0.05 significance level, except for those indicated with an asterisk (*).

In an initial evaluation, the correlation between water depth and the TWI was assessed using linear regression, yielding a coefficient of determination (R^2) value of 0.227 (Figure 28). The overall trend suggests that TWI could be a promising variable for developing an empirical model to predict water depth. Therefore, variations of the TWI (Equations 5 to 7) were fitted and compared. As shown in Figure 29, the Modified TWI 3 model (Equation 7) demonstrated a relatively better goodness of fit ($R^2 = 0.558$) compared to the other two models, making it the optimal choice for predicting water depth.

In terms of water velocity model development, the goodness of fit from the four models modified from SPI and STI (Equations 8 to 11) were relatively low with $R^2 \leq 0.2$ (Figure 30). Therefore, they were not considered in a further stage. In contrast, the models modified based on the Manning's equation (Equations 13 to 16) demonstrated a greater goodness of fit with $R^2 > 0.48$ (Figure 31). Although the Modified Manning 3 model (Equation 14) yielded a slightly higher R^2 compared to the Modified Manning 2 model (Equation 14), the difference was minimal. Given that the Modified Manning 2 model is simpler and offers a similar R^2 value, it was selected as the optimal model for predicting water velocity.

4.3 Model validation and flood map generation

As shown in Figure 32, the R^2 values for the calculated water depth and velocity from the empirical models (0.557 for water depth and 0.527 for water velocity) are comparable to those obtained during calibration (0.558 for water depth and 0.557 for water velocity), thereby confirming the models' validity. The empirical models for water depth and velocity were employed to create stormwater flood maps for the sites listed in Table 1. It is noteworthy that the calculated water depth and velocity exhibited considerable variation across building blocks in most areas. This variation arises because DEMs used for calculations often remove buildings or structures during their creation, but open spaces like streets and walkways remain largely unaffected by this process. The maps depicting water depth at each site are shown in Figures 33 to 52, while Figures 53 to 72 present the maps for water velocity. These maps can be utilized to assist in flood risk assessment and mitigation planning.

5. Conclusions

The empirical models developed in this project significantly reduce the complexity and resource demands of traditional flood prediction methods by bypassing resource-intensive hydraulic simulations. This advancement allows for rapid and efficient flood risk assessments across diverse urban environments. By incorporating these empirical models into routine urban planning processes, cities can enhance their resilience to increasing flood risks and develop more effective transportation and infrastructure strategies. The practical advantages of this approach are substantial. For cities like Newark, which face ongoing challenges with stormwater flooding, these models provide a means to improve both the accuracy and timeliness of flood predictions without the need for extensive technical resources. This capability supports more informed decision-making, enabling cities to prioritize flood mitigation investments, optimize emergency response plans, and ultimately mitigate the impacts of flooding on urban communities. Furthermore, the accessibility of these empirical models extends their utility to a broad range of stakeholders, including city planners and community organizations, promoting a more inclusive approach to urban flood management. However, it is important to note that this project focused on a single city (Newark, NJ) and a specific precipitation condition (1.25 inches in 2 hours). Future work should aim to enhance the models' capacity to handle various precipitation scenarios and validate their accuracy across different cities and regions. Continued validation with actual flood records will be crucial for further improving model precision and reliability.

6. Acknowledgements

This study is the result of work sponsored by The Center for Social and Economic Mobility for People and Communities through Transportation (SEMPACT). The authors gratefully acknowledge Nicole Miller and Dr. Christopher Obropta for providing information on the selected sites used for simulations.

7. References

Azizi K, Diko SK, Saija L, Zamani MG, Meier CI. Integrated community-based approaches to urban pluvial flooding research, trends and future directions: A review. Urban Climate 2022; 44.

Bates PD, Quinn N, Sampson C, Smith A, Wing O, Sosa J, et al. Combined Modeling of US Fluvial, Pluvial, and Coastal Flood Hazard Under Current and Future Climates. Water Resources Research 2021; 57.

Beven KJ, Kirkby MJ. A physically based, variable contributing area model of basin hydrology / Un modèle à base physique de zone d'appel variable de l'hydrologie du bassin versant. Hydrological Sciences Bulletin 1979; 24: 43-69.

Boufadel MC. Unit Hydrographs Derived from The Nash Model. Journal of the American Water Resources Association 1998; 34: 167-177.

Boufadel MC. Estimation of the HEC1 loss parameters for routing the probably maximum flood. Journal of the American Water Resources Association 2000; 36: 203-213.

Brunner GW. HEC-RAS 2D User's Manual. Version 6.2. US Army Corps of Engineers-Hydrologic Engineering Center 2022.

Chen T, Chen L, Shao Z, Chai H. Enhanced resilience in urban stormwater management through model predictive control and optimal layout schemes under extreme rainfall events. Journal of Environmental Management 2024; 366: 121767.

Choo K-S, Kang D-H, Kim B-S. Impact Assessment of Urban Flood on Traffic Disruption using Rainfall–Depth–Vehicle Speed Relationship. Water 2020; 12: 926.

Coles D, Yu D, Wilby RL, Green D, Herring Z. Beyond 'flood hotspots': Modelling emergency service accessibility during flooding in York, UK. Journal of hydrology 2017; 546: 419-436.

Costa-Cabral MC, Burges SJ. Digital elevation model networks (DEMON): A model of flow over hillslopes for computation of contributing and dispersal areas. Water resources research 1994; 30: 1681-1692.

Han S, Xu J, Yan M, Gao S, Li X, Huang X, et al. Predicting the water film depth: A model based on the geometric features of road and capacity of drainage facilities. Plos one 2021; 16: e0252767.

Horn BK. Hill shading and the reflectance map. Proceedings of the IEEE 1981; 69: 14-47.

Le HN, Vo DP, Nguyen QD, Nguyen BQ, Nguyen CC. Assessing the impacts of urbanization and climate change on urban drainage system. River 2024.

Li J, Hou H, Zhang Y, Huang R, Hu T. Scenario-Based Simulation of Impervious Surfaces for Detecting the Effects of Landscape Patterns on Urban Waterlogging. Remote Sensing 2024; 16: 2130.

Luo P, Luo M, Li F, Qi X, Huo A, Wang Z, et al. Urban flood numerical simulation: Research, methods and future perspectives. Environmental Modelling & Software 2022; 156: 105478.

Machiels O, Erpicum S, Dewals B, Archambeau P, Pirotton M. Continuous formulation for bottom friction in free surface flows modelling. River Basin Management V; WIT Press: Hampshire, UK 2009: 81-92.

Maidment D, Olivera F, Calver A, Eatherall A, Fraczek W. Unit hydrograph derived from a spatially distributed velocity field. Hydrological processes 1996; 10: 831-844.

Manning R. On the flow of water in open channels and pipes: Institute of Civil Engineers of Ireland Transactions, v. 20. 1891.

Martínez-Gomariz E, Gómez M, Russo B. Experimental study of the stability of pedestrians exposed to urban pluvial flooding. Natural Hazards 2016; 82: 1259-1278.

Moore I, Burch G. Sediment transport capacity of sheet and rill flow: application of unit stream power theory. Water resources research 1986; 22: 1350-1360.

Moore I, Burch G, Mackenzie D. Topographic effects on the distribution of surface soil water and the location of ephemeral gullies. Transactions of the ASAE 1988; 31: 1098-1107.
Muthusamy M, Casado MR, Butler D, Leinster P. Understanding the effects of Digital Elevation Model resolution in urban fluvial flood modelling. Journal of Hydrology 2021; 596: 126088.
Quinn P, Beven K, Chevallier P, Planchon O. The prediction of hillslope flow paths for distributed hydrological modelling using digital terrain models. Hydrological processes 1991; 5: 59-79.
Russo B, Gómez M, Macchione F. Pedestrian hazard criteria for flooded urban areas. Natural Hazards 2013; 69: 251-265.
Xiao K, Hui B, Qu X, Wang H, Diab A, Cao M. Asphalt pavement water film thickness detection and prediction model: A review. Journal of Traffic and Transportation Engineering (English Edition) 2023; 10: 349-367.

List of Figures

List of Tables

Appendix

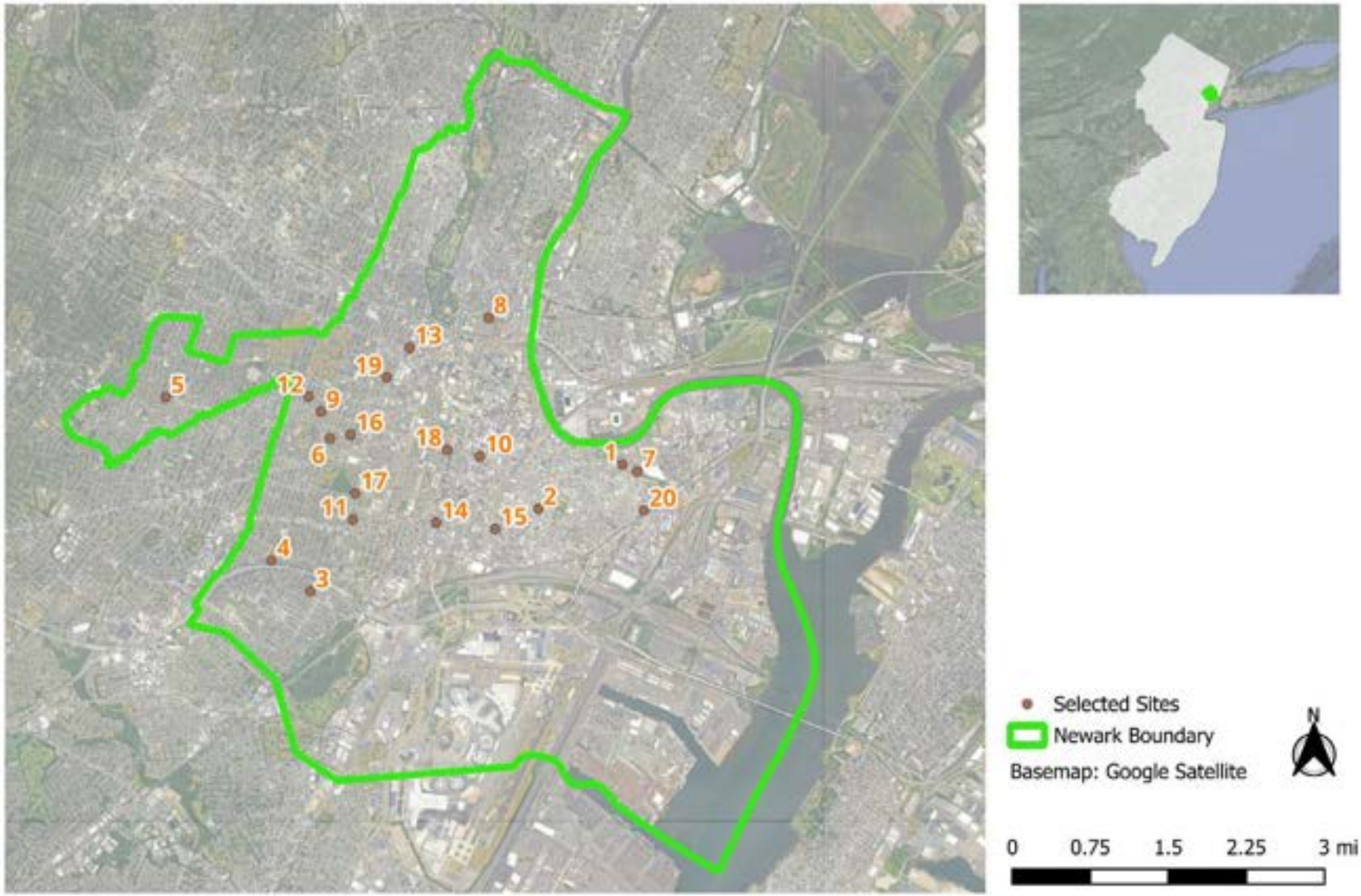

Figure 2 Selected sites in Newark, New Jersey

Appendix

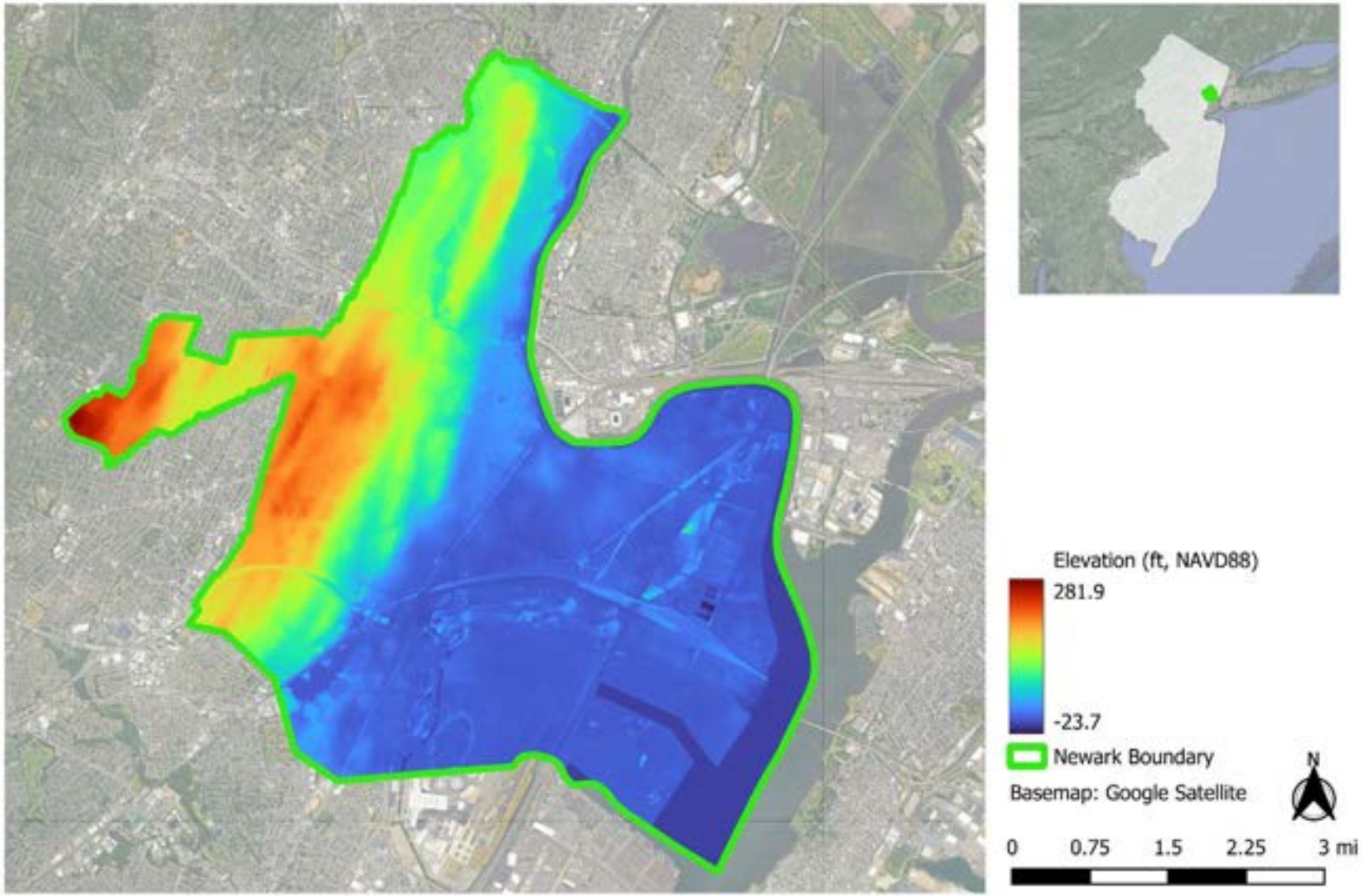

Figure 3 Elevation (Vertical datum: NAVD88) in Newark, New Jersey

Appendix

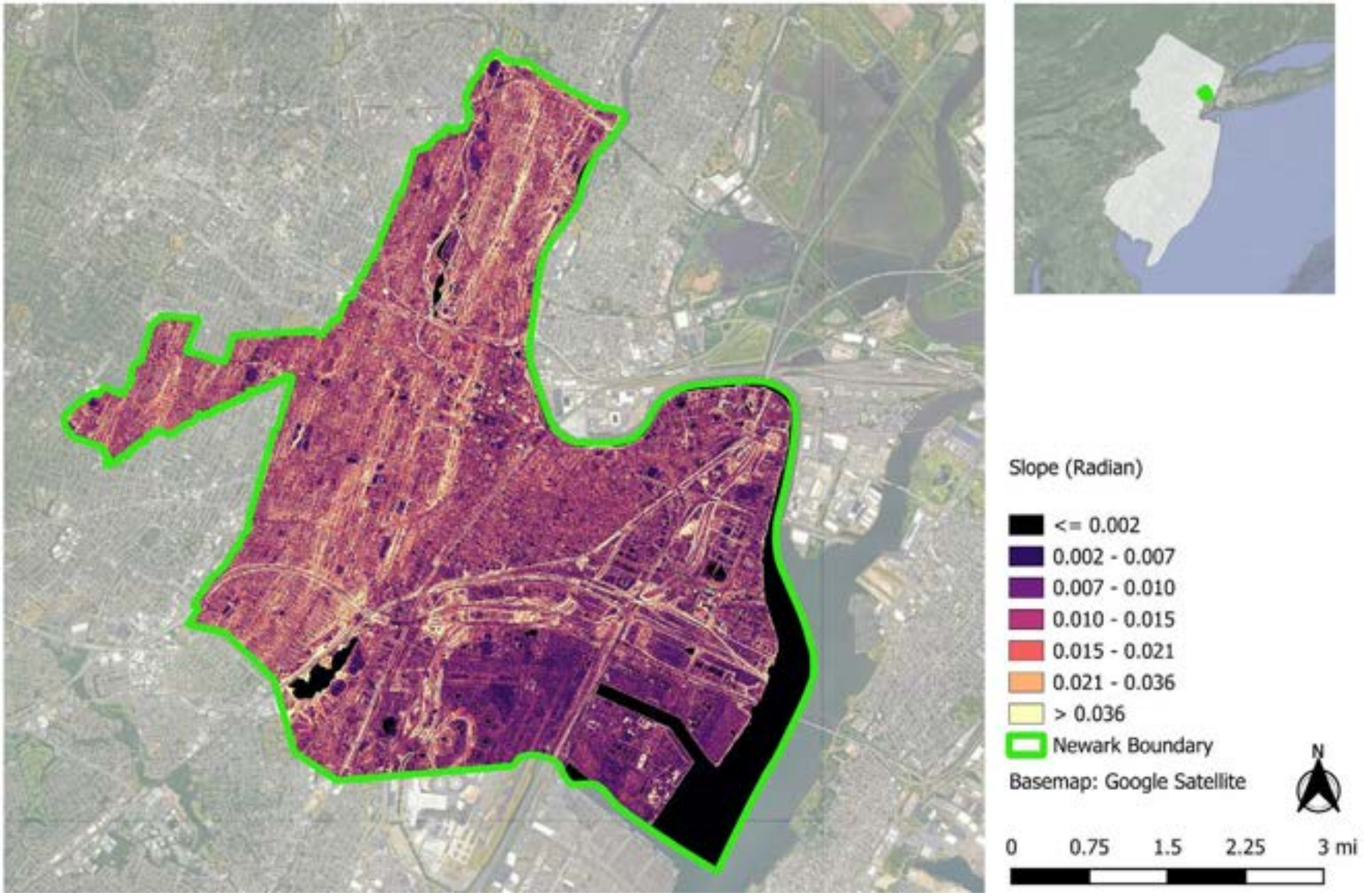

Figure 4 Slope in Newark, New Jersey

Appendix

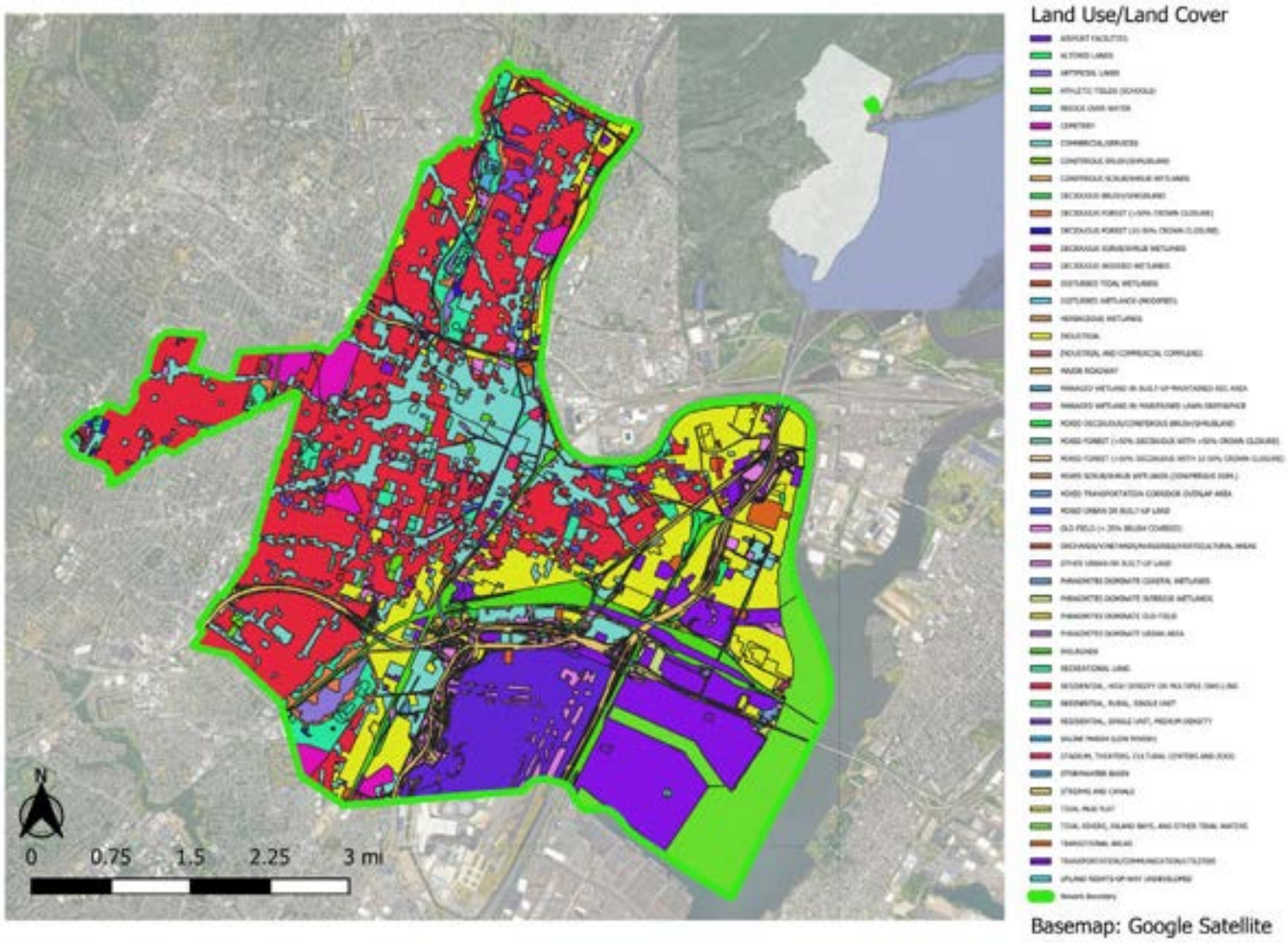

Figure 5 Land use/land cover in Newark, New Jersey

Appendix

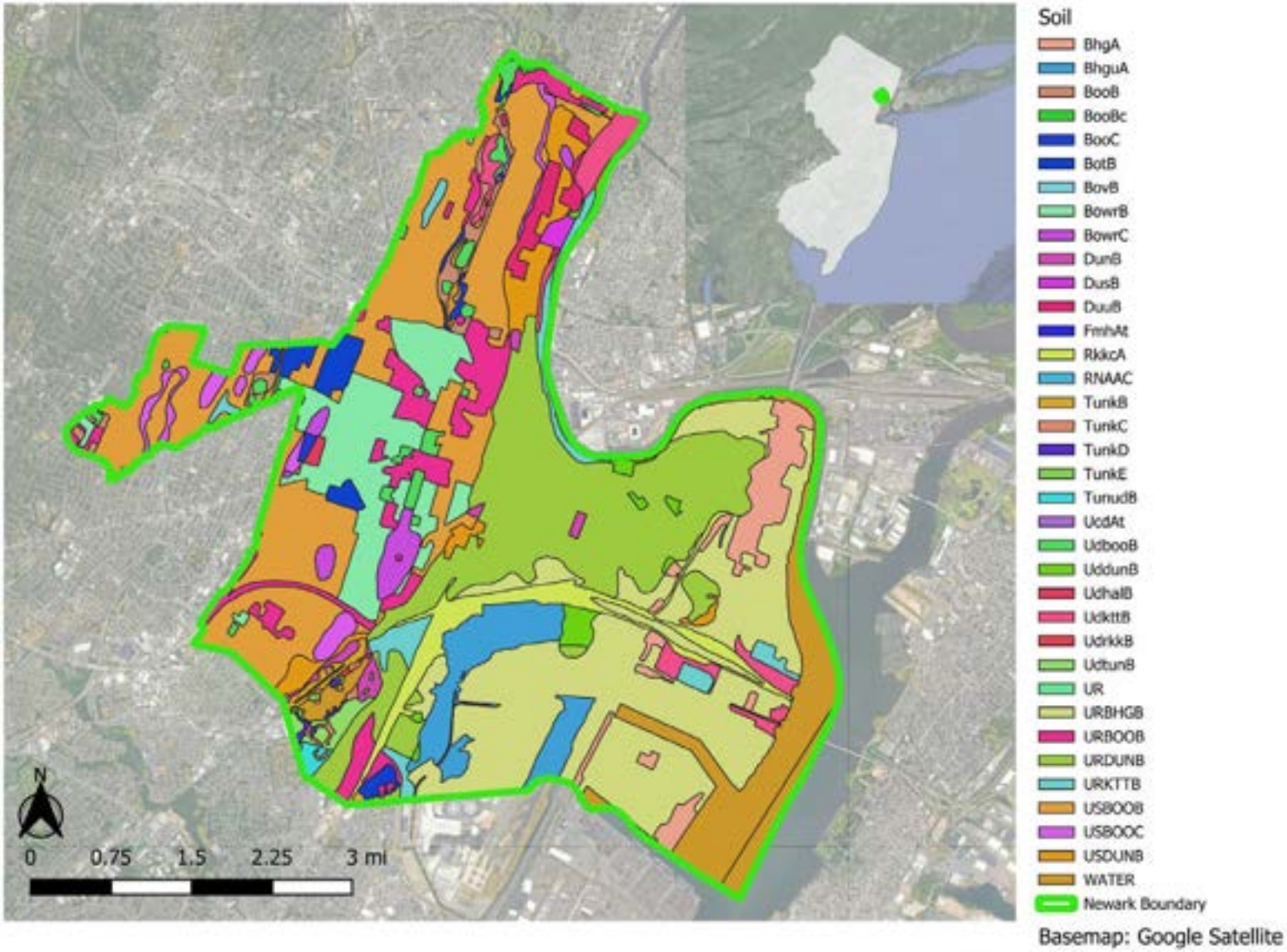

Figure 6 Soil in Newark, New Jersey

Appendix

a)

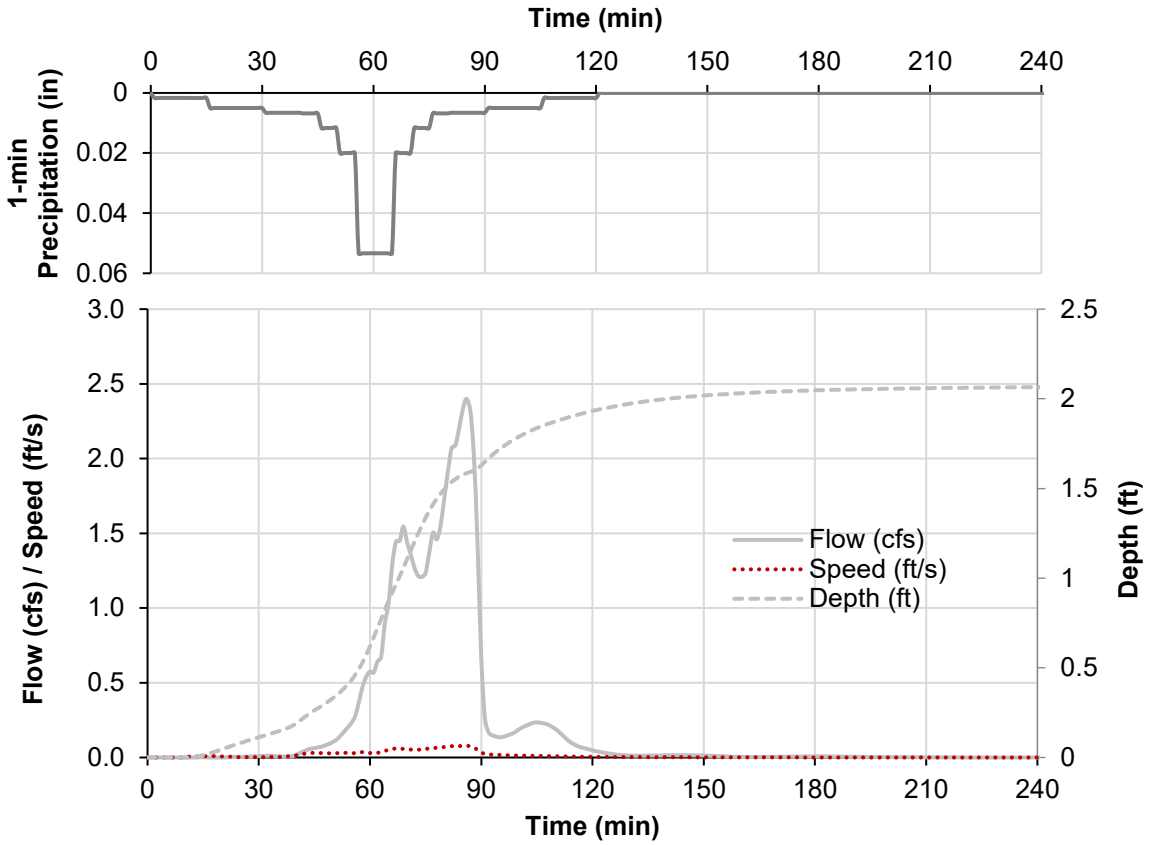

b)

Figure 7 a) Water flow, depth, and speed at the Newark Police Station 3rd Precinct site. b) Aerial photo of the site indicating the reference line (yellow line) where flow was extracted, and the reference point (green point) where depth and speed were measured.

Appendix

a)

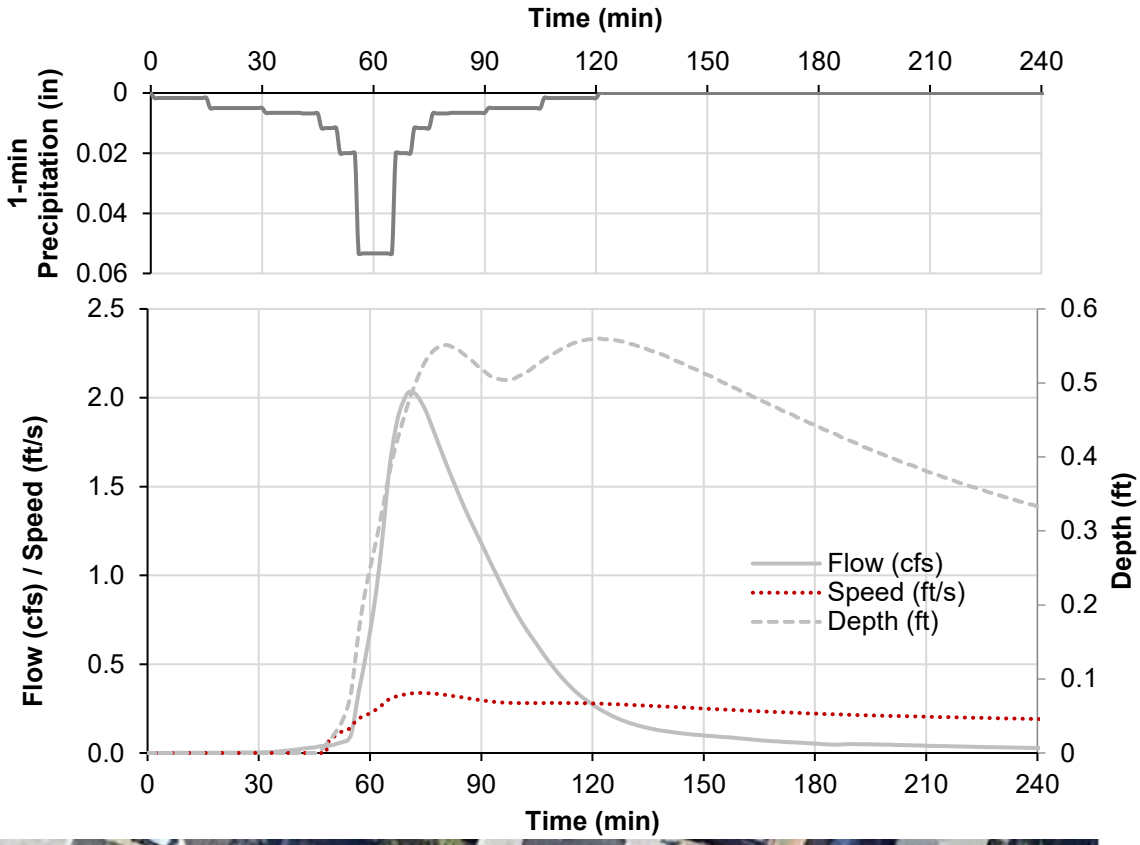

b)

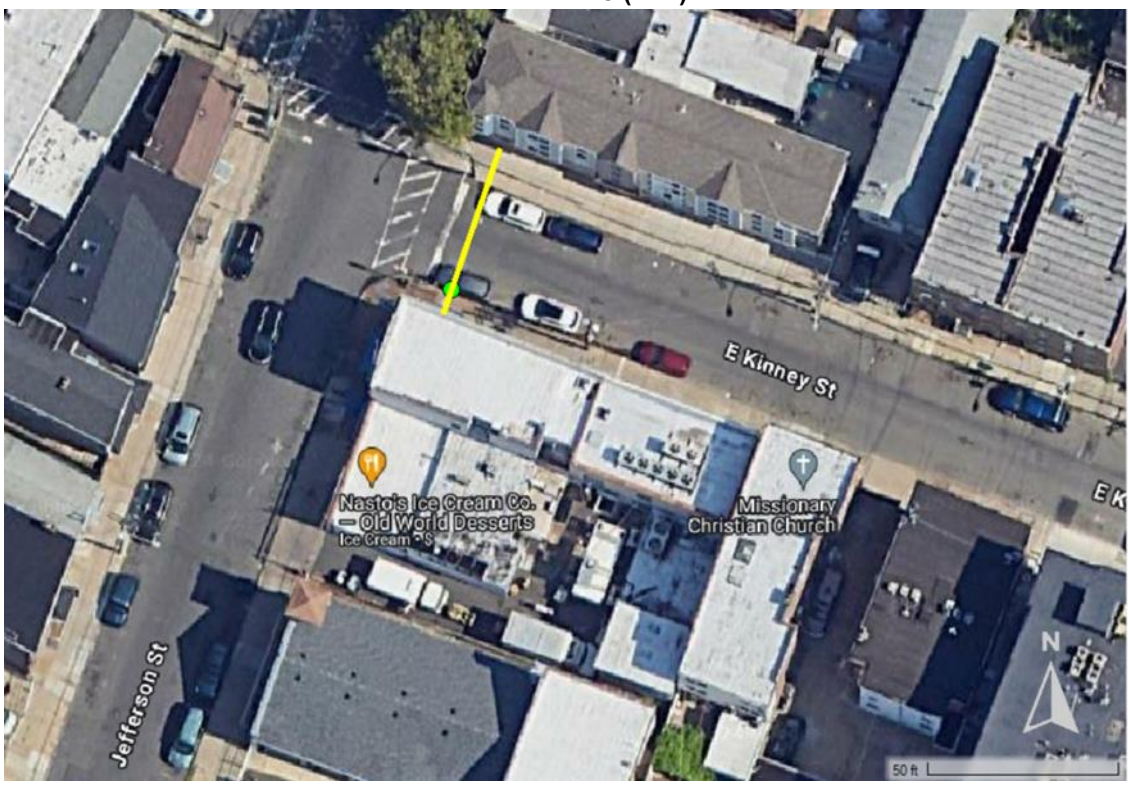

Figure 8 a) Water flow, depth, and speed at the Nasto's Ice Cream site. b) Aerial photo of the site indicating the reference line (yellow line) where flow was extracted, and the reference point (green point) where depth and speed were measured.

Appendix

a)

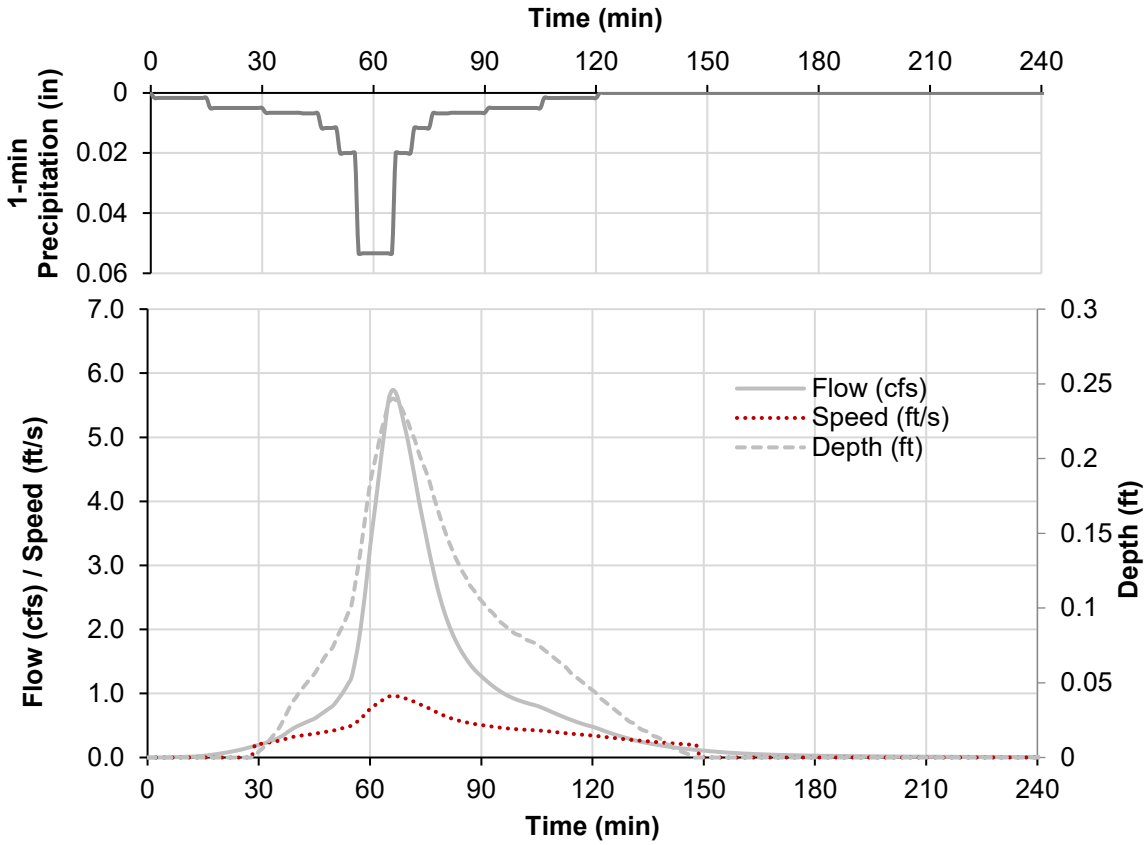

b)

Figure 9 a) Water flow, depth, and speed at the Art of Survival Garden site from HEC-RAS simulation. b) Aerial photo of the site indicating the reference line (yellow line) where flow was extracted, and the reference point (green point) where depth and speed were measured.

Appendix

a)

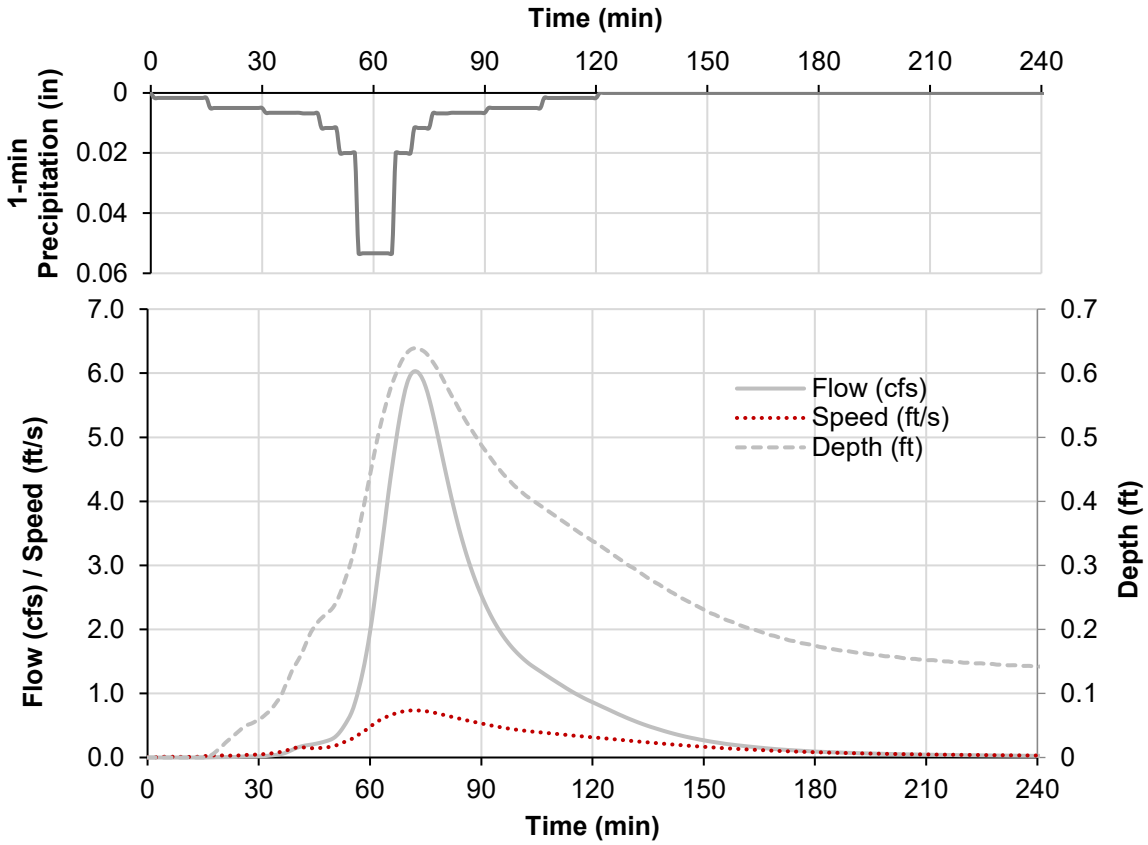

b)

Figure 10 a) Water flow, depth, and speed at the Hawthorne Hawks Healthy Harvest Farm site from HEC-RAS simulation. b) Aerial photo of the site indicating the reference line (yellow line) where flow was extracted, and the reference point (green point) where depth and speed were measured.

Appendix

a)

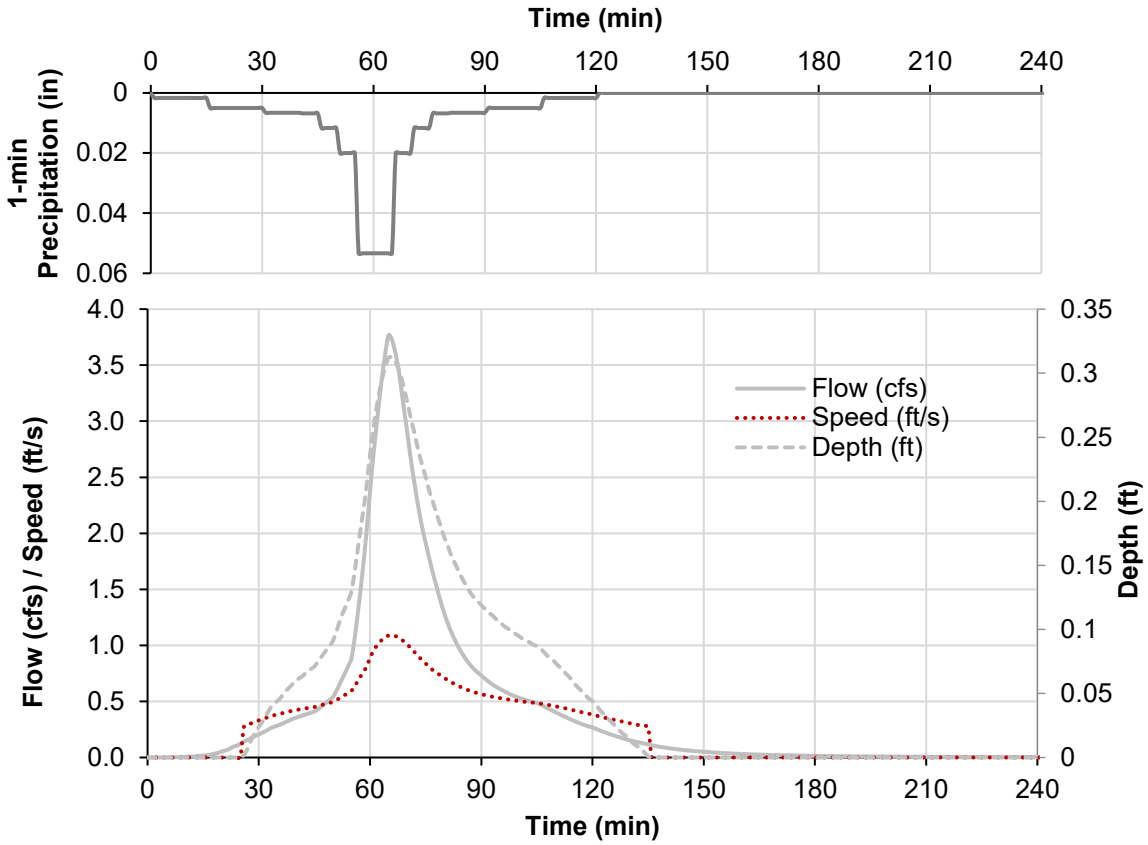

b)

Figure 11 a) Water flow, depth, and speed at the HOV Healthy Haven Garden site from HEC-RAS simulation. b) Aerial photo of the site indicating the reference line (yellow line) where flow was extracted, and the reference point (green point) where depth and speed were measured.

Appendix

a)

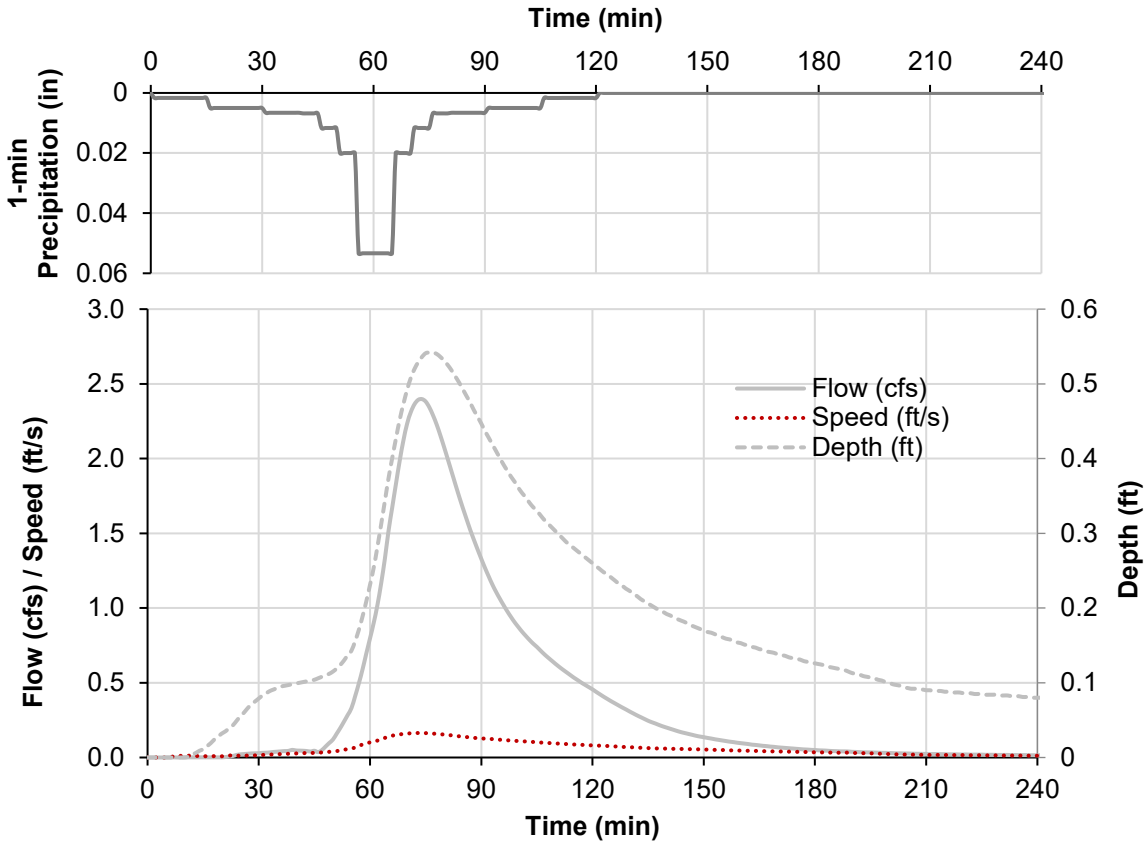

b)

Figure 12 a) Water flow, depth, and speed at the Harriet Tubman Elementary School site from HEC-RAS simulation. b) Aerial photo of the site indicating the reference line (yellow line) where flow was extracted, and the reference point (green point) where depth and speed were measured.

Appendix

a)

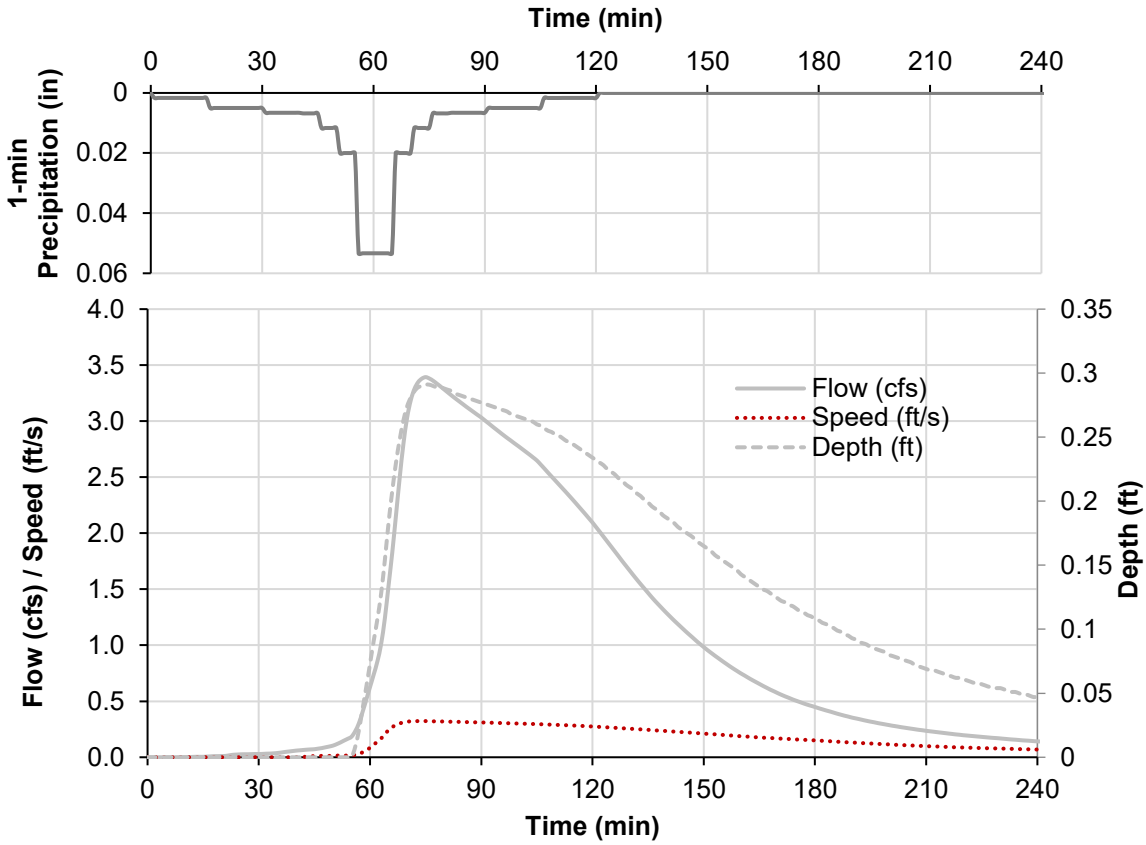

b)

Figure 13 a) Water flow, depth, and speed at the Down Bottom Farms Traffic Triangle site from HEC-RAS simulation. b) Aerial photo of the site indicating the reference line (yellow line) where flow was extracted, and the reference point (green point) where depth and speed were measured.

Appendix

a)

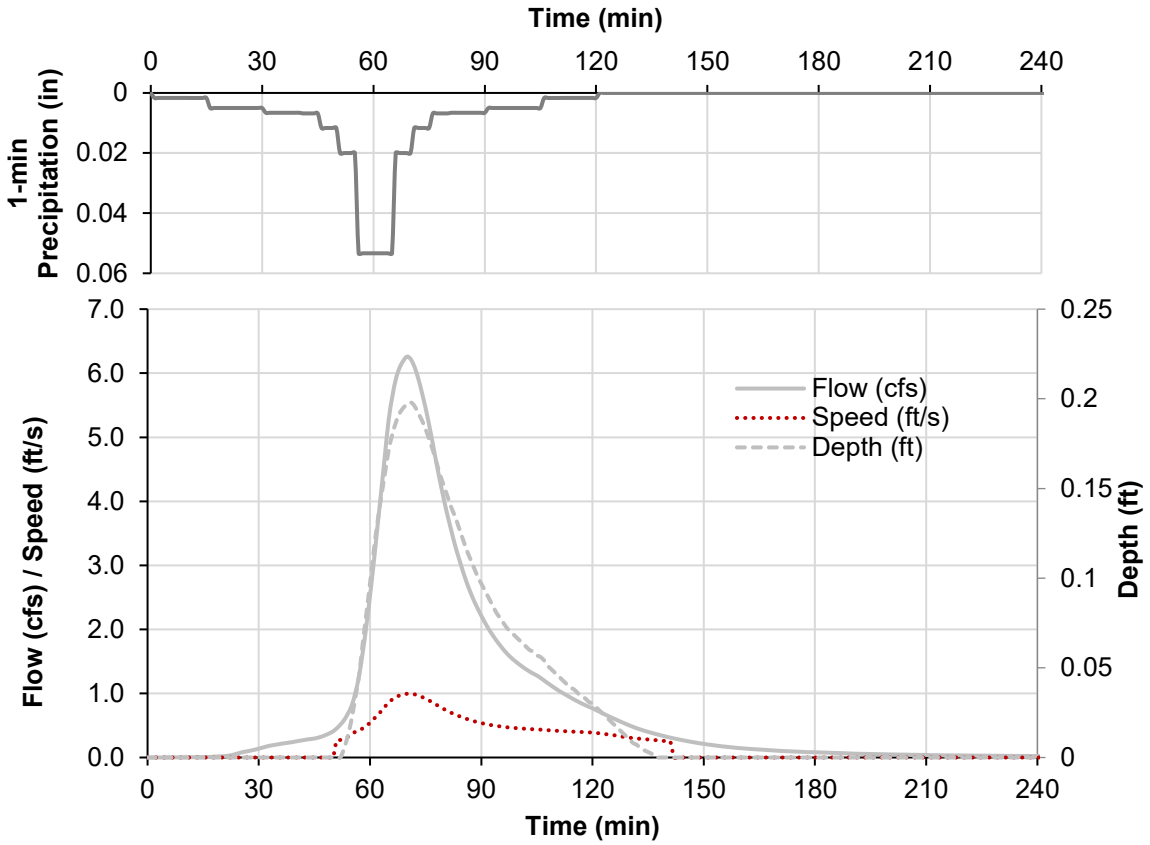

b)

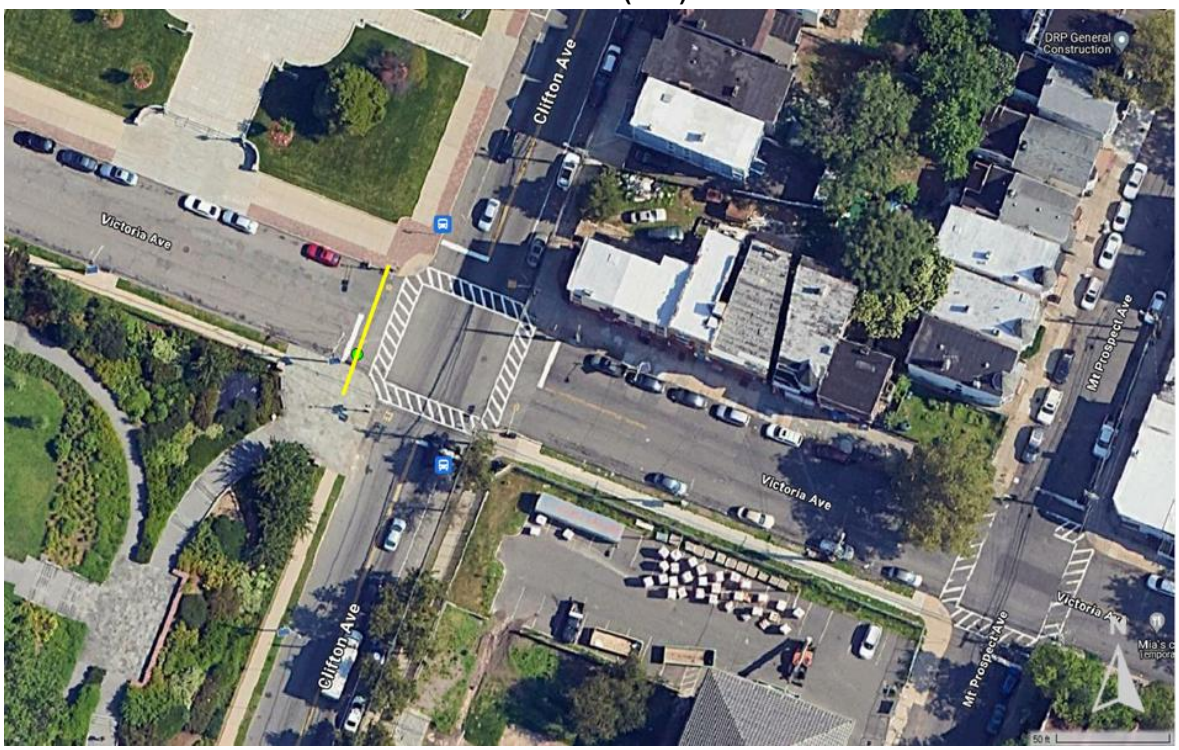

Figure 14 a) Water flow, depth, and speed at the Branck Brook Alliance site from HEC-RAS simulation. b) Aerial photo of the site indicating the reference line (yellow line) where flow was extracted, and the reference point (green point) where depth and speed were measured.

Appendix

a)

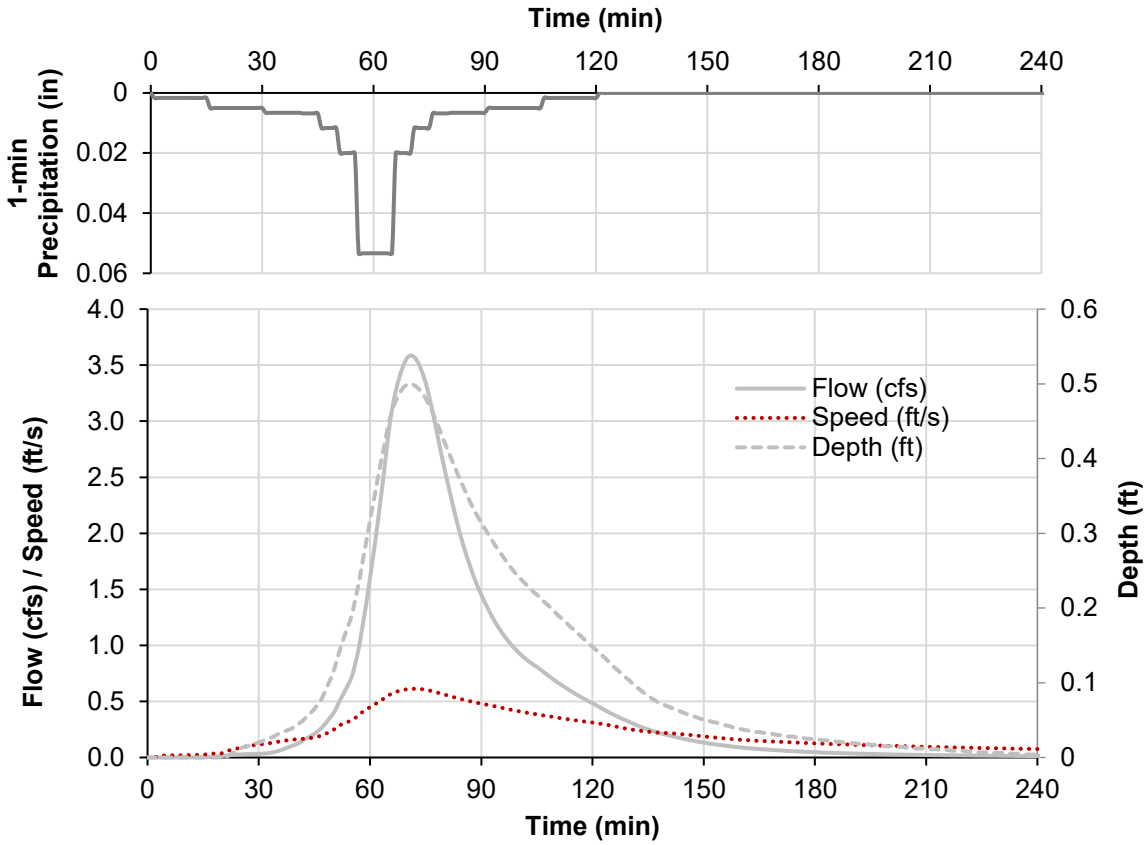

b)

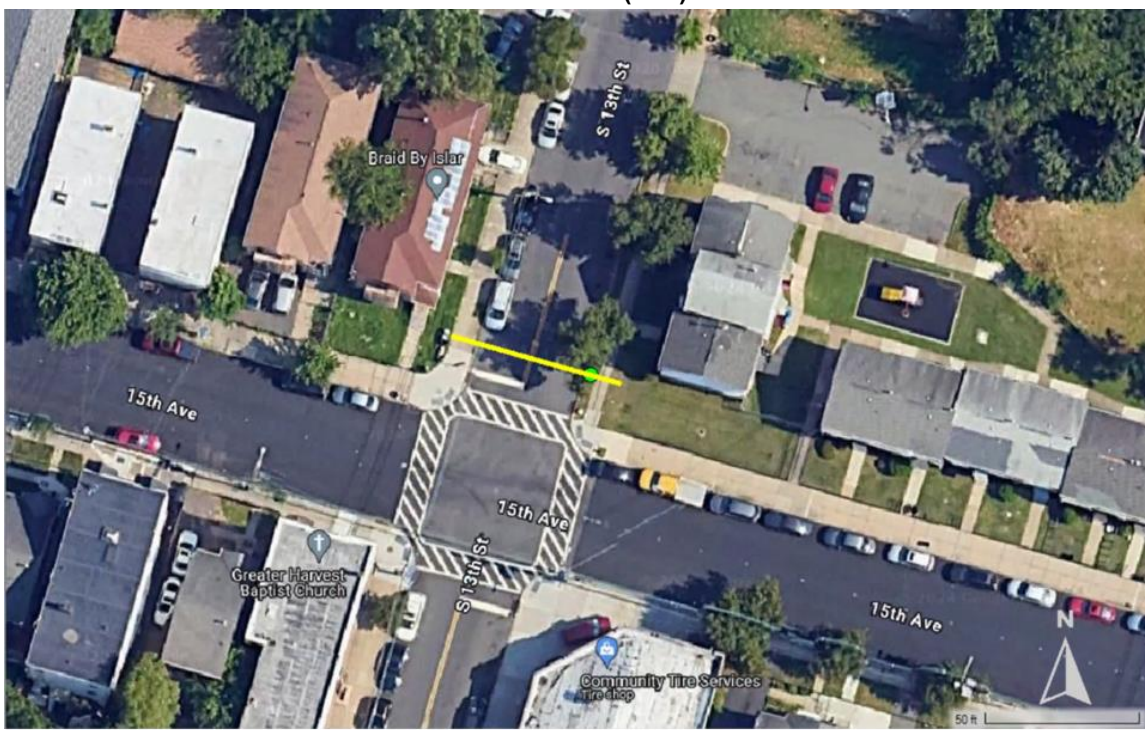

Figure 15 a) Water flow, depth, and speed at the Wanda Upshaw Meditation Garden site from HEC-RAS simulation. b) Aerial photo of the site indicating the reference line (yellow line) where flow was extracted, and the reference point (green point) where depth and speed were measured.

Appendix

a)

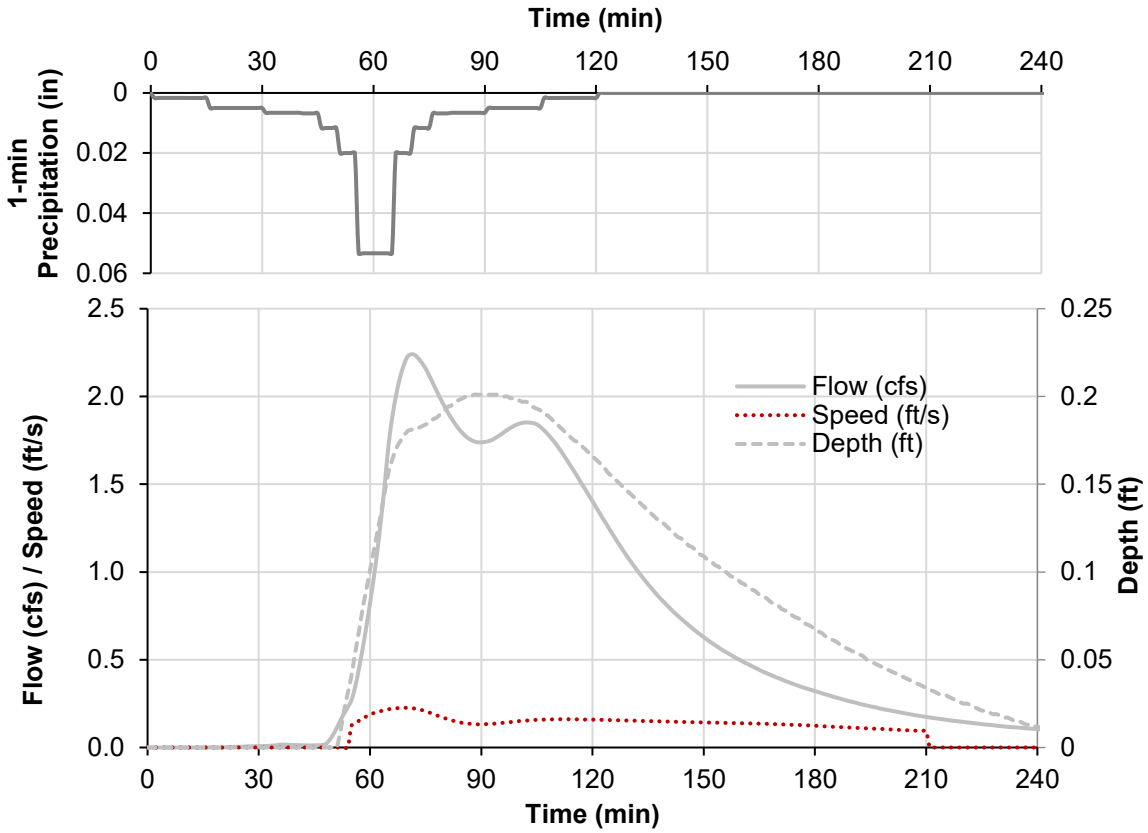

b)

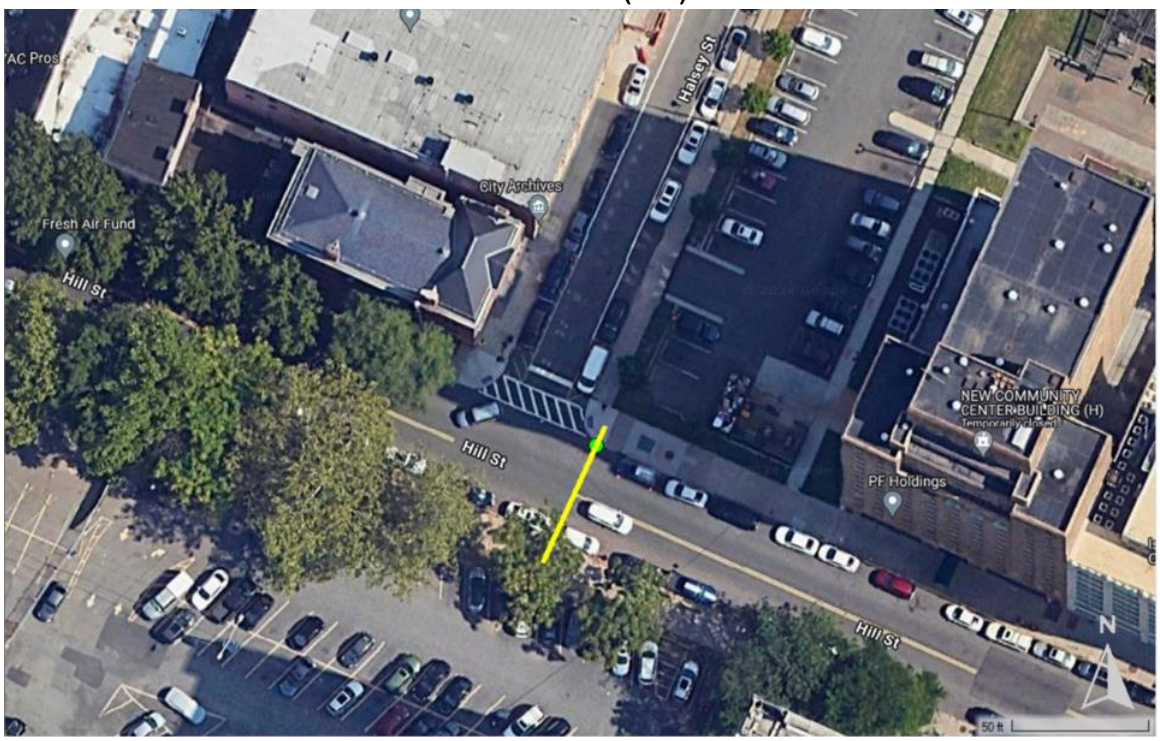

Figure 16 a) Water flow, depth, and speed at the Newark Educators Community Charter School site from HEC-RAS simulation. b) Aerial photo of the site indicating the reference line (yellow line) where flow was extracted, and the reference point (green point) where depth and speed were measured.

Appendix

a)

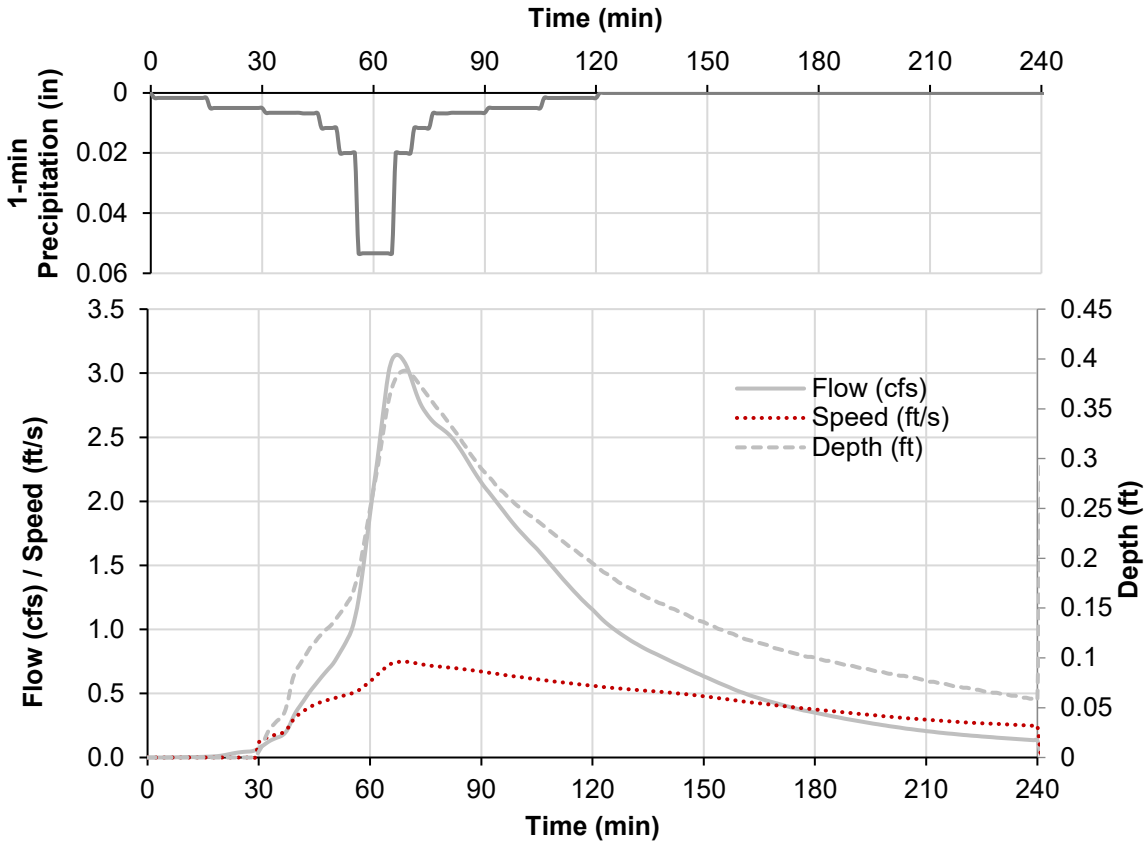

b)

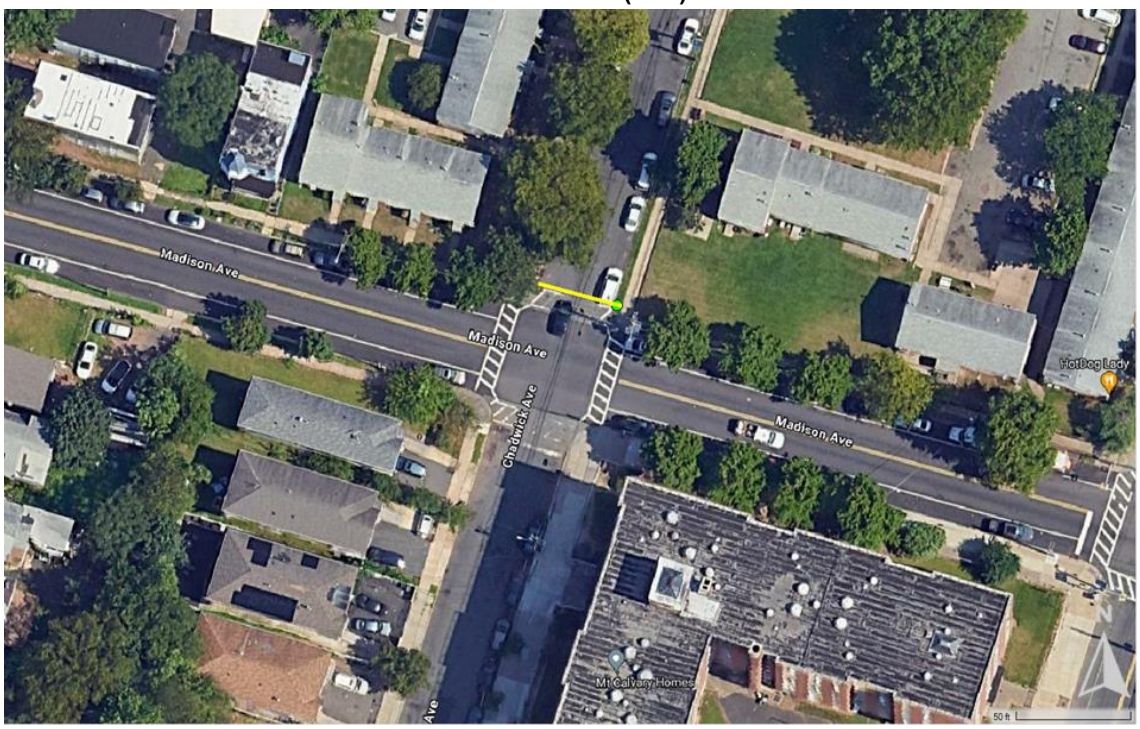

Figure 17 a) Water flow, depth, and speed at the Bergen Street Community Garden site from HEC-RAS simulation. b) Aerial photo of the site indicating the reference line (yellow line) where flow was extracted, and the reference point (green point) where depth and speed were measured.

a)

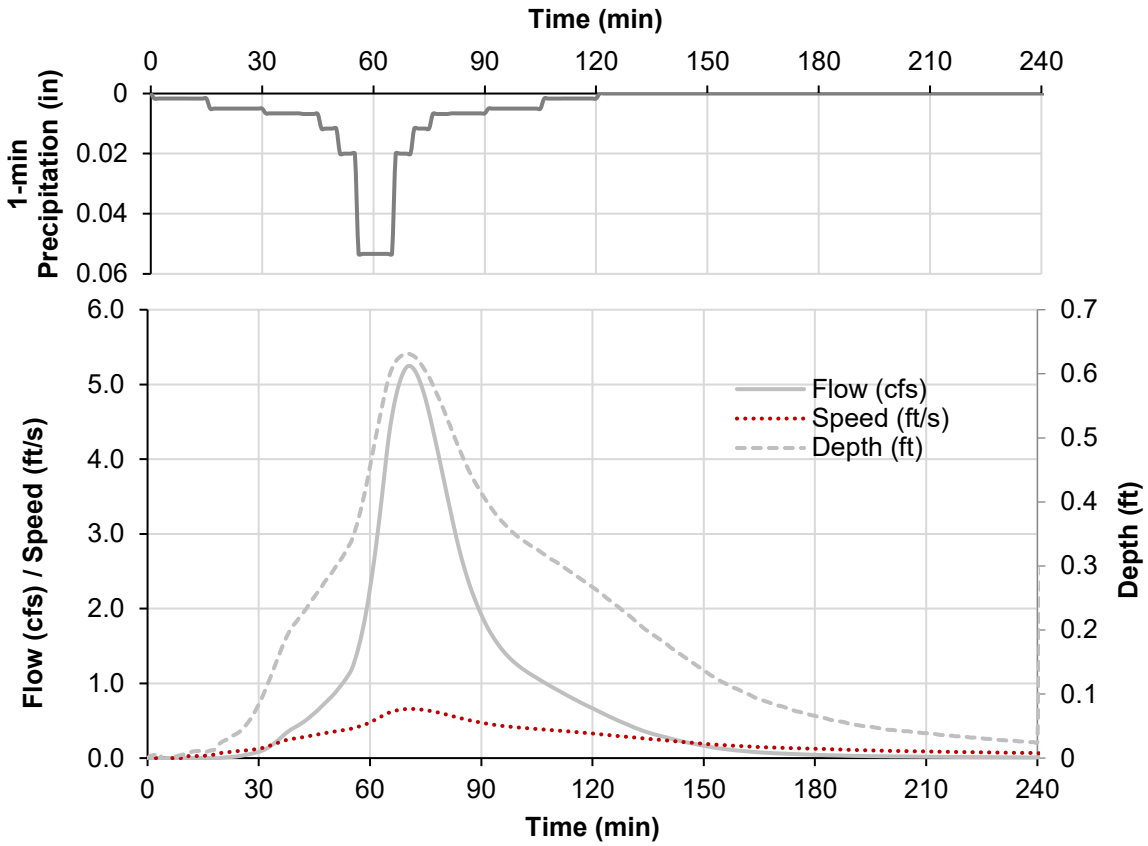

b)

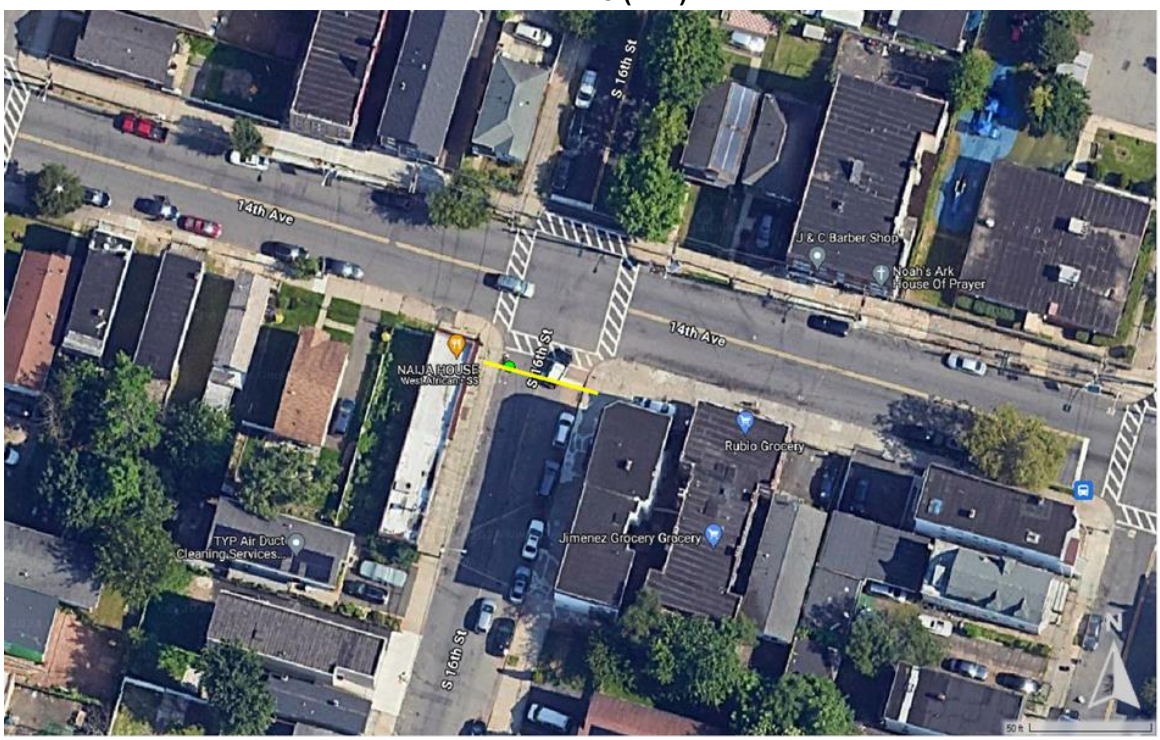

Figure 18 a) Water flow, depth, and speed at the 14th Avenue Community Garden site from HEC-RAS simulation. b) Aerial photo of the site indicating the reference line (yellow line) where flow was extracted, and the reference point (green point) where depth and speed were measured.

Appendix

a)

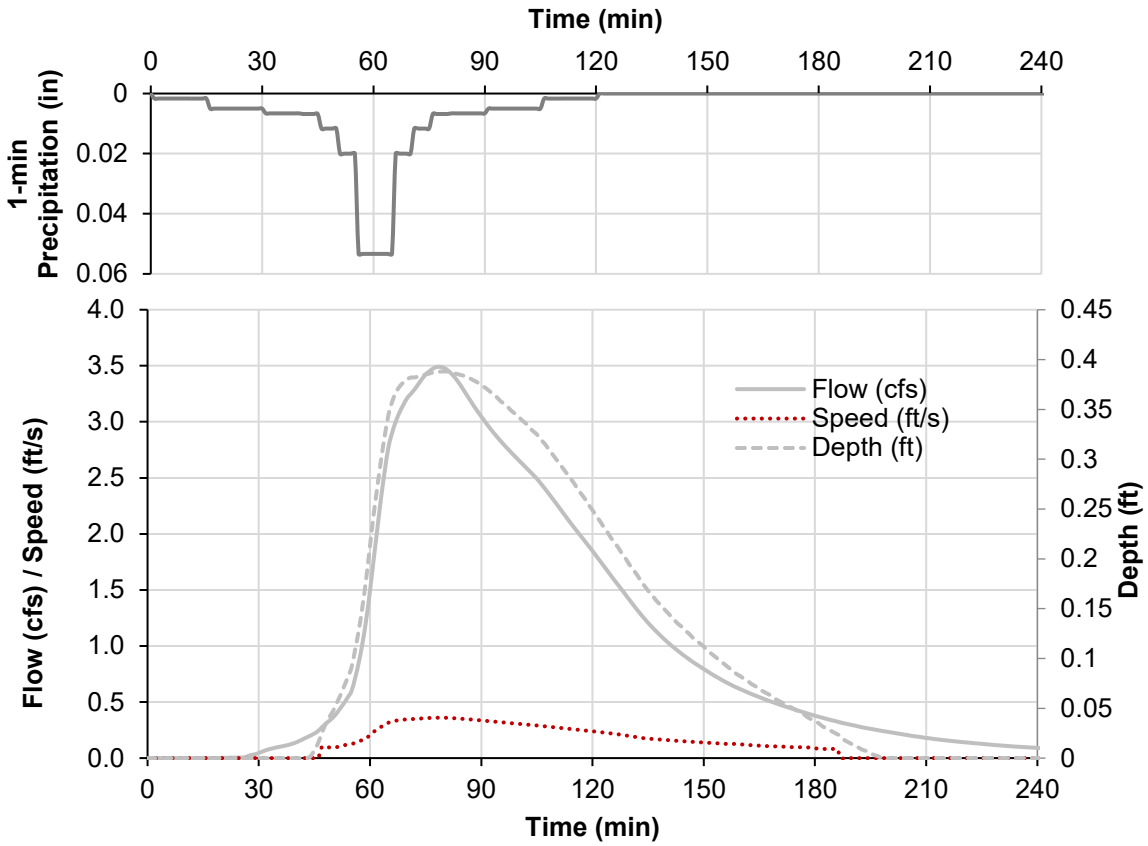

b)

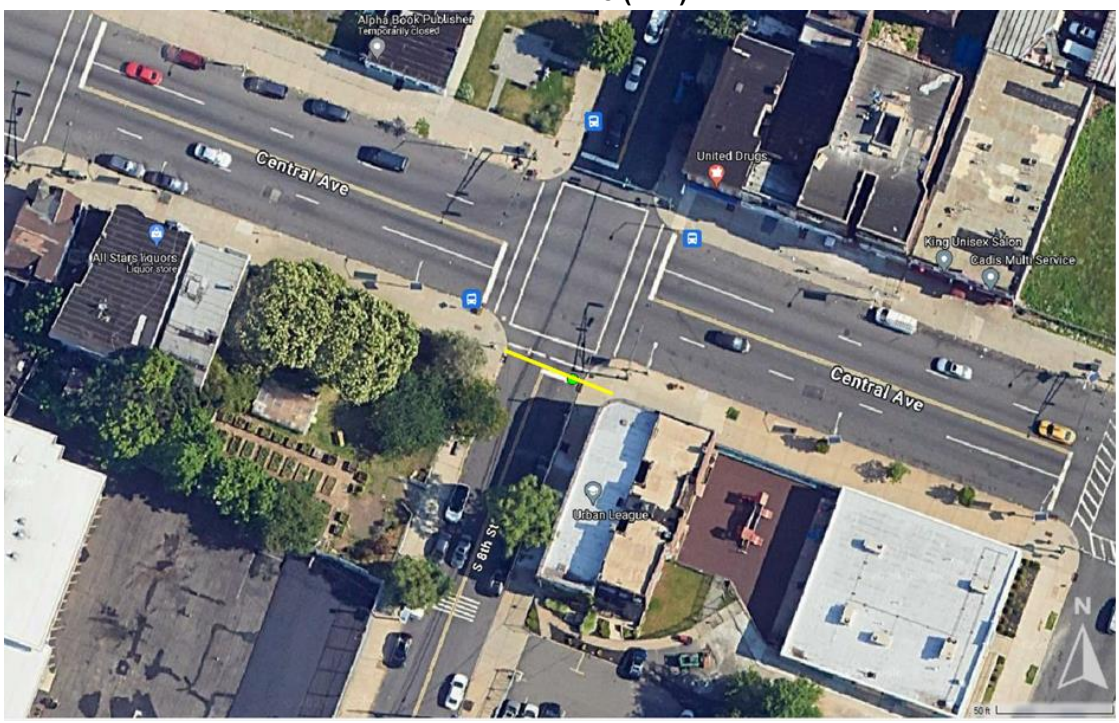

Figure 19 a) Water flow, depth, and speed at the Urban League of Essex County site from HEC-RAS simulation. b) Aerial photo of the site indicating the reference line (yellow line) where flow was extracted, and the reference point (green point) where depth and speed were measured.

Appendix

a)

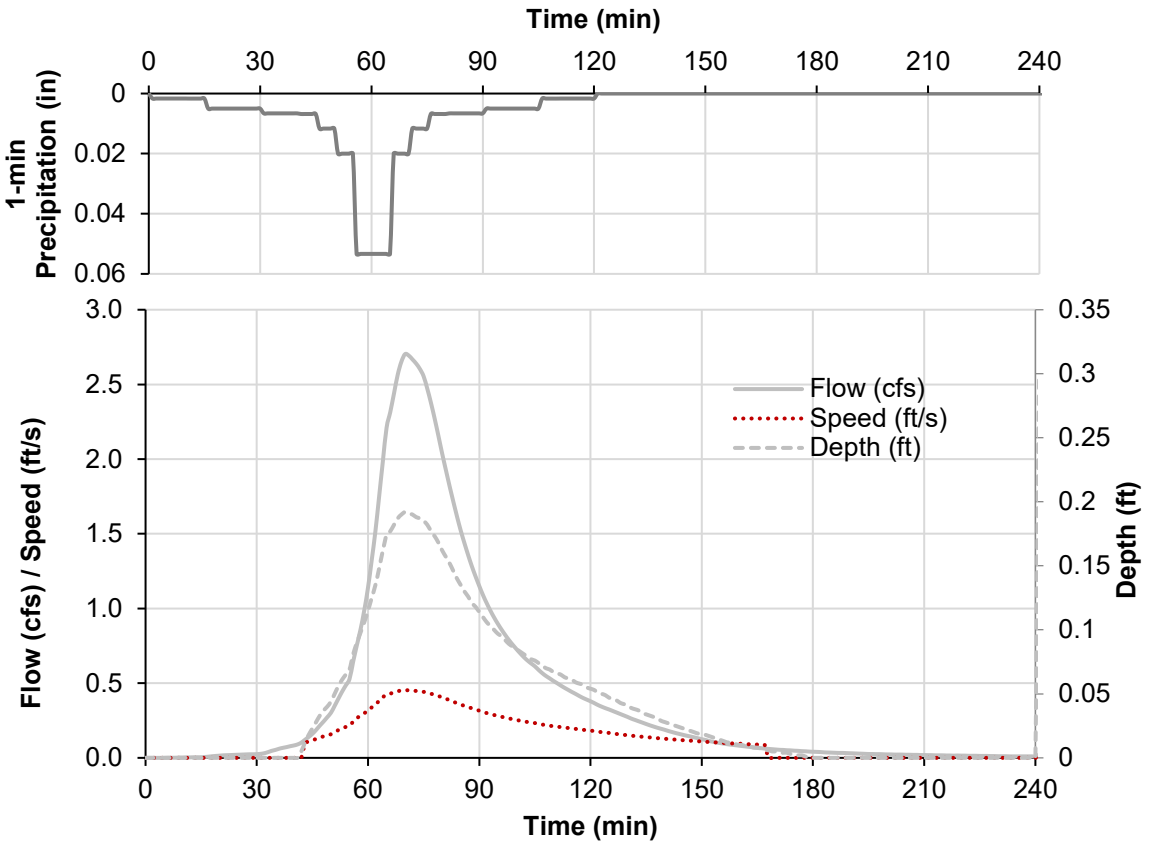

b)

Figure 20 a) Water flow, depth, and speed at the Astor Street Community Garden site from HEC-RAS simulation. b) Aerial photo of the site indicating the reference line (yellow line) where flow was extracted, and the reference point (green point) where depth and speed were measured.

Appendix

a)

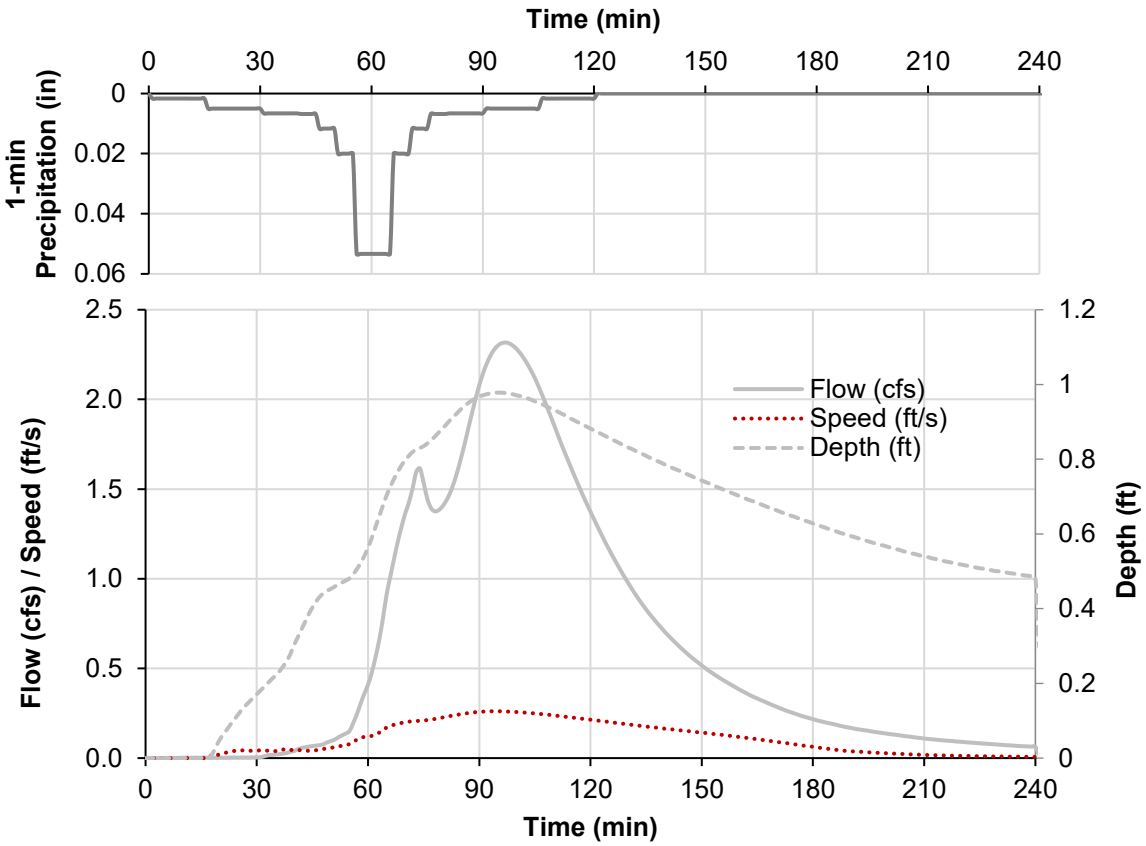

b)

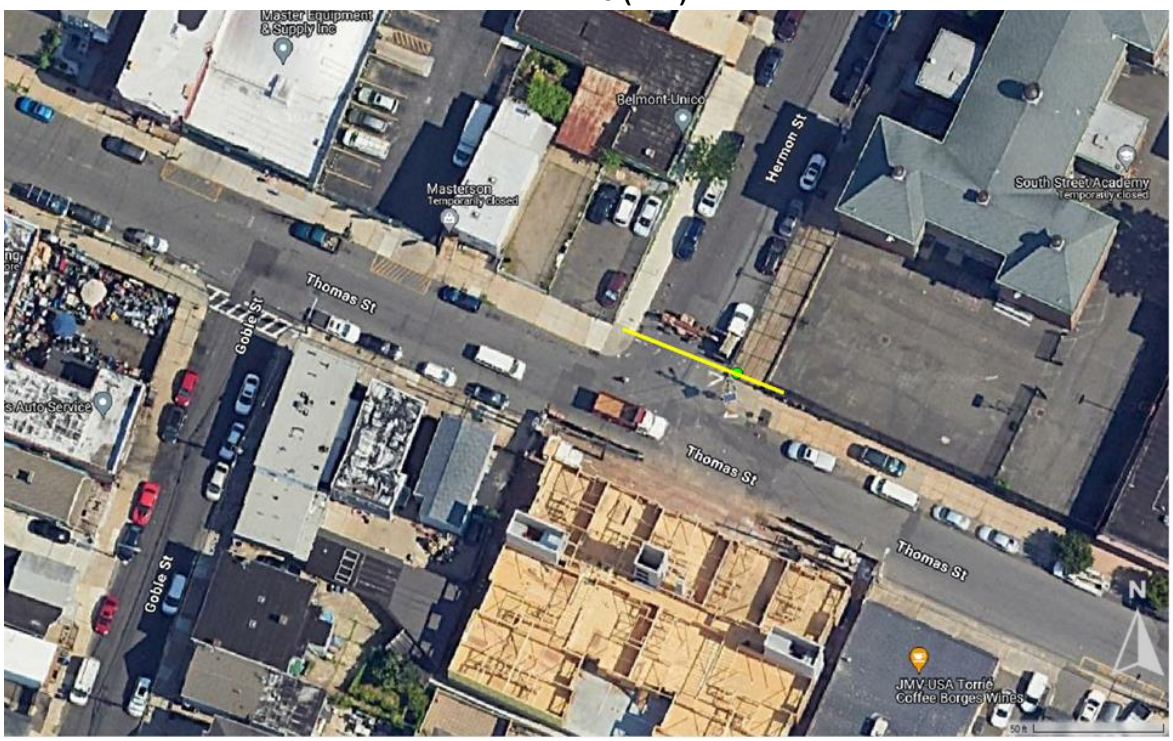

Figure 21 a) Water flow, depth, and speed at the South Street Academy site from HEC-RAS simulation. b) Aerial photo of the site indicating the reference line (yellow line) where flow was extracted, and the reference point (green point) where depth and speed were measured.

Appendix

a)

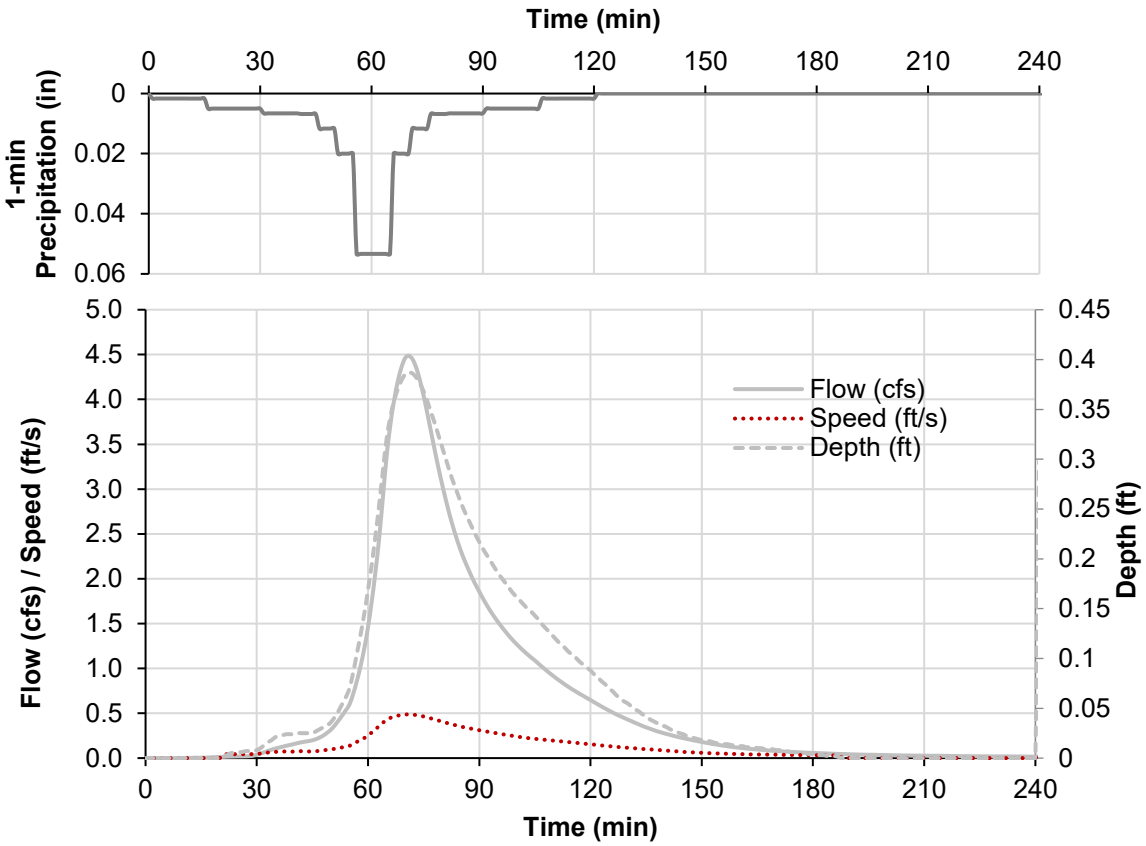

b)

Figure 22 a) Water flow, depth, and speed at the St. Ann's Church site from HEC-RAS simulation. b) Aerial photo of the site indicating the reference line (yellow line) where flow was extracted, and the reference point (green point) where depth and speed were measured.

Appendix

a)

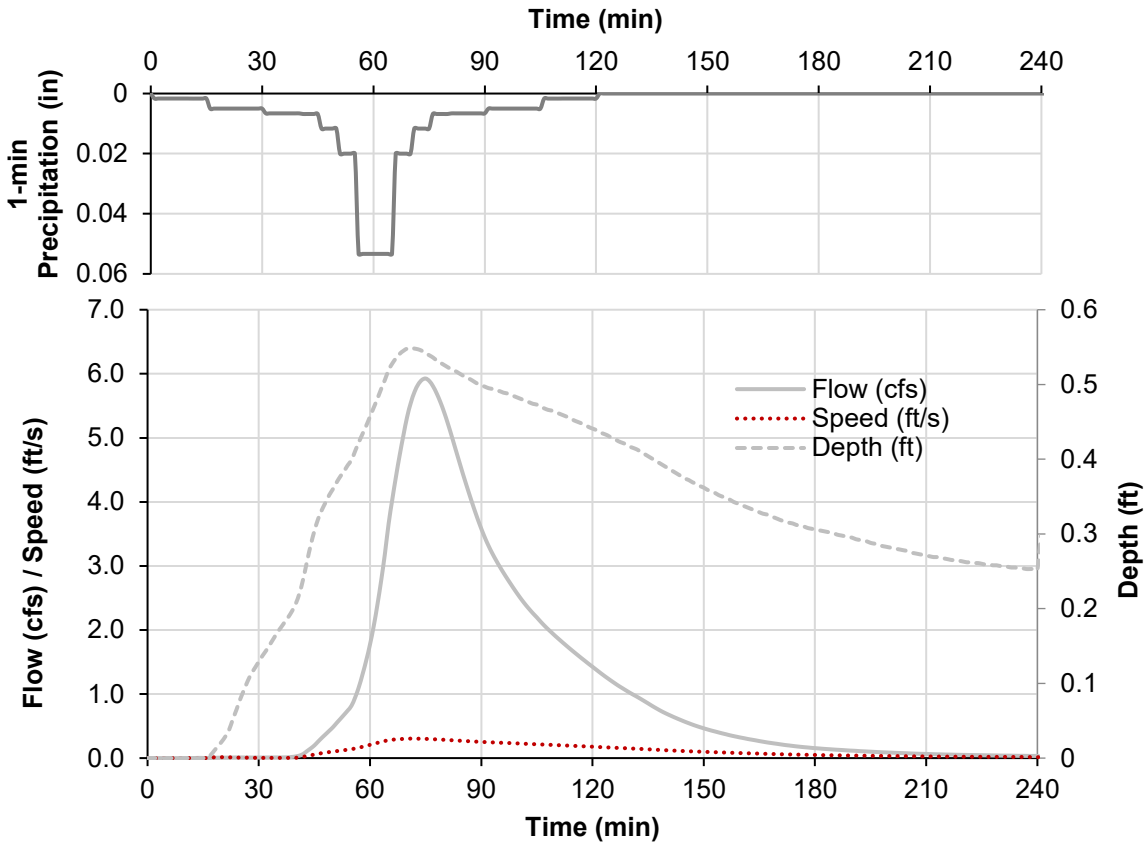

b)

Figure 23 a) Water flow, depth, and speed at the James C. White Manor Senior Housing site from HEC-RAS simulation. b) Aerial photo of the site indicating the reference line (yellow line) where flow was extracted, and the reference point (green point) where depth and speed were measured.

Appendix

a)

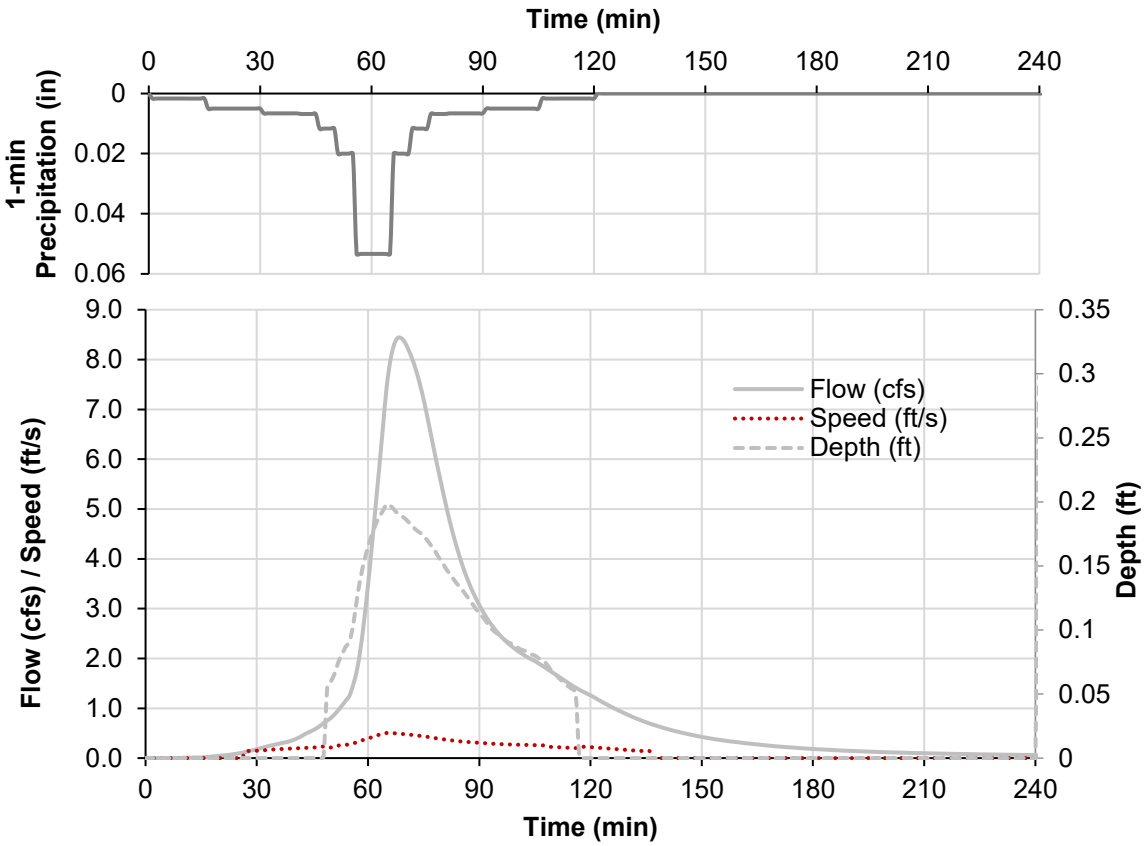

b)

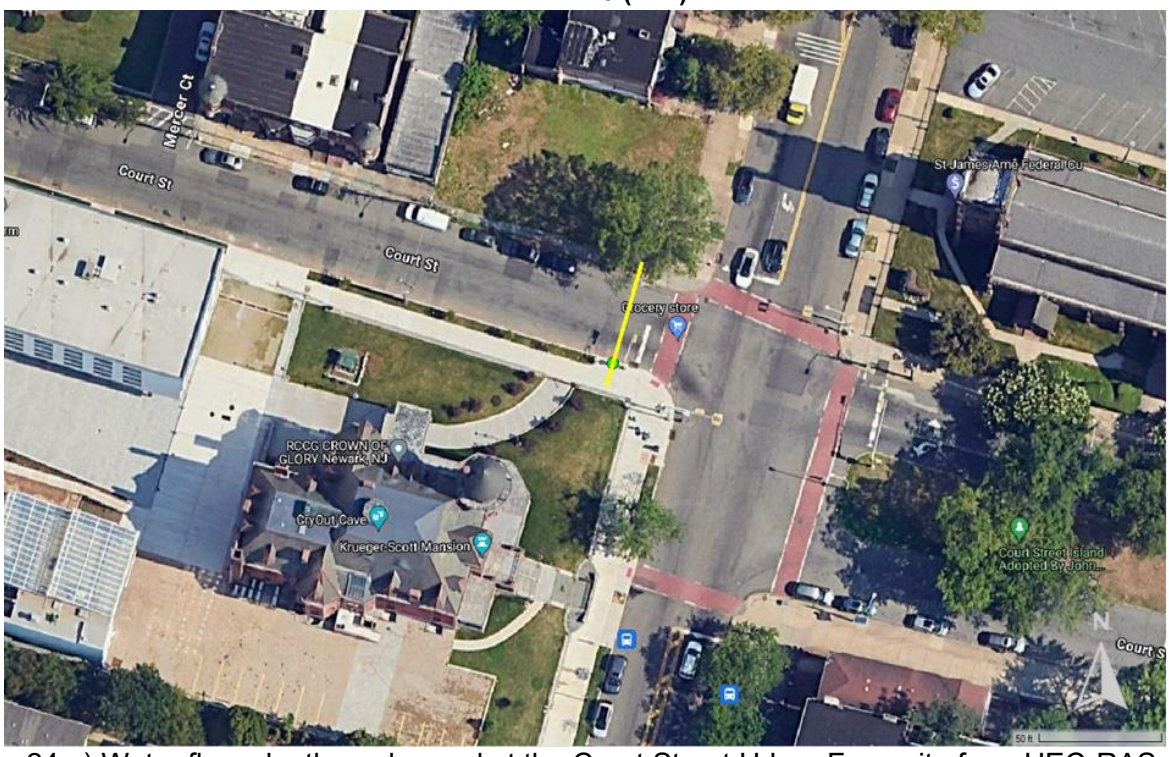

Figure 24 a) Water flow, depth, and speed at the Court Street Urban Farm site from HEC-RAS simulation. b) Aerial photo of the site indicating the reference line (yellow line) where flow was extracted, and the reference point (green point) where depth and speed were measured.

Appendix

a)

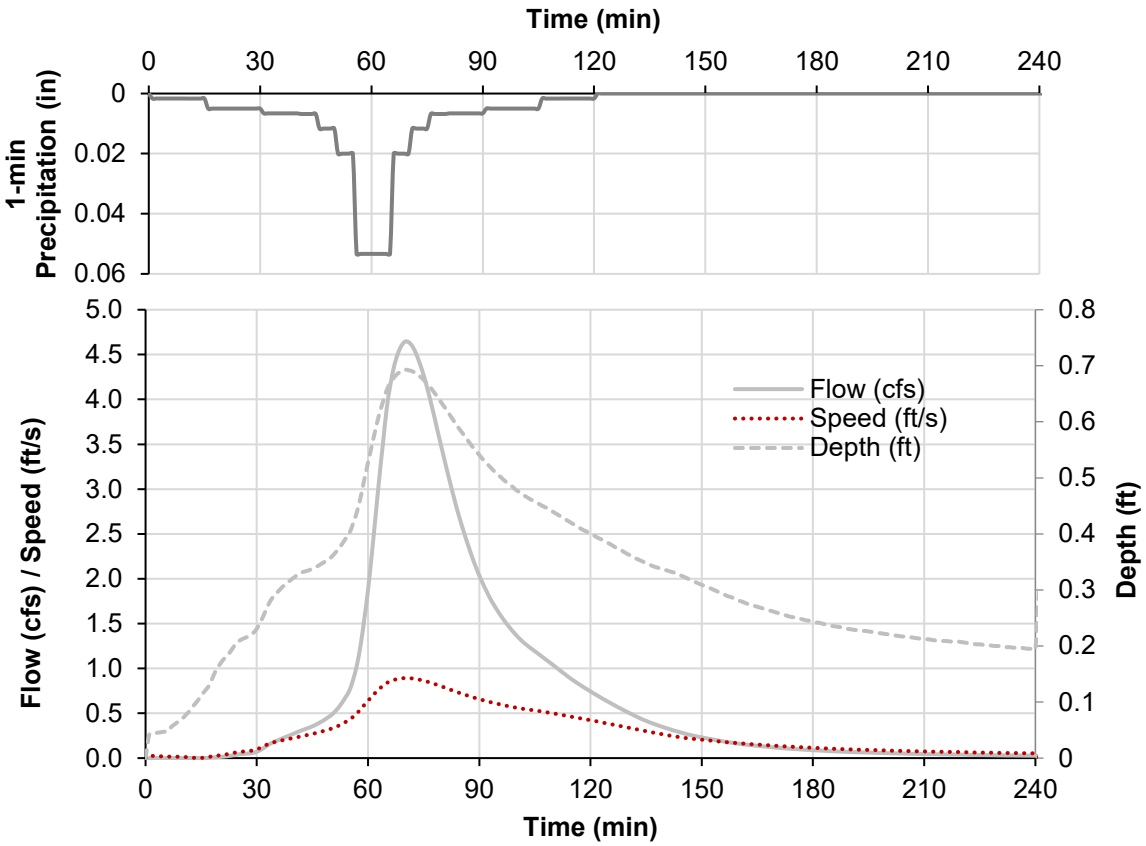

b)

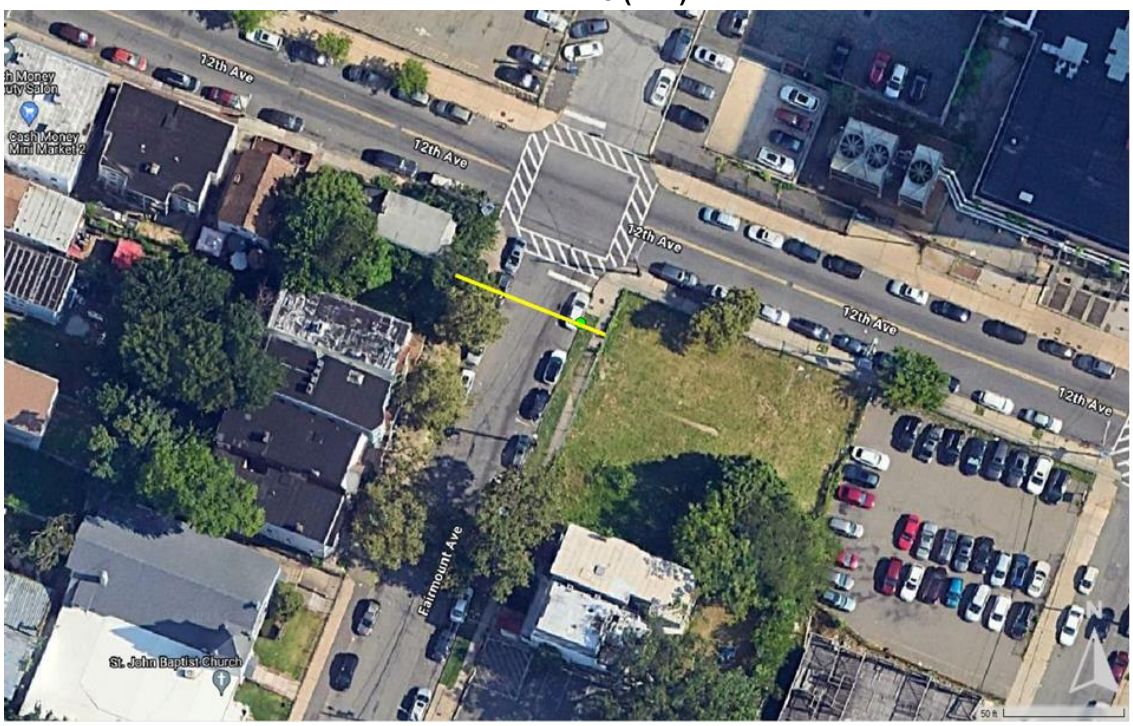

Figure 25 a) Water flow, depth, and speed at the Rutgers School of Health Professions site from HEC-RAS simulation. b) Aerial photo of the site indicating the reference line (yellow line) where flow was extracted, and the reference point (green point) where depth and speed were measured.

a)

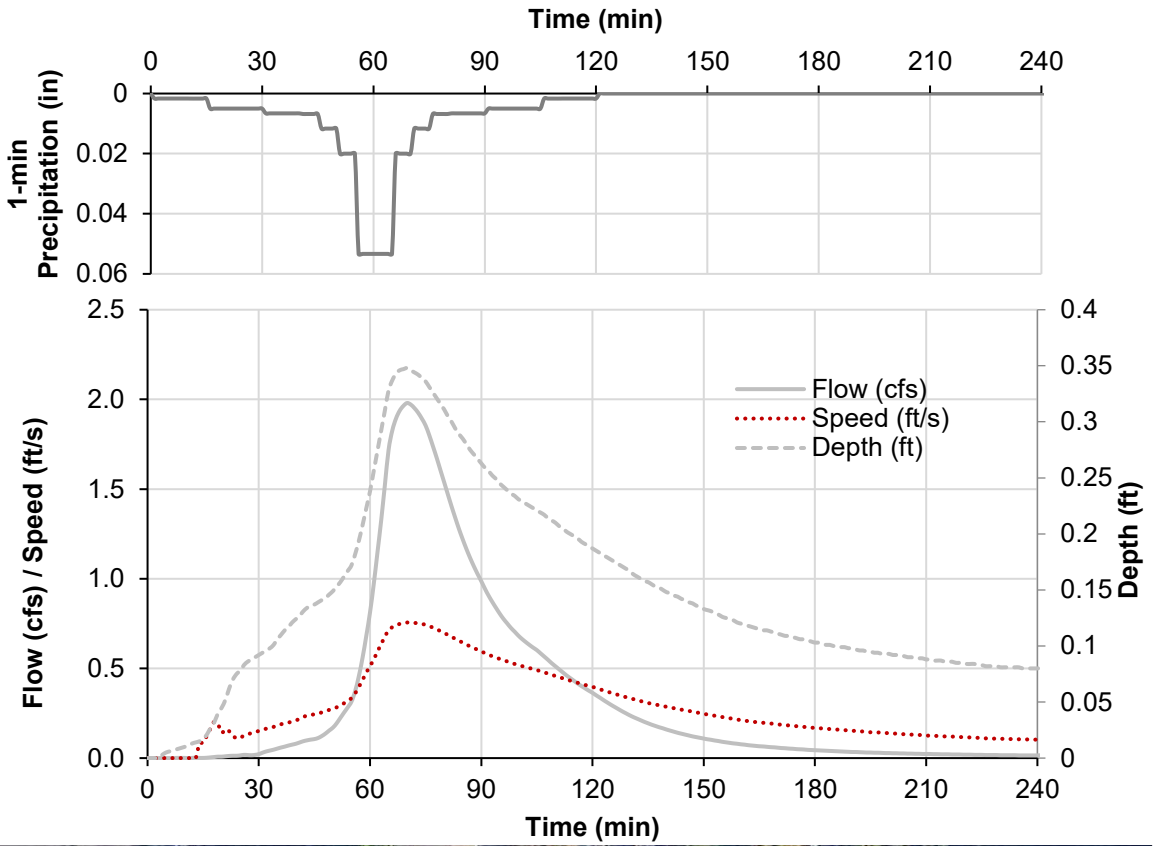

b)

Figure 26 a) Water flow, depth, and speed at the Robert Treat Academy Charter School site from HEC-RAS simulation. b) Aerial photo of the site indicating the reference line (yellow line) where flow was extracted, and the reference point (green point) where depth and speed were measured.

Appendix

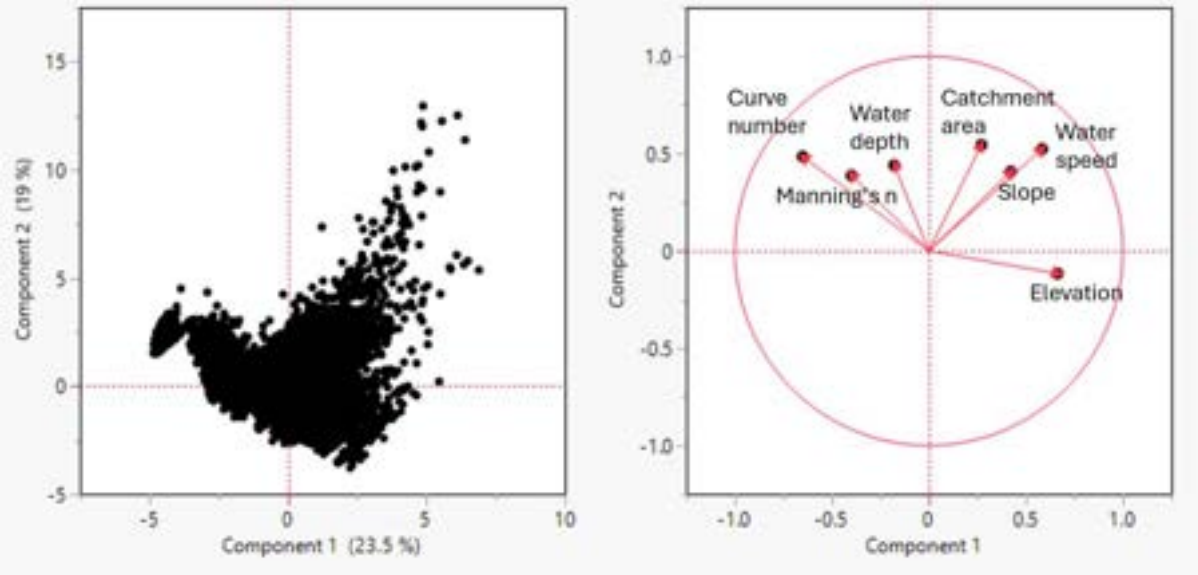

Figure 27 Principal component score plot (left) and loading plot (right).

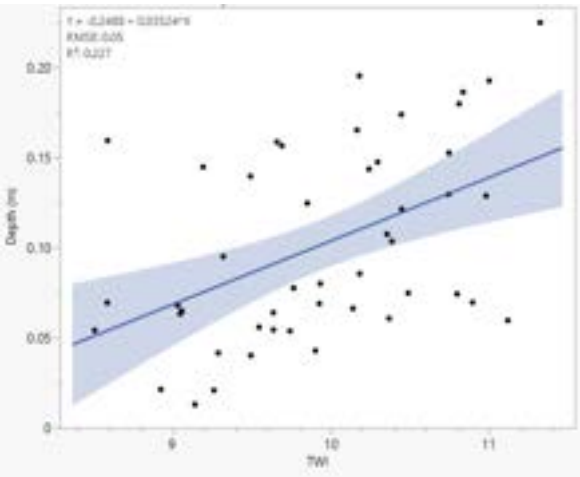

Figure 28 Correlation between water depth from the HEC-RAS simulations and TWI

Appendix

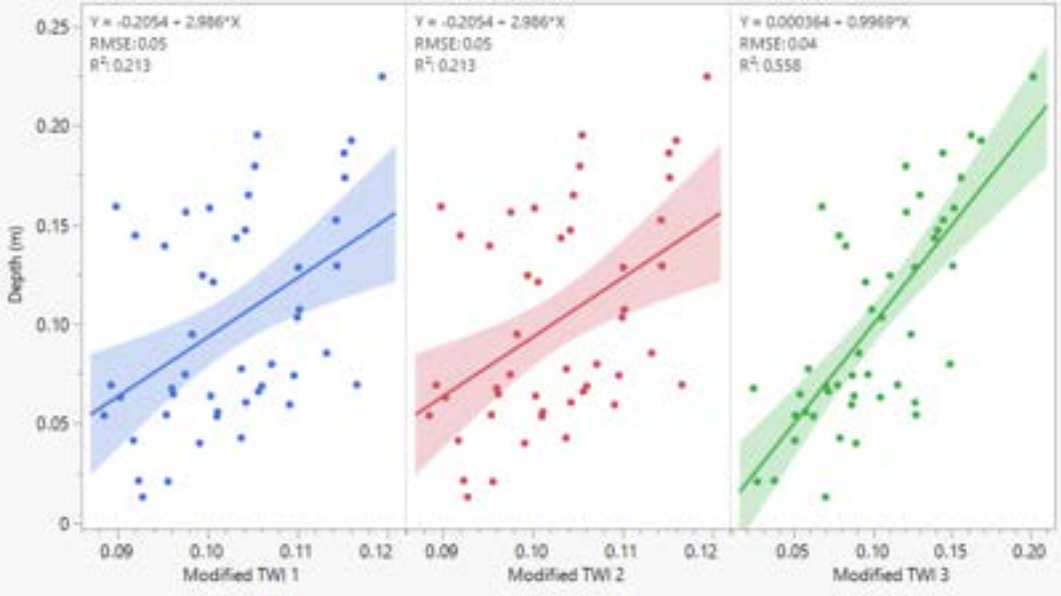

Figure 29 Correlation between water depth from the HEC-RAS simulations and predicted water depth from the three models.

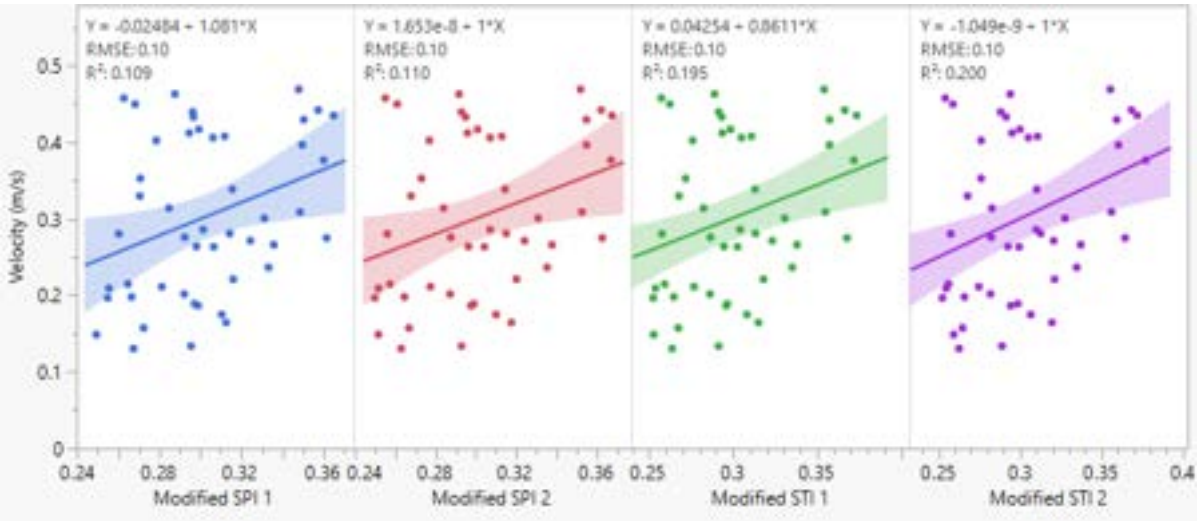

Figure 30 Correlation between water velocity from the HEC-RAS simulations and predicted water velocity from Equations 8 to 11.

Appendix

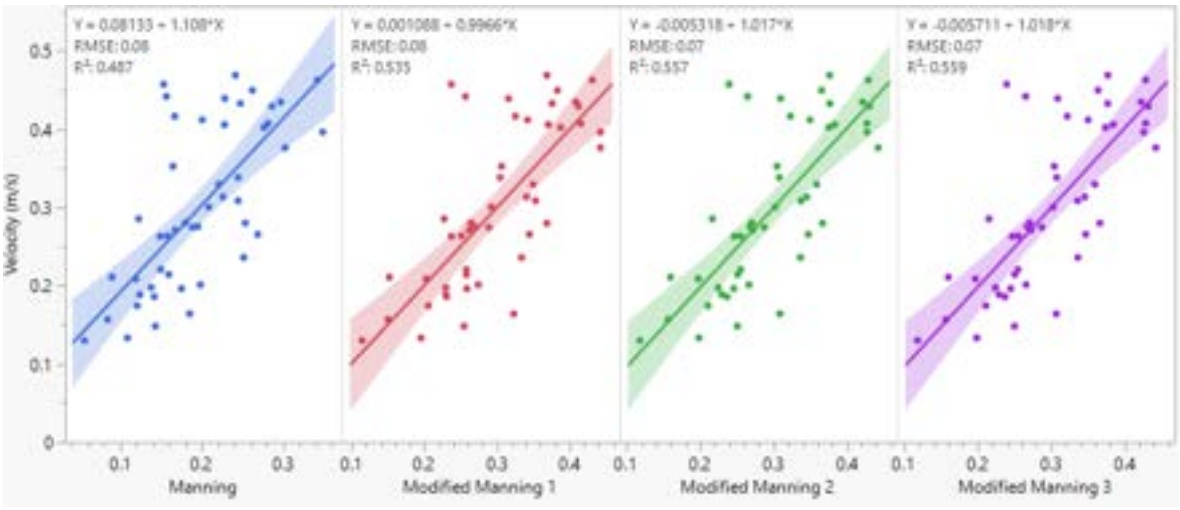

Figure 31 Correlation between water velocity from the HEC-RAS simulations and predicted water velocity from Equations 13 to 16.

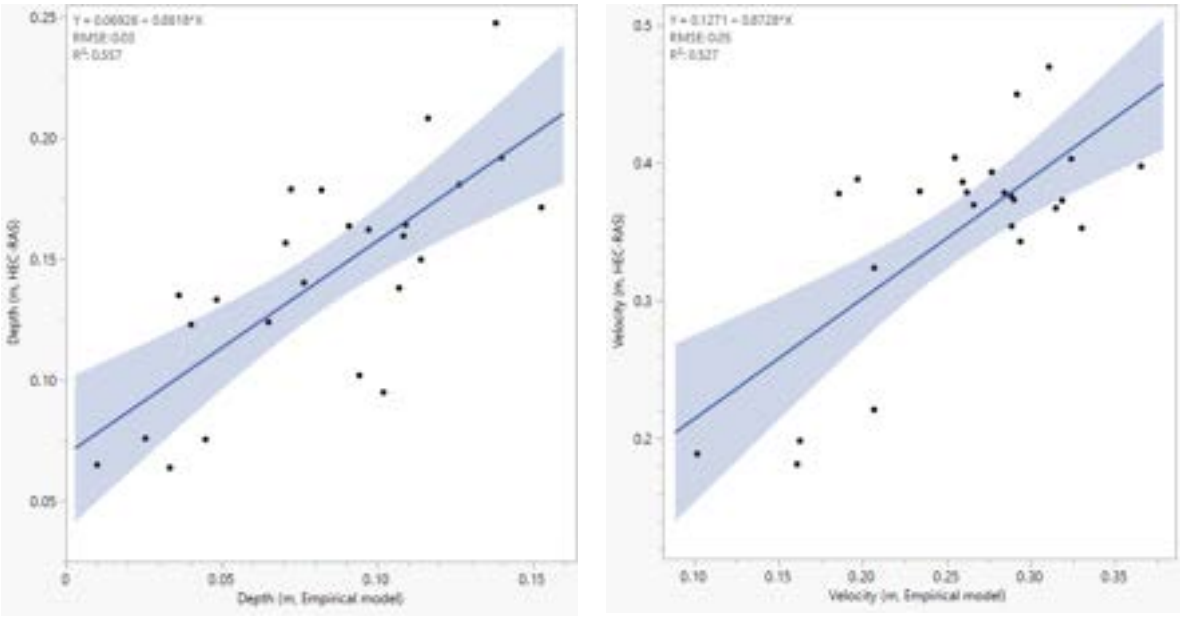

(a) (b)

Figure 32 Correlation between (a) water depth and (b) water velocity from the HEC-RAS simulations and calculated values from the respective empirical models based on the data from five new locations as shown in Table 2.

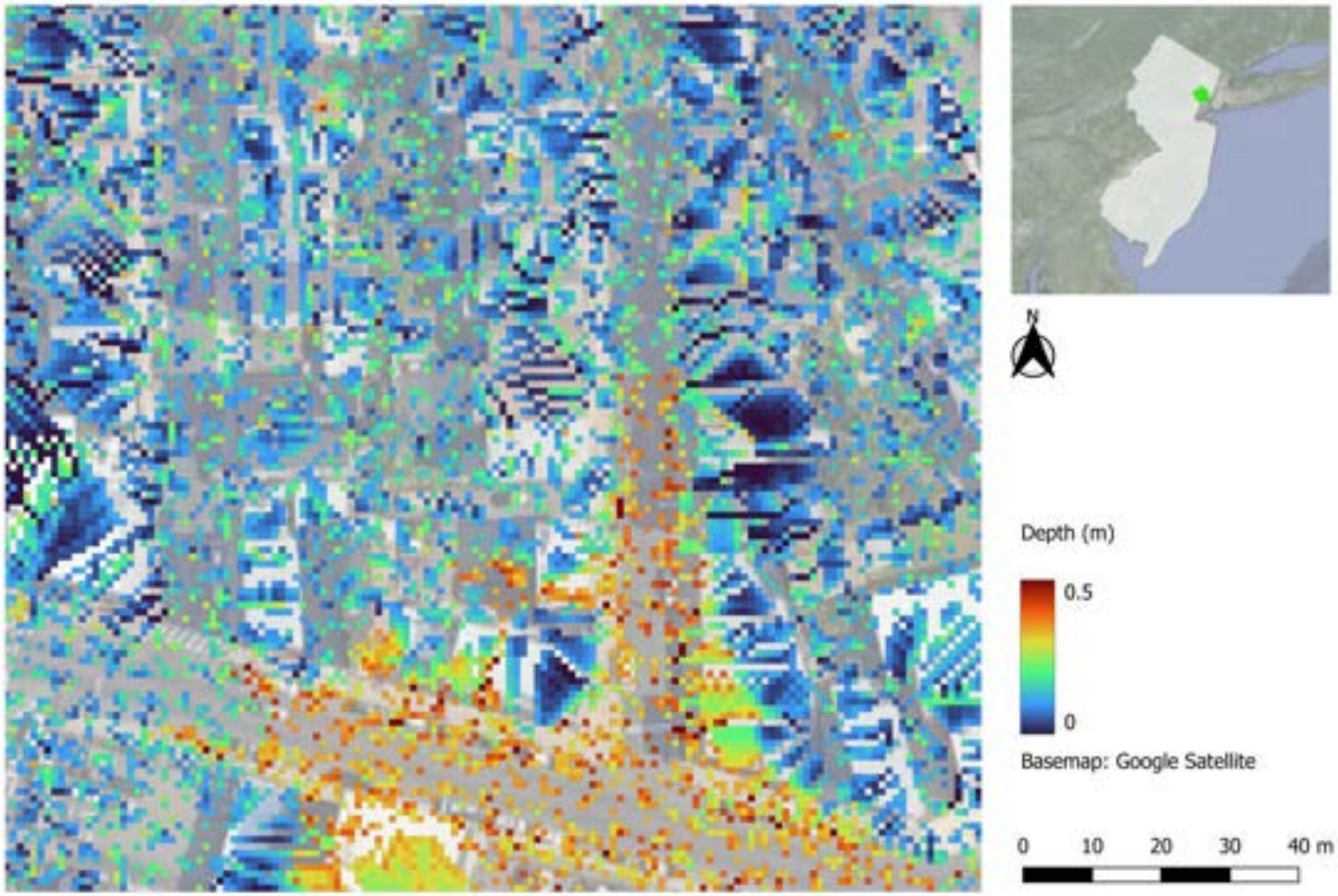

Figure 33 Calculated water depth based on the empirical model at the Newark Police Station 3rd Precinct site.

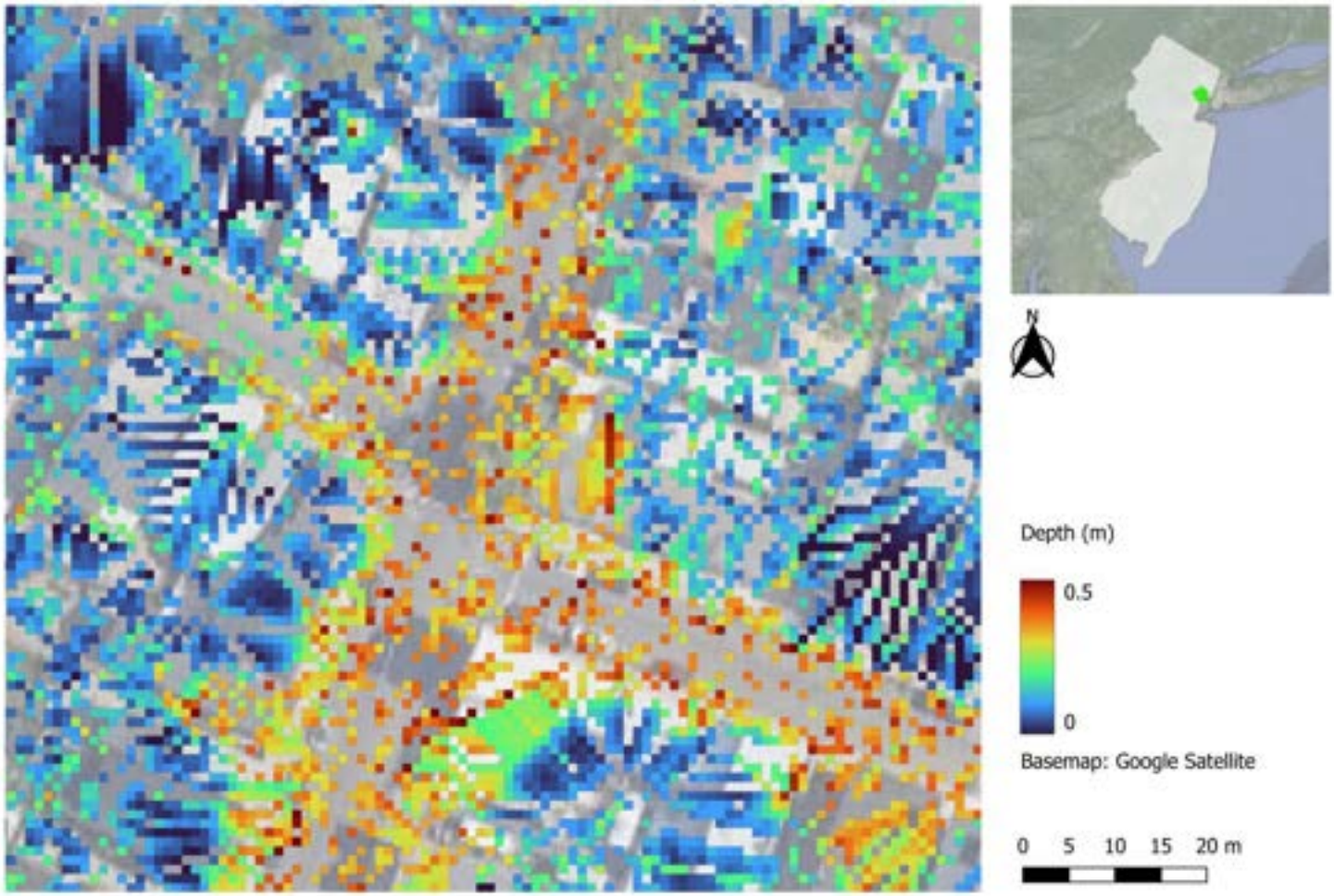

Figure 34 Calculated water depth based on the empirical model at the Nasto's Ice Cream site.

Appendix

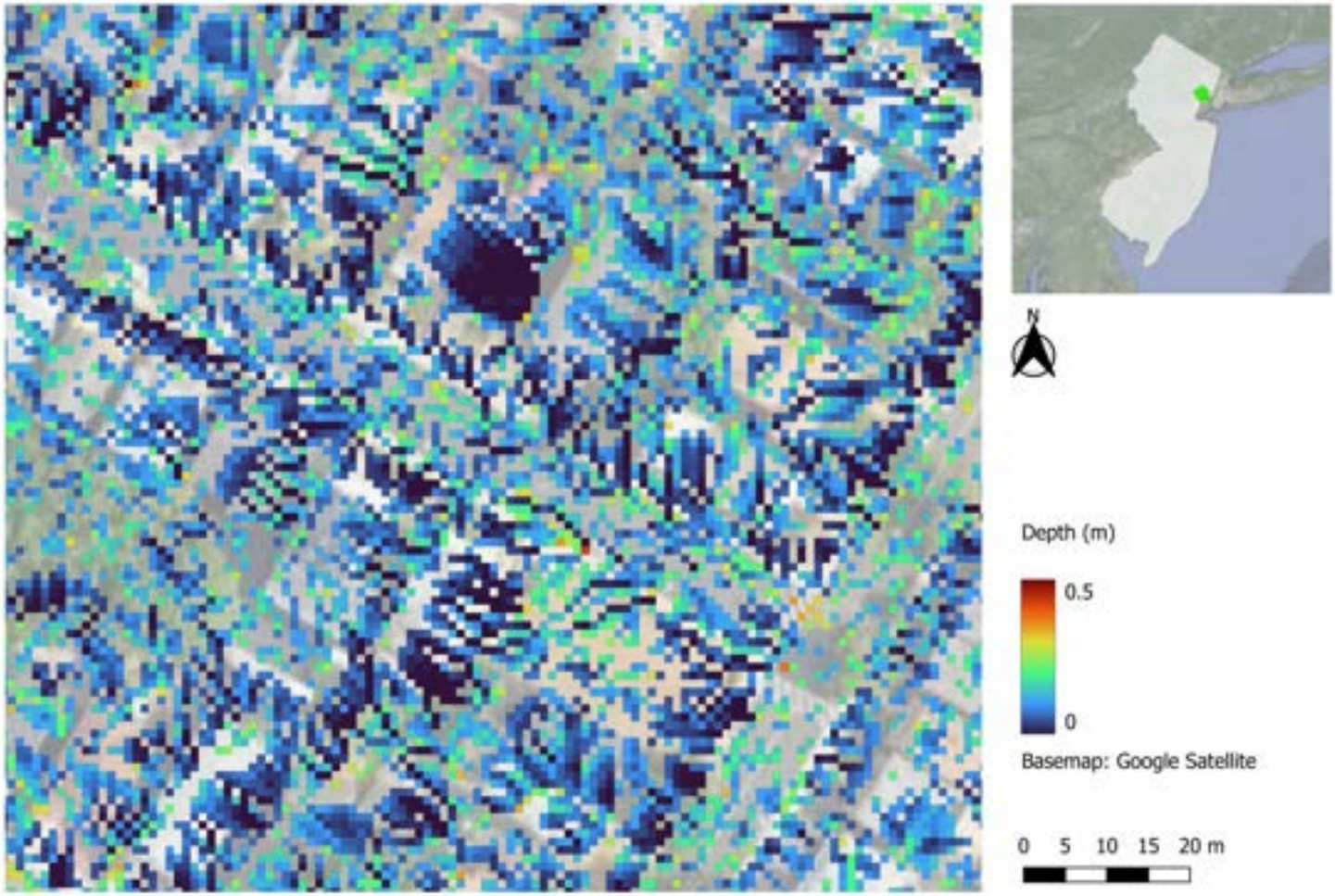

Figure 35 Calculated water depth based on the empirical model at the Art of Survival Garden site.

Appendix

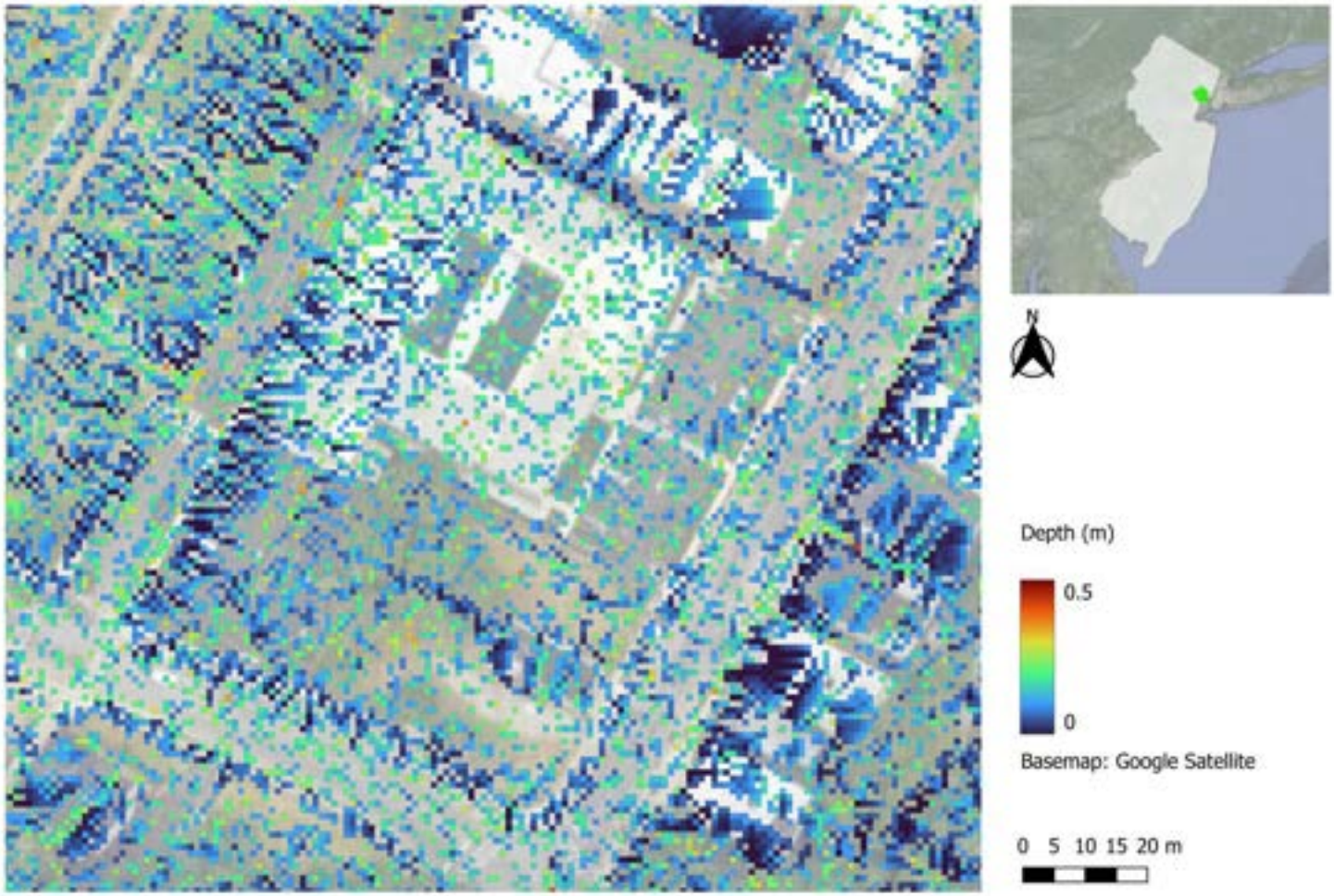

Figure 36 Calculated water depth based on the empirical model at the Hawthorne Hawks Healthy Harvest Farm site.

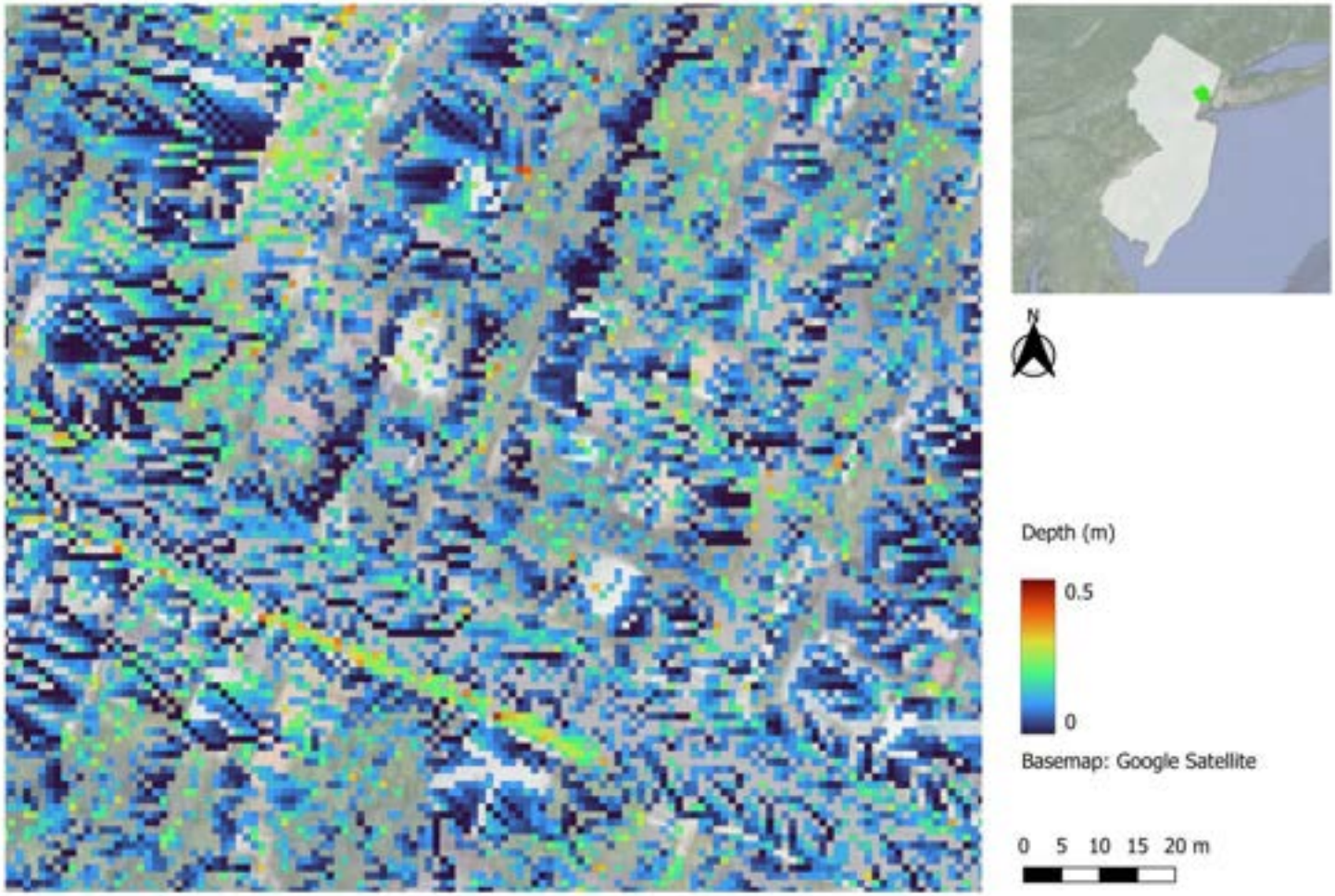

Figure 37 Calculated water depth based on the empirical model at the HOV Healthy Haven Garden site.

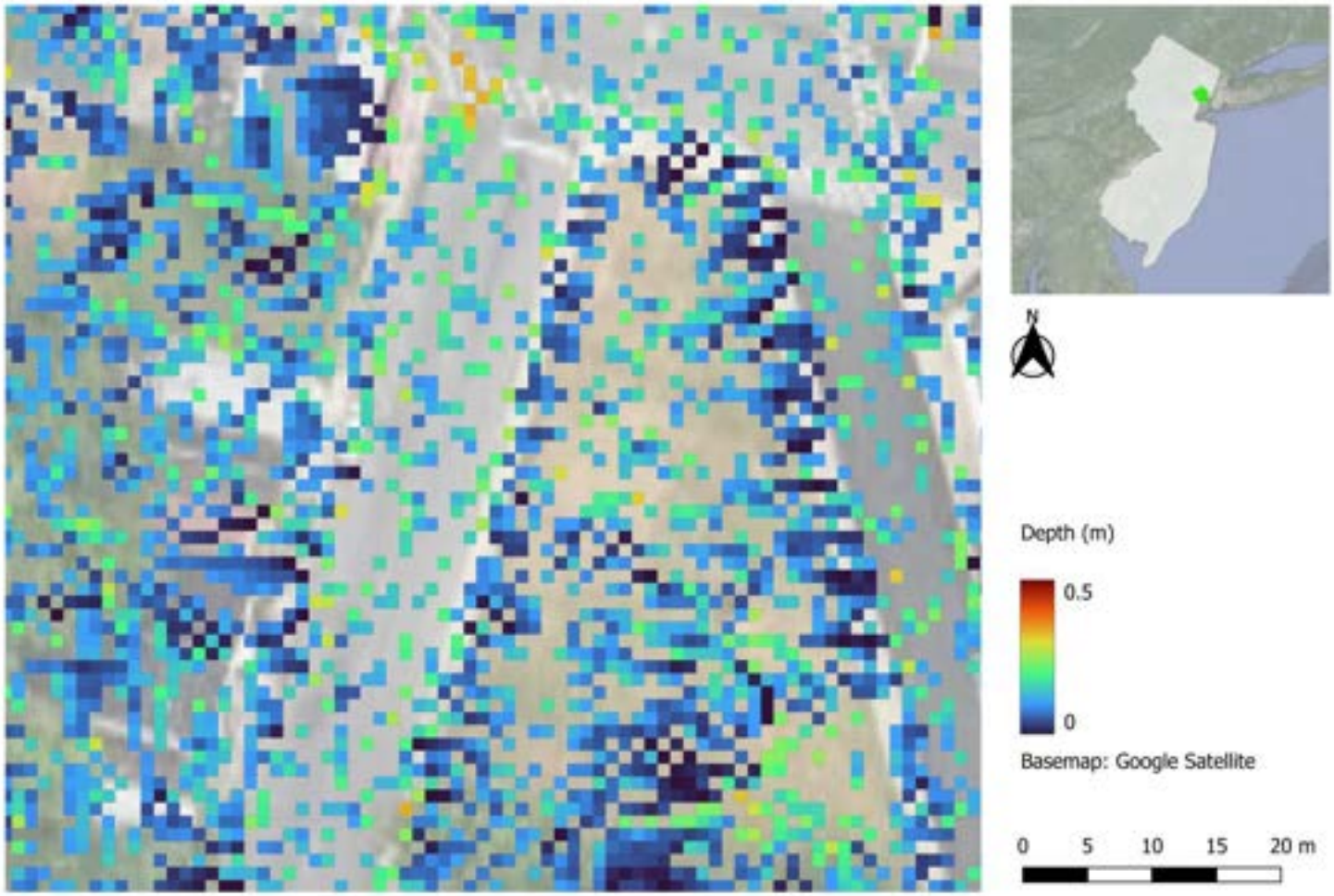

Figure 38 Calculated water depth based on the empirical model at the Harriet Tubman Elementary School site.

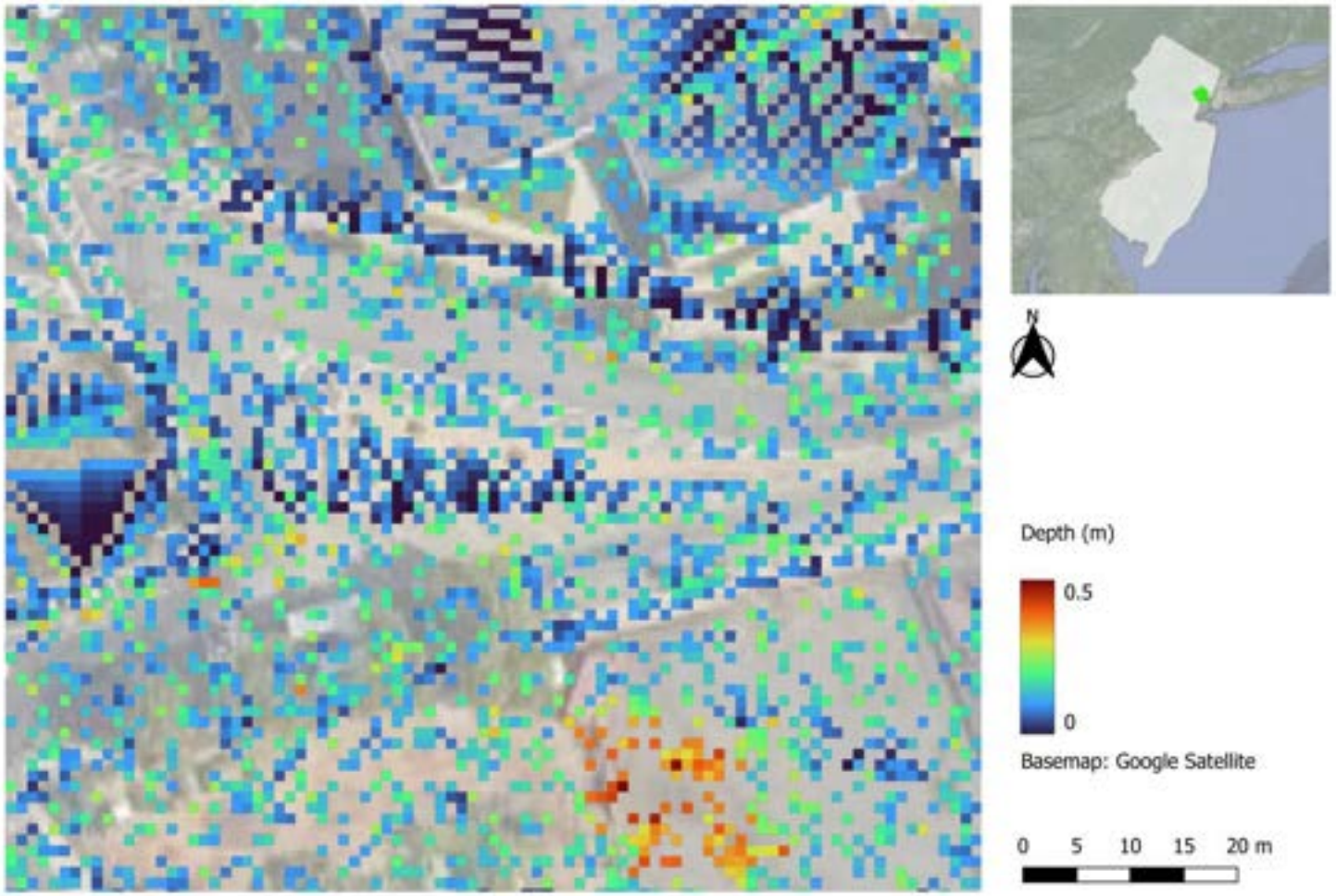

Figure 39 Calculated water depth based on the empirical model at the Down Bottom Farms Traffic Triangle site.

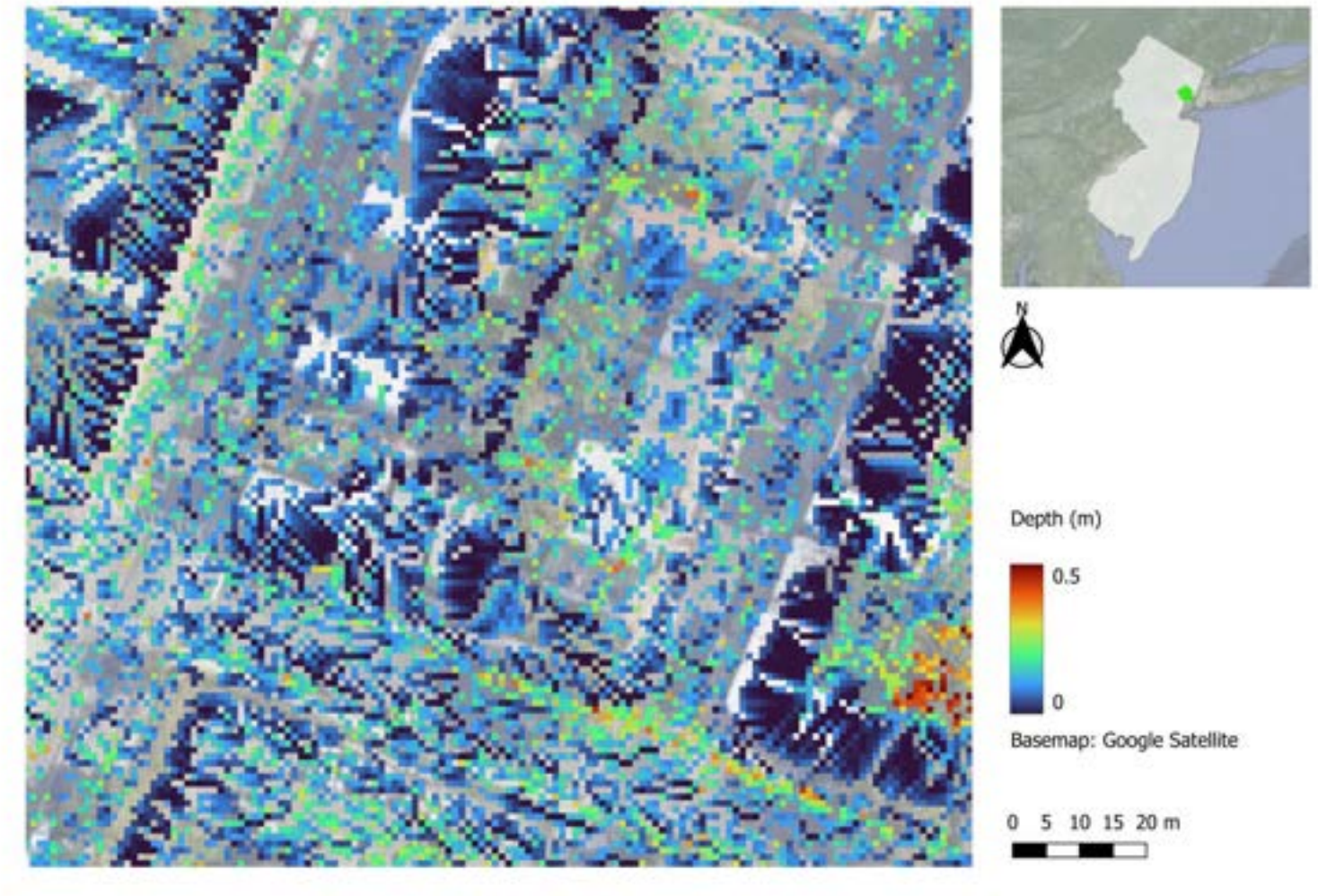

Figure 40 Calculated water depth based on the empirical model at the Branck Brook Alliance site.

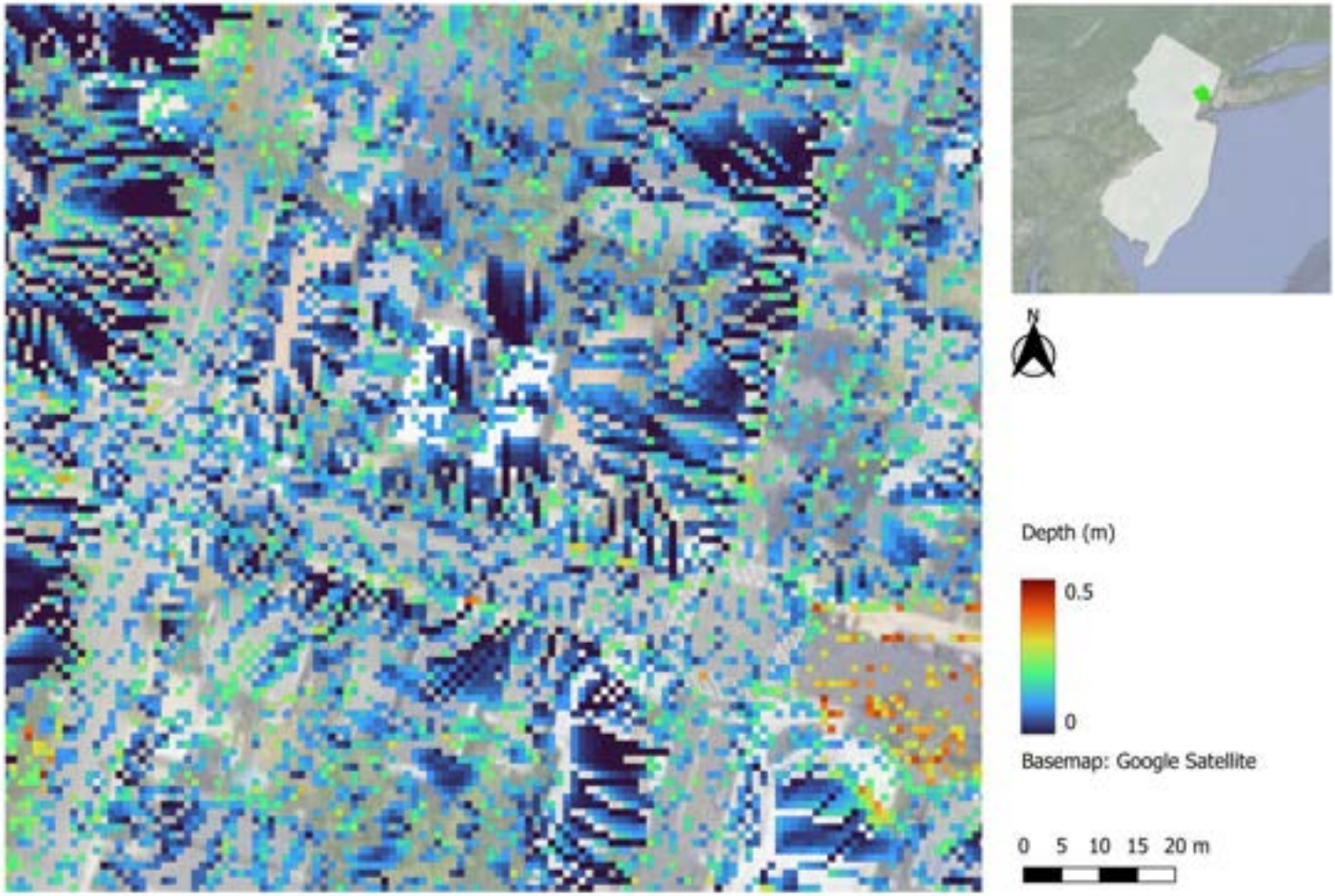

Figure 41 Calculated water depth based on the empirical model at the Wanda Upshaw Meditation Garden site.

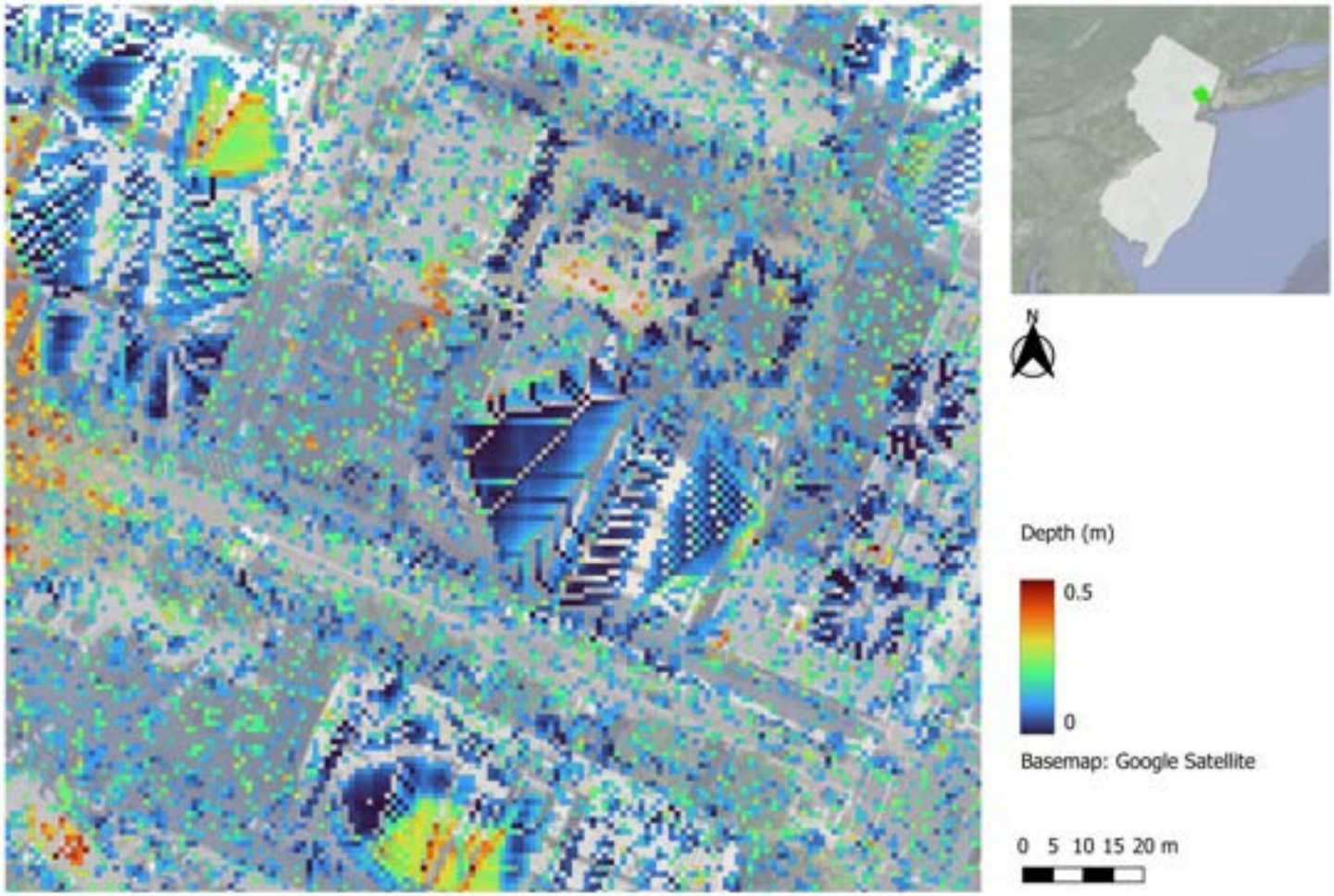

Figure 42 Calculated water depth based on the empirical model at the Newark Educators Community Charter School site.

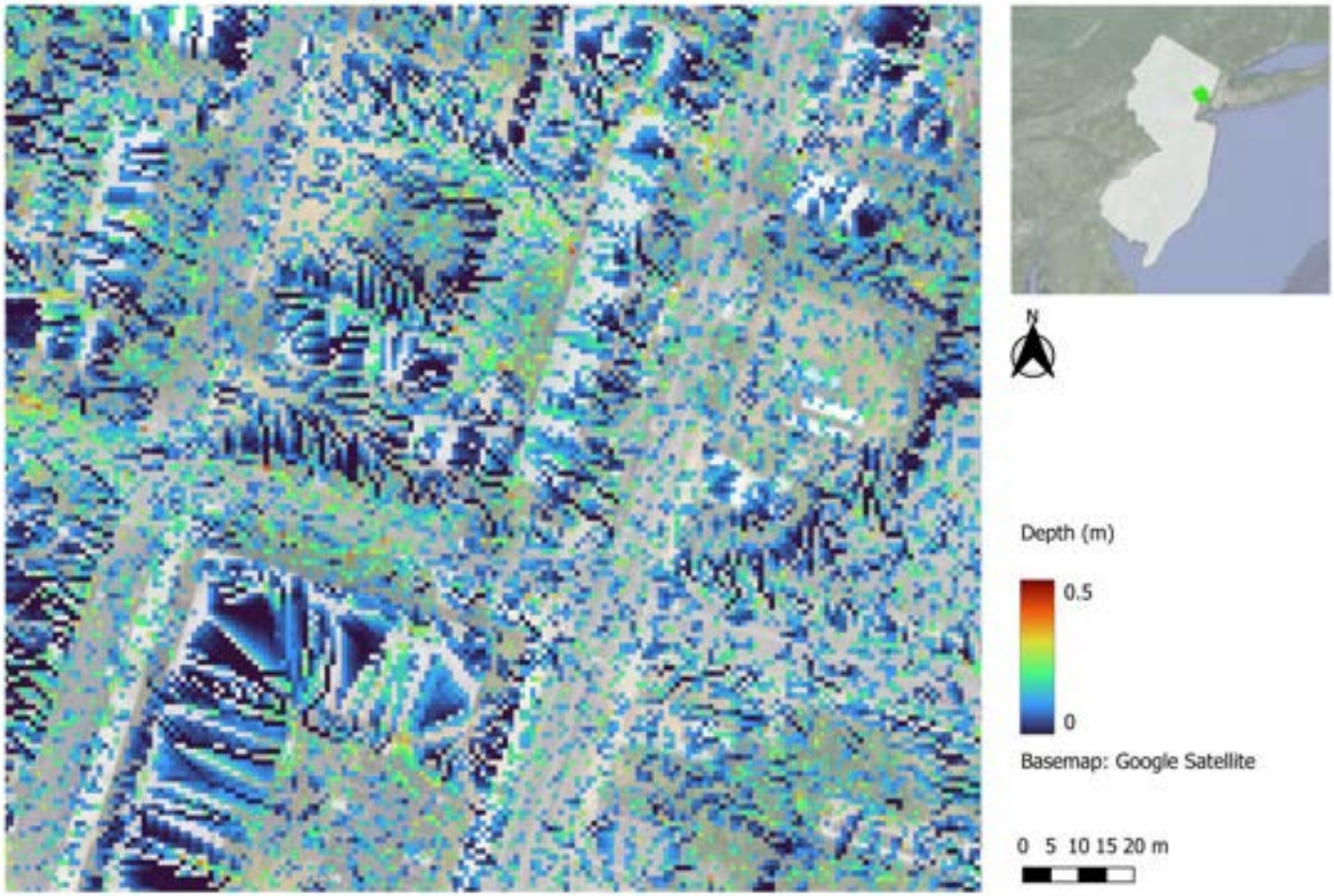

Figure 43 Calculated water depth based on the empirical model at the Bergen Street Community Garden site.

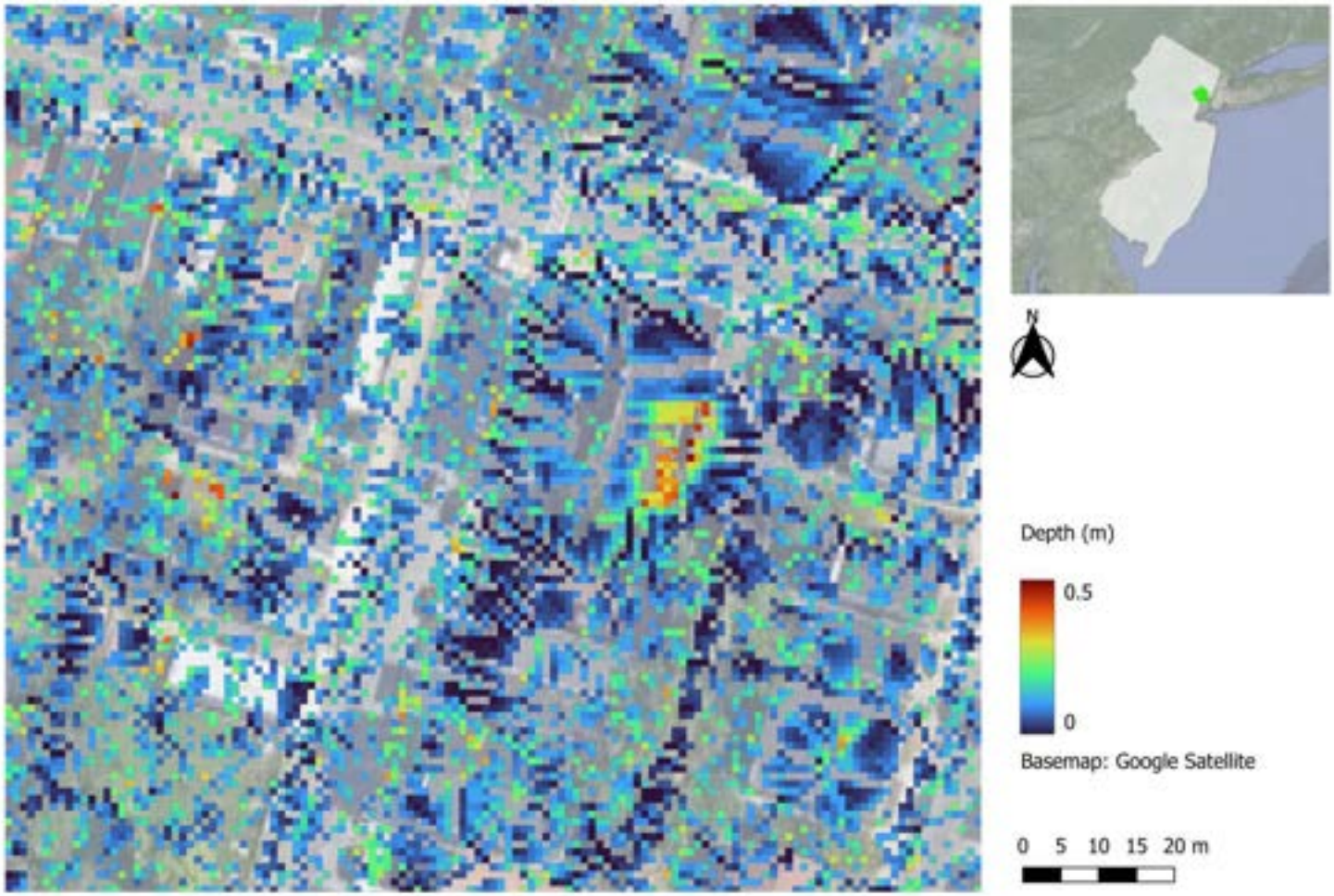

Figure 44 Calculated water depth based on the empirical model at the 14th Avenue Community Garden site.

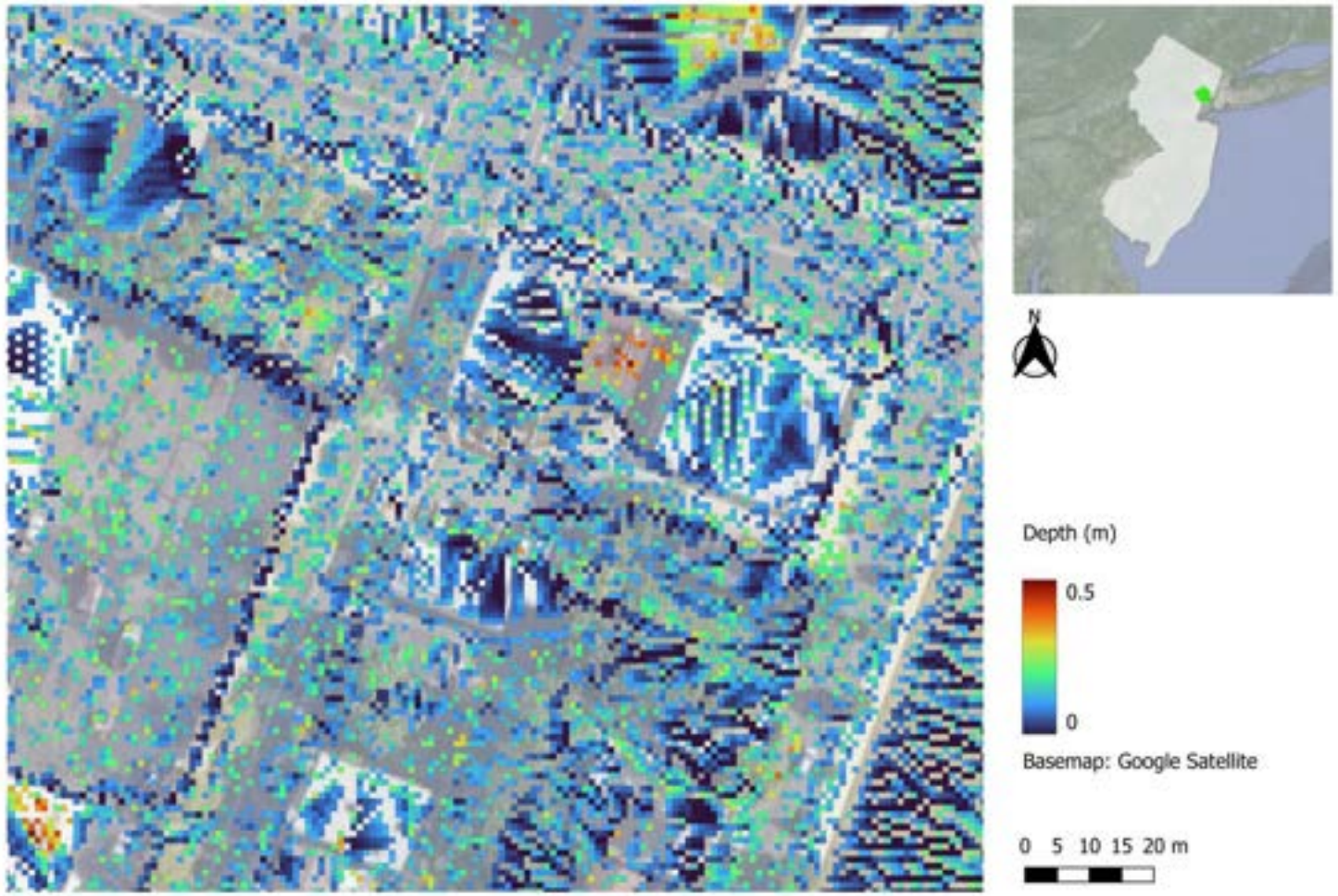

Figure 45 Calculated water depth based on the empirical model at the Urban League of Essex County site.

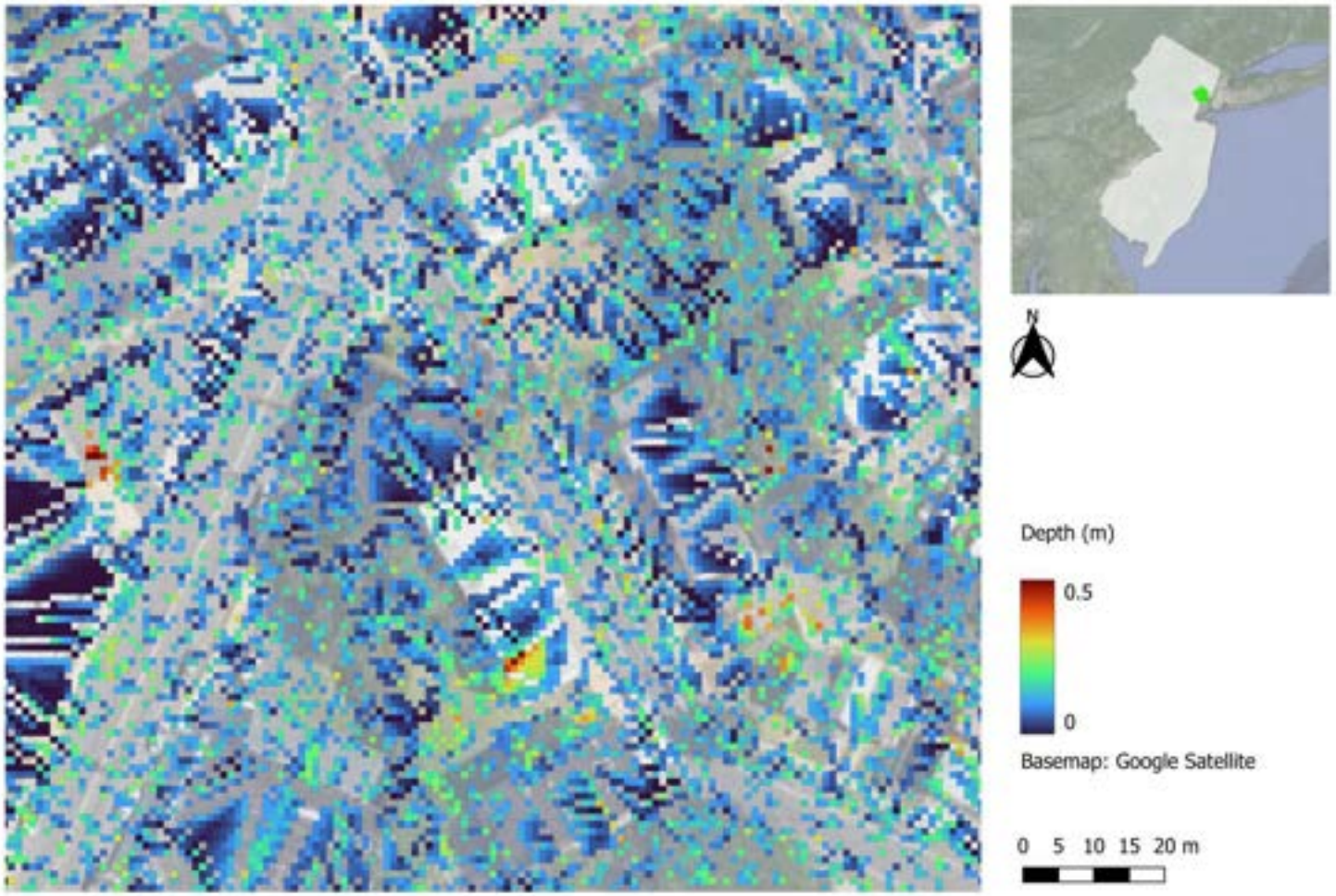

Figure 46 Calculated water depth based on the empirical model at the Astor Street Community Garden site.

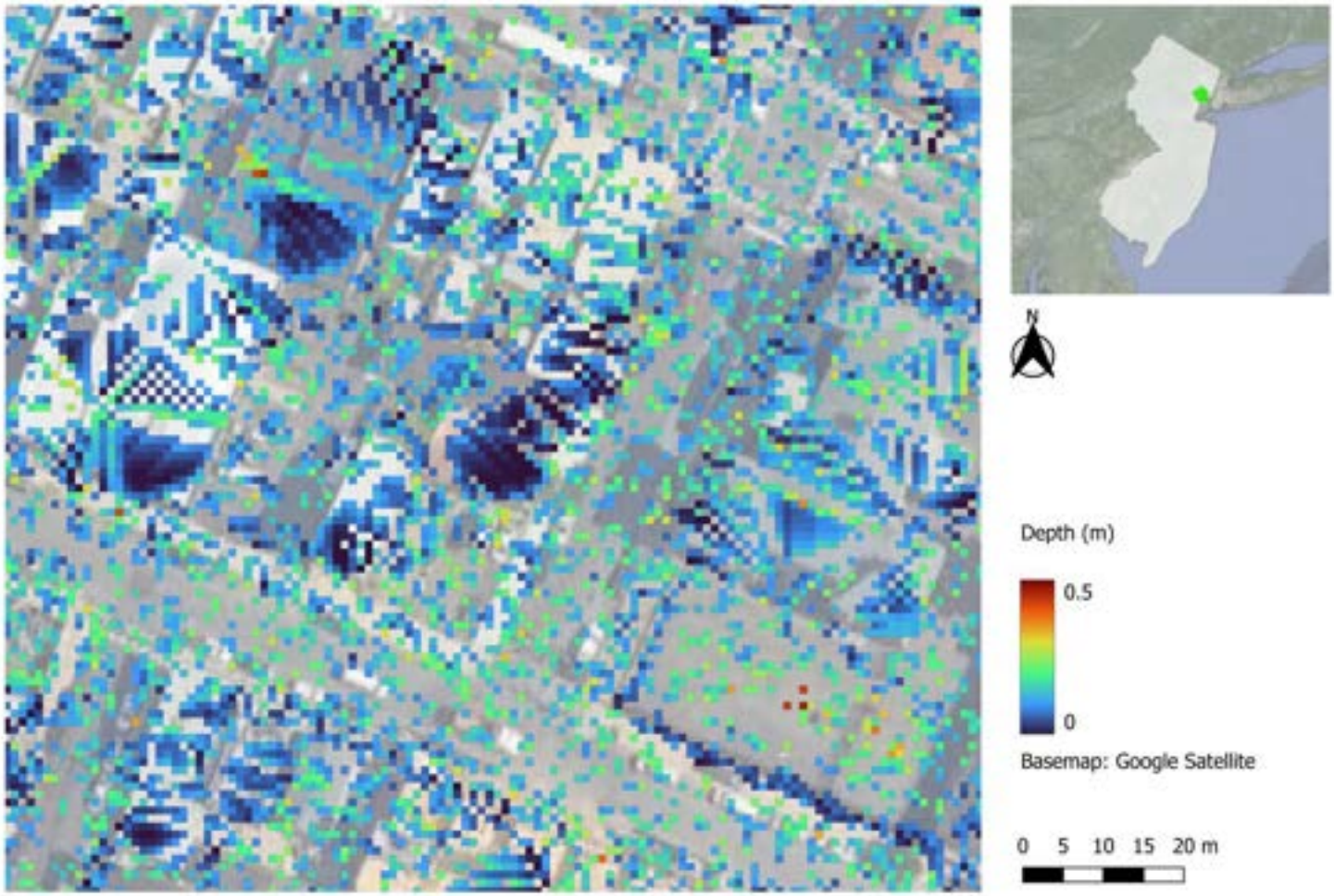

Figure 47 Calculated water depth based on the empirical model at the South Street Academy site.

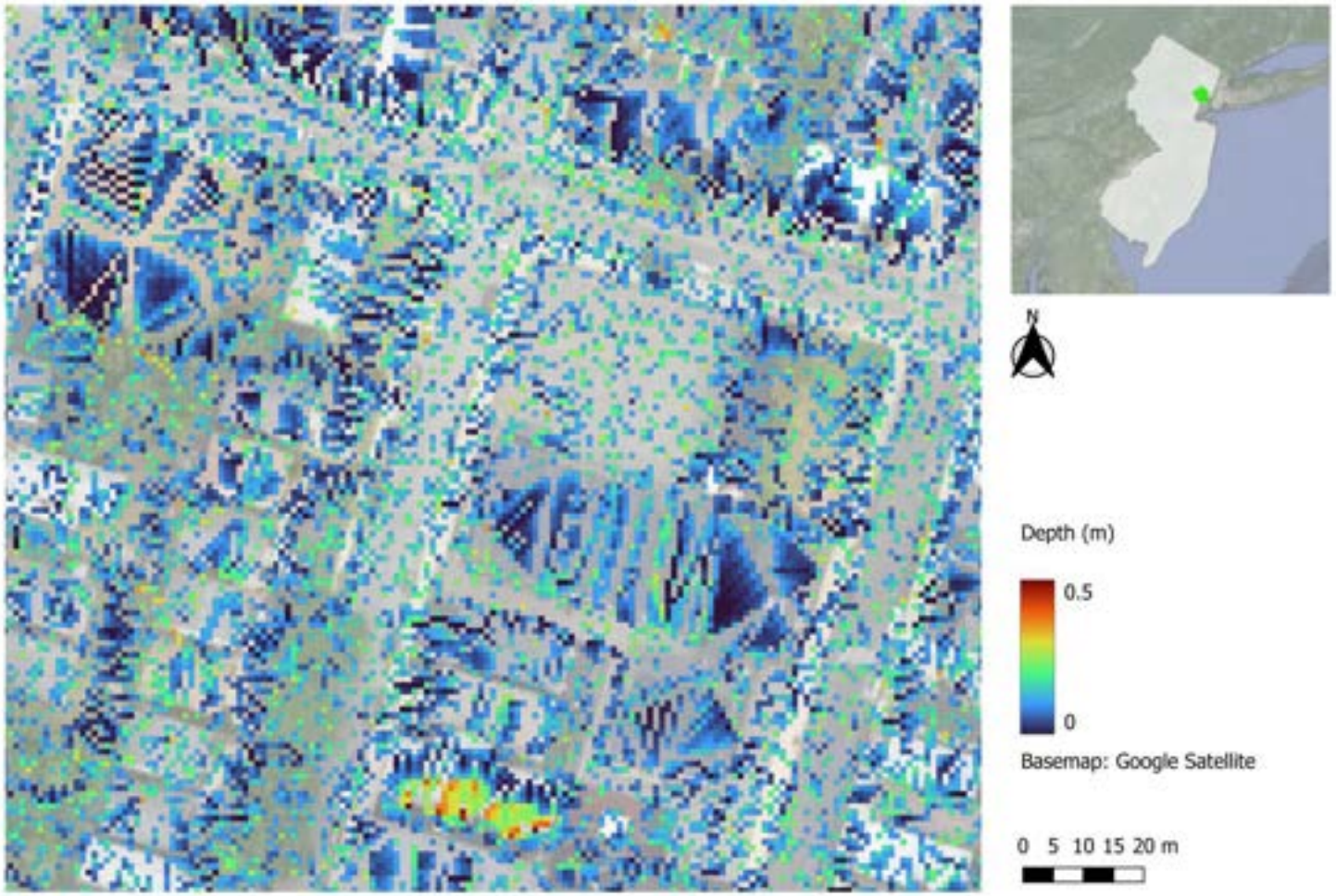

Figure 48 Calculated water depth based on the empirical model at the St. Ann's Church site.

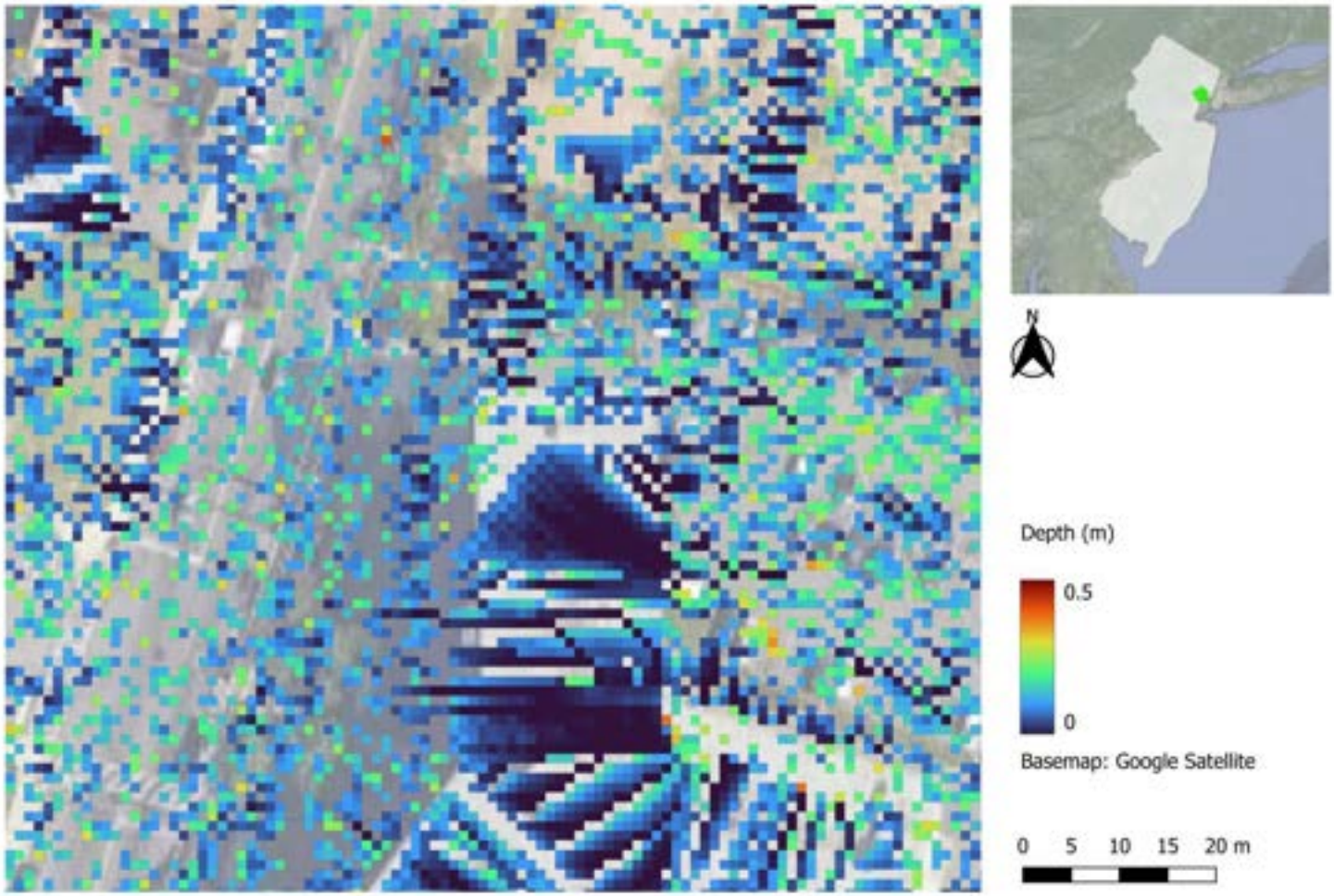

Figure 49 Calculated water depth based on the empirical model at the James C. White Manor Senior Housing site.

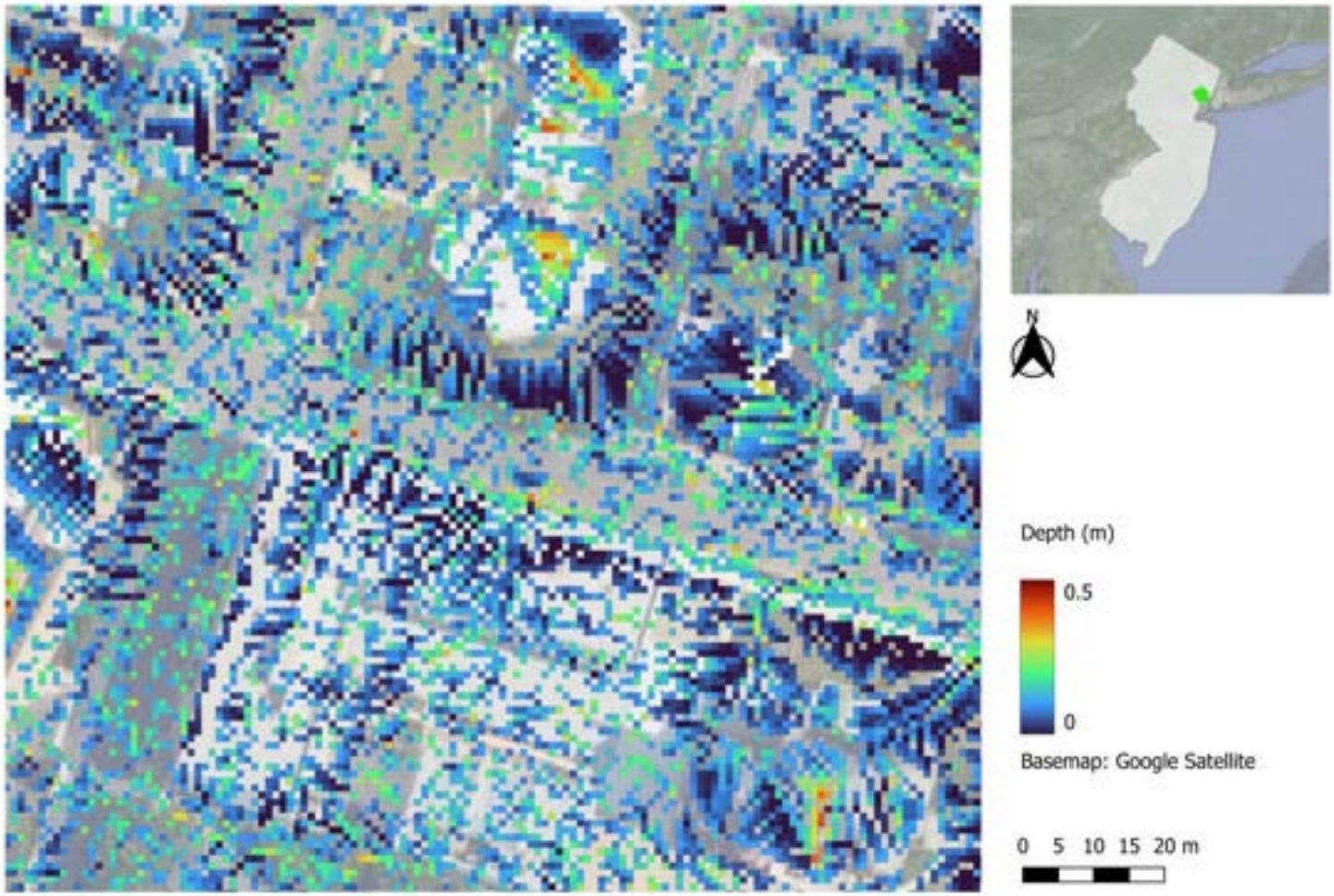

Figure 50 Calculated water depth based on the empirical model at the Court Street Urban Farm site.

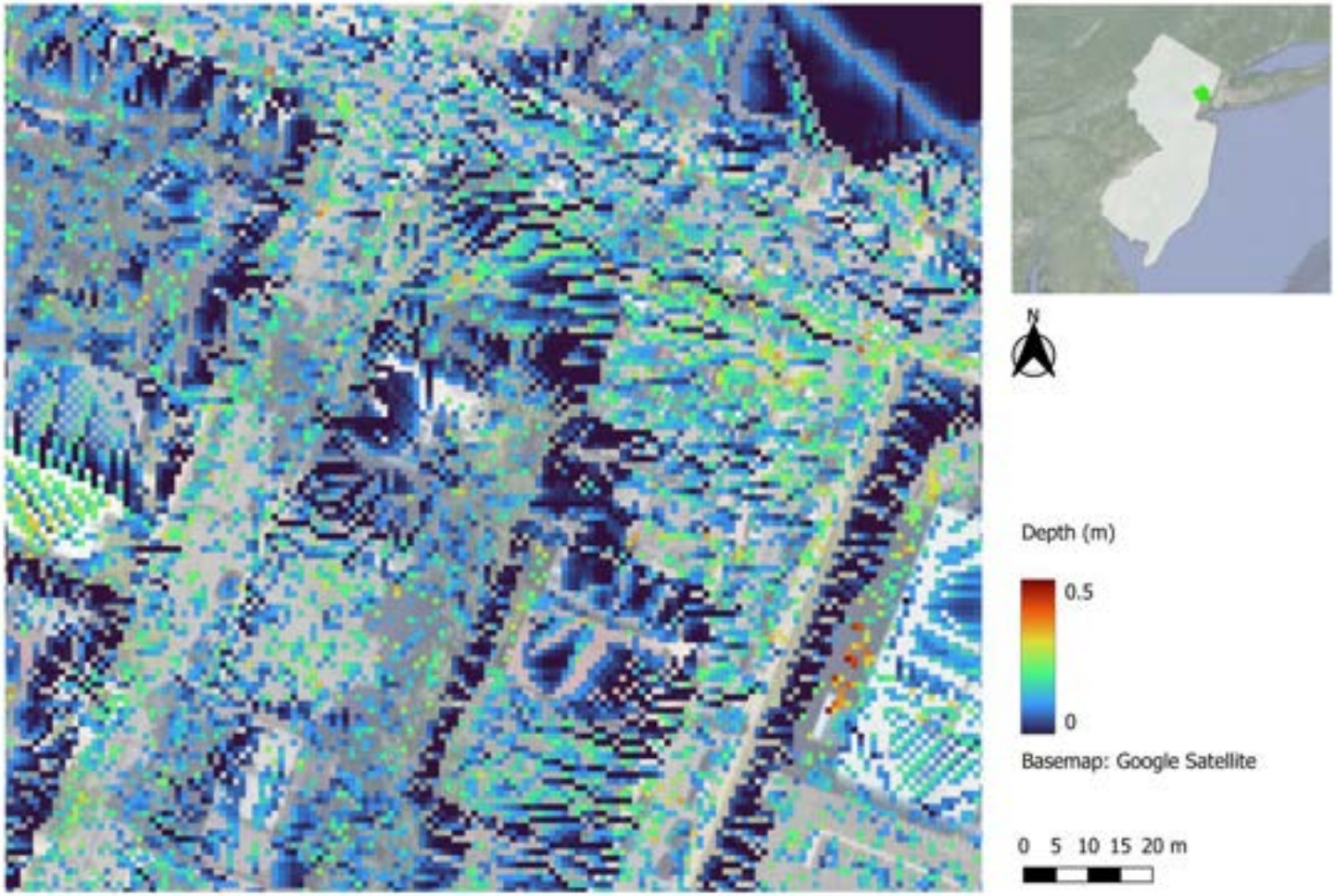

Figure 51 Calculated water depth based on the empirical model at the Rutgers School of Health Professions site.

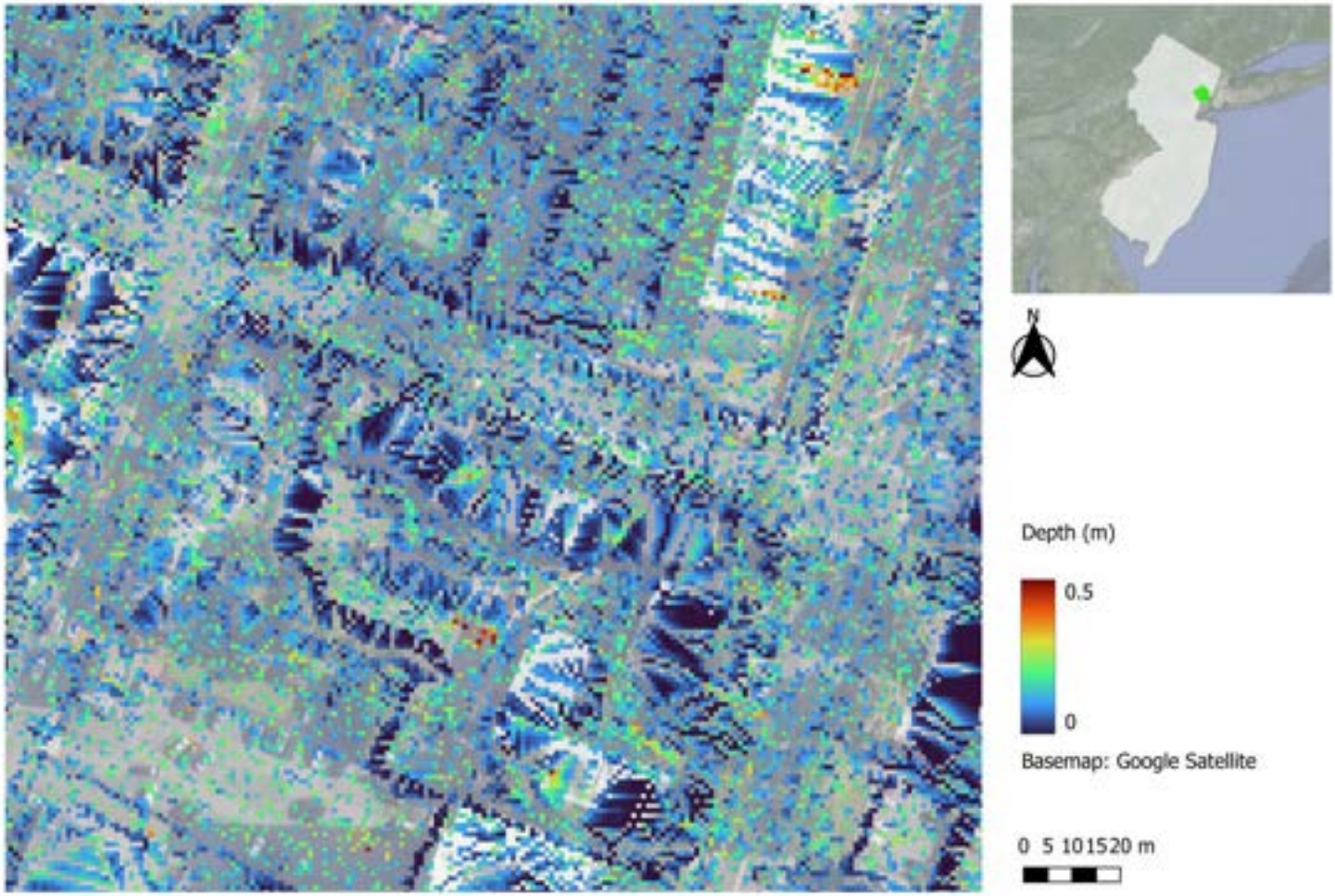

Figure 52 Calculated water depth based on the empirical model at the Robert Treat Academy Charter School site.

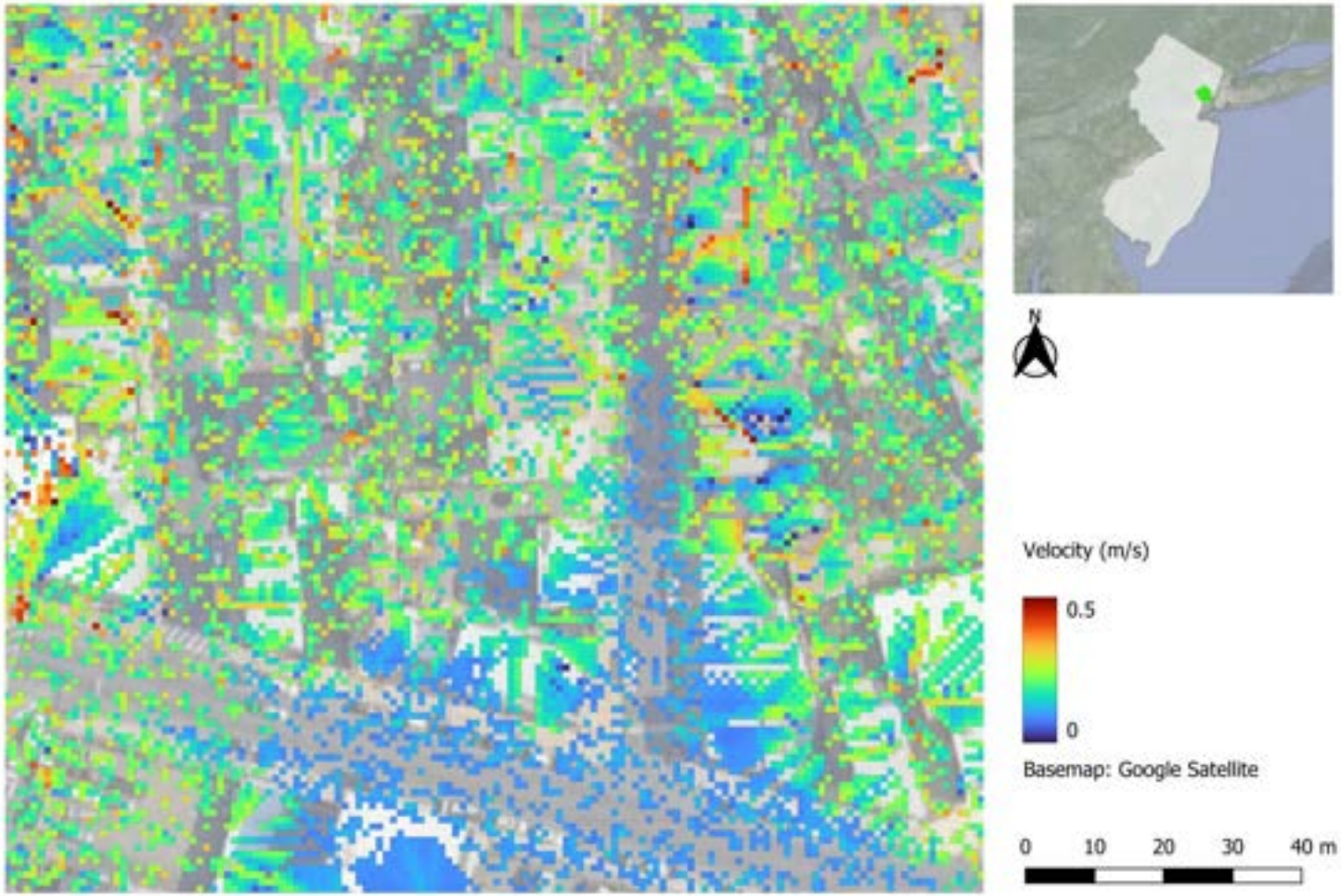

Figure 53 Calculated water velocity based on the empirical model at the Newark Police Station 3rd Precinct site.

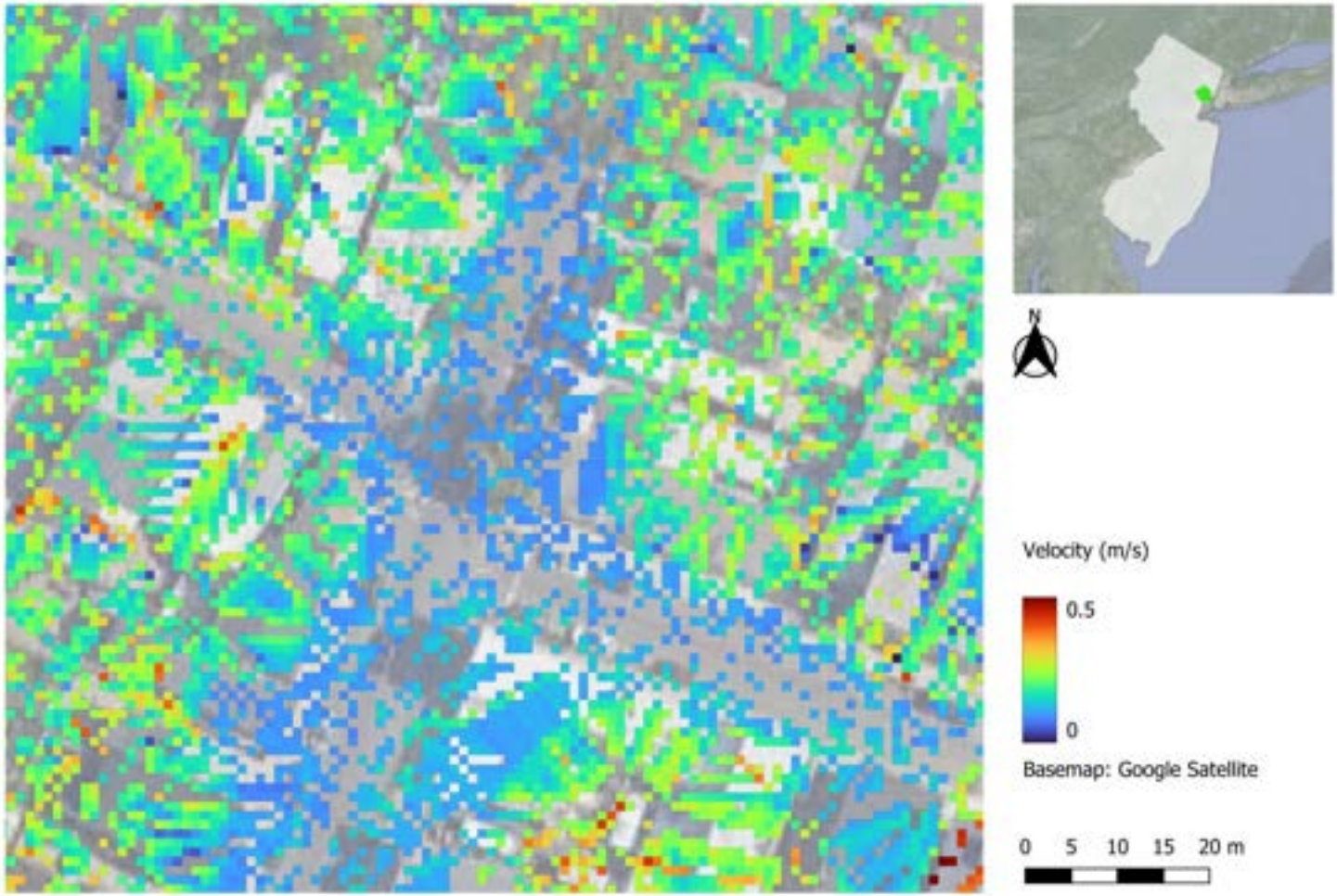

Figure 54 Calculated water velocity based on the empirical model at the Nasto's Ice Cream site.

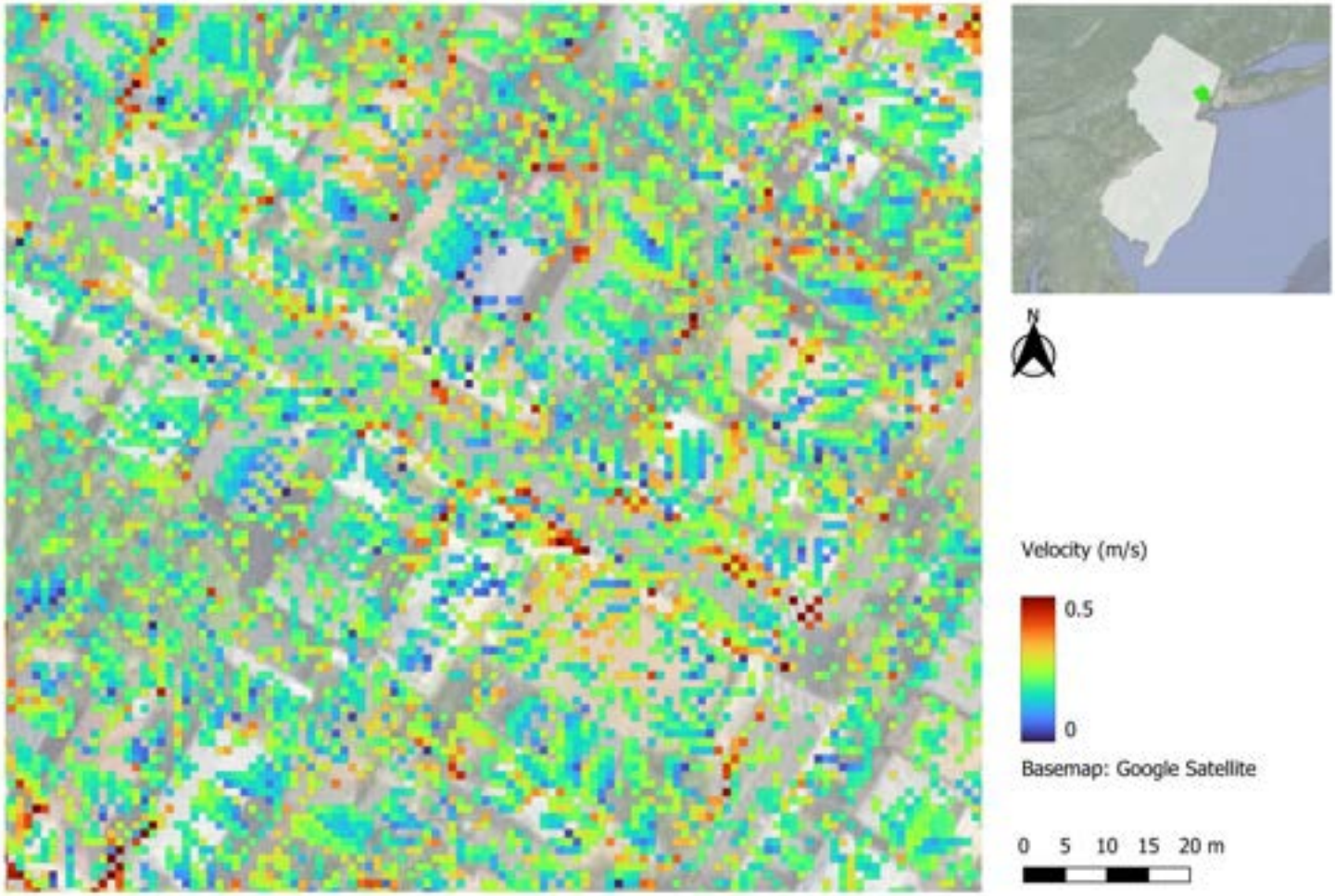

Figure 55 Calculated water velocity based on the empirical model at the Art of Survival Garden site.

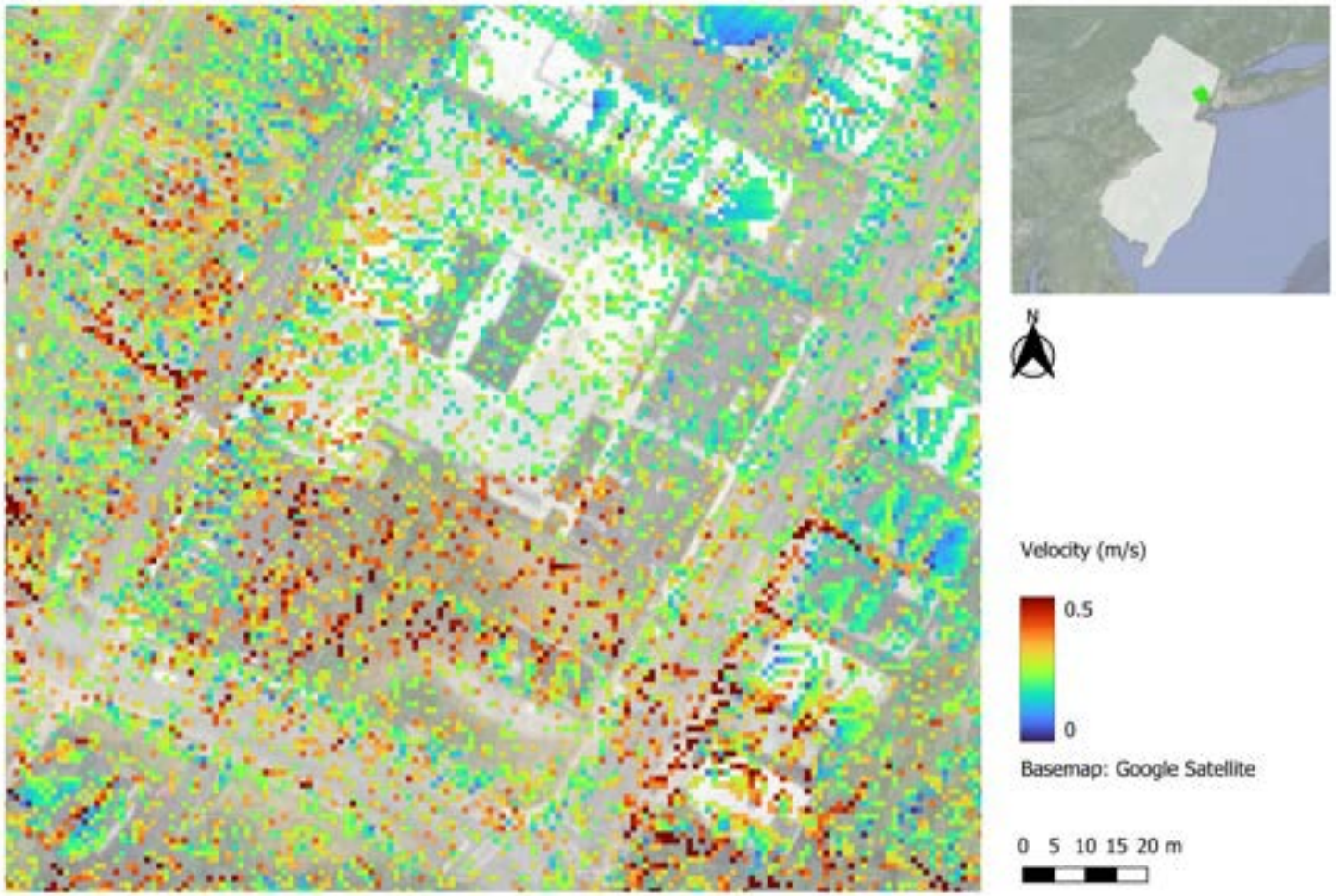

Figure 56 Calculated water velocity based on the empirical model at the Hawthorne Hawks Healthy Harvest Farm site.

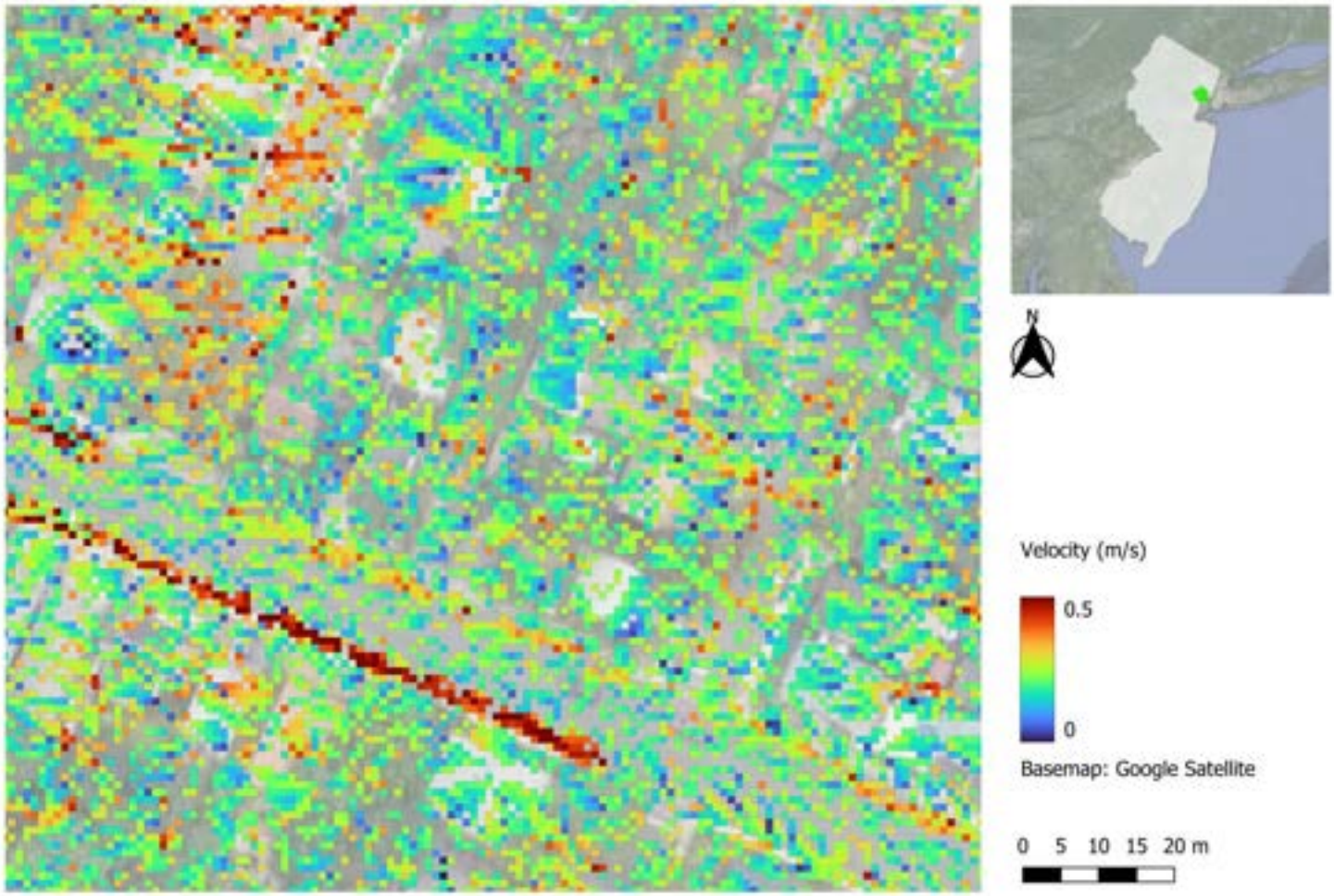

Figure 57 Calculated water velocity based on the empirical model at the HOV Healthy Haven Garden site.

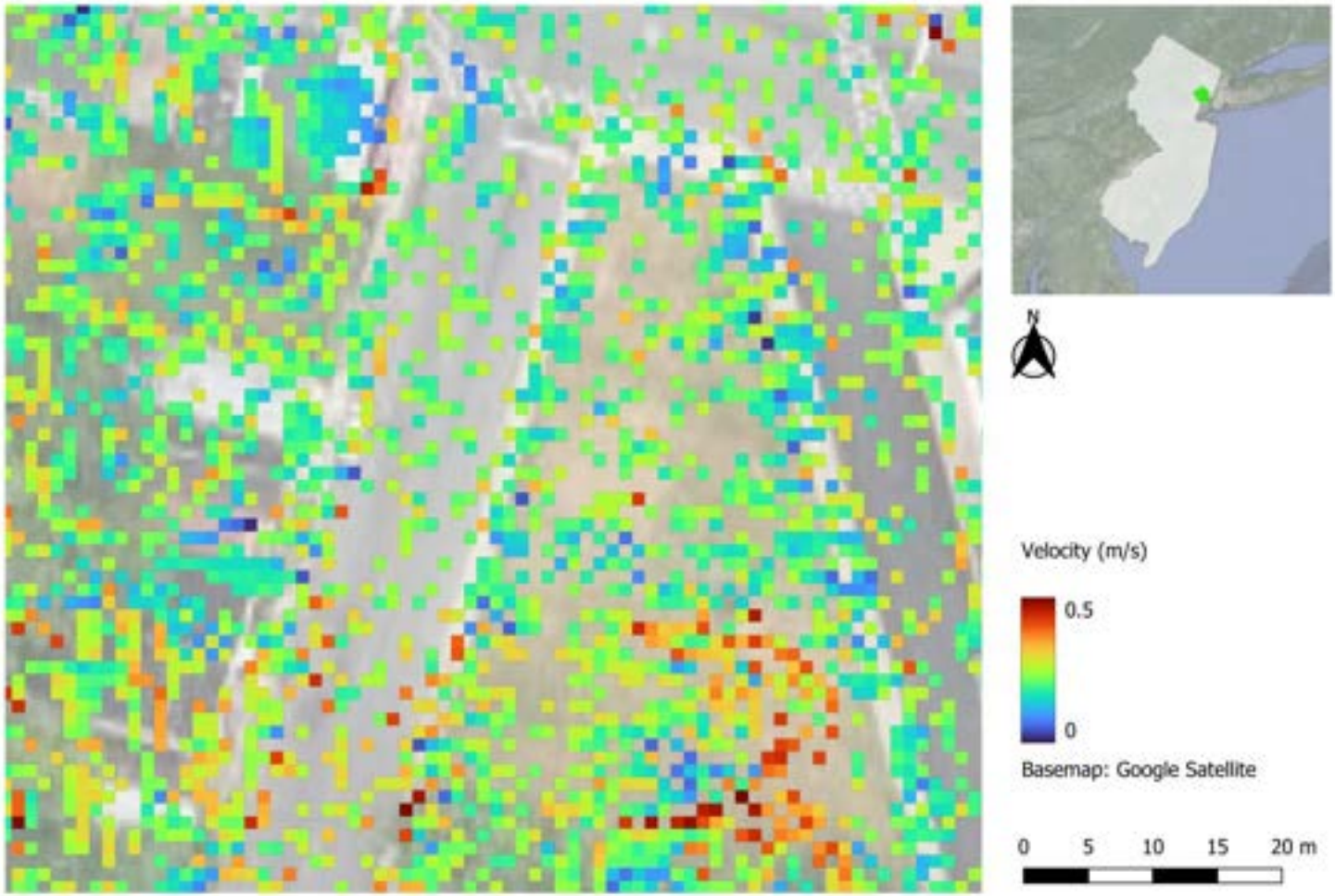

Figure 58 Calculated water velocity based on the empirical model at the Harriet Tubman Elementary School site.

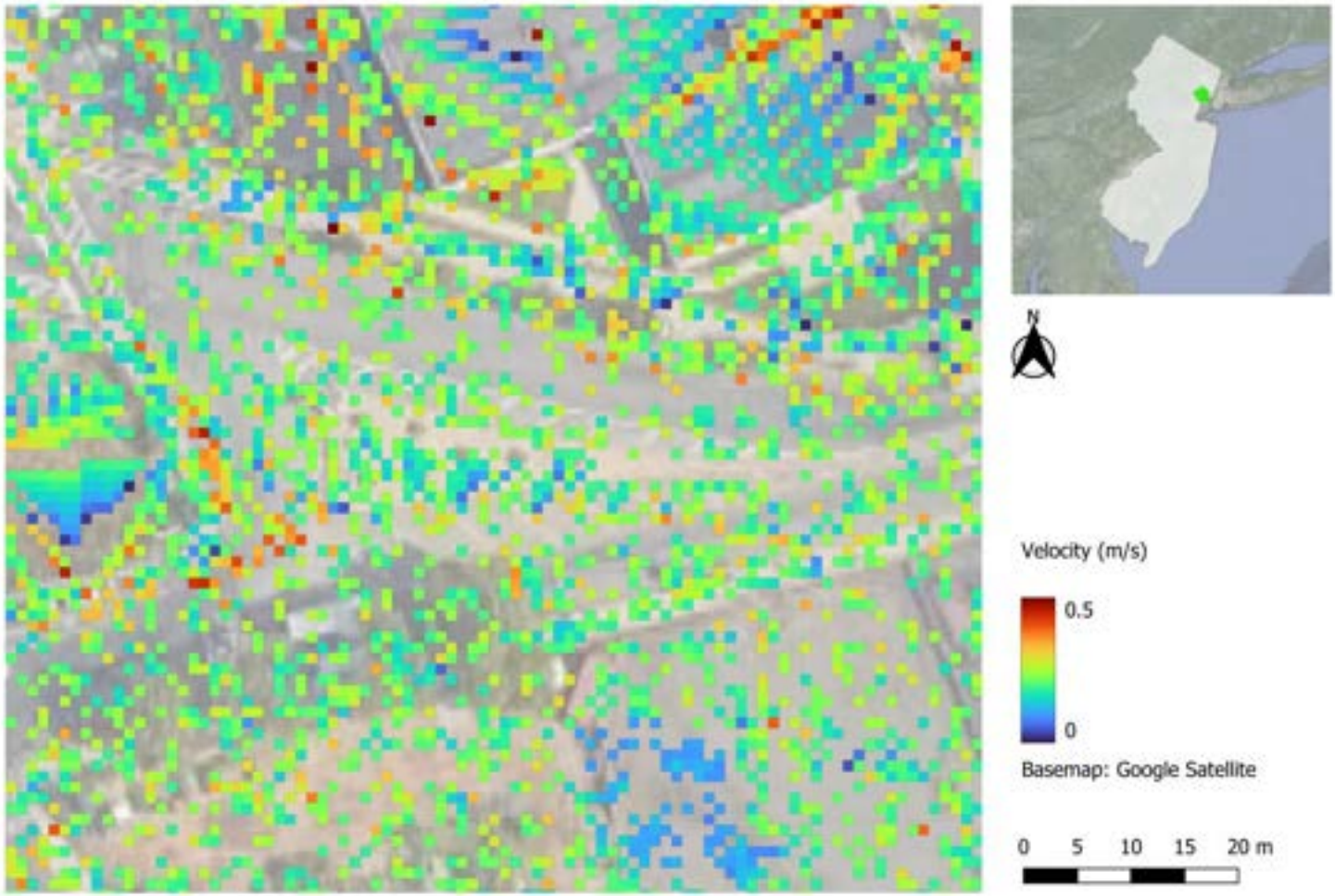

Figure 59 Calculated water velocity based on the empirical model at the Down Bottom Farms Traffic Triangle site.

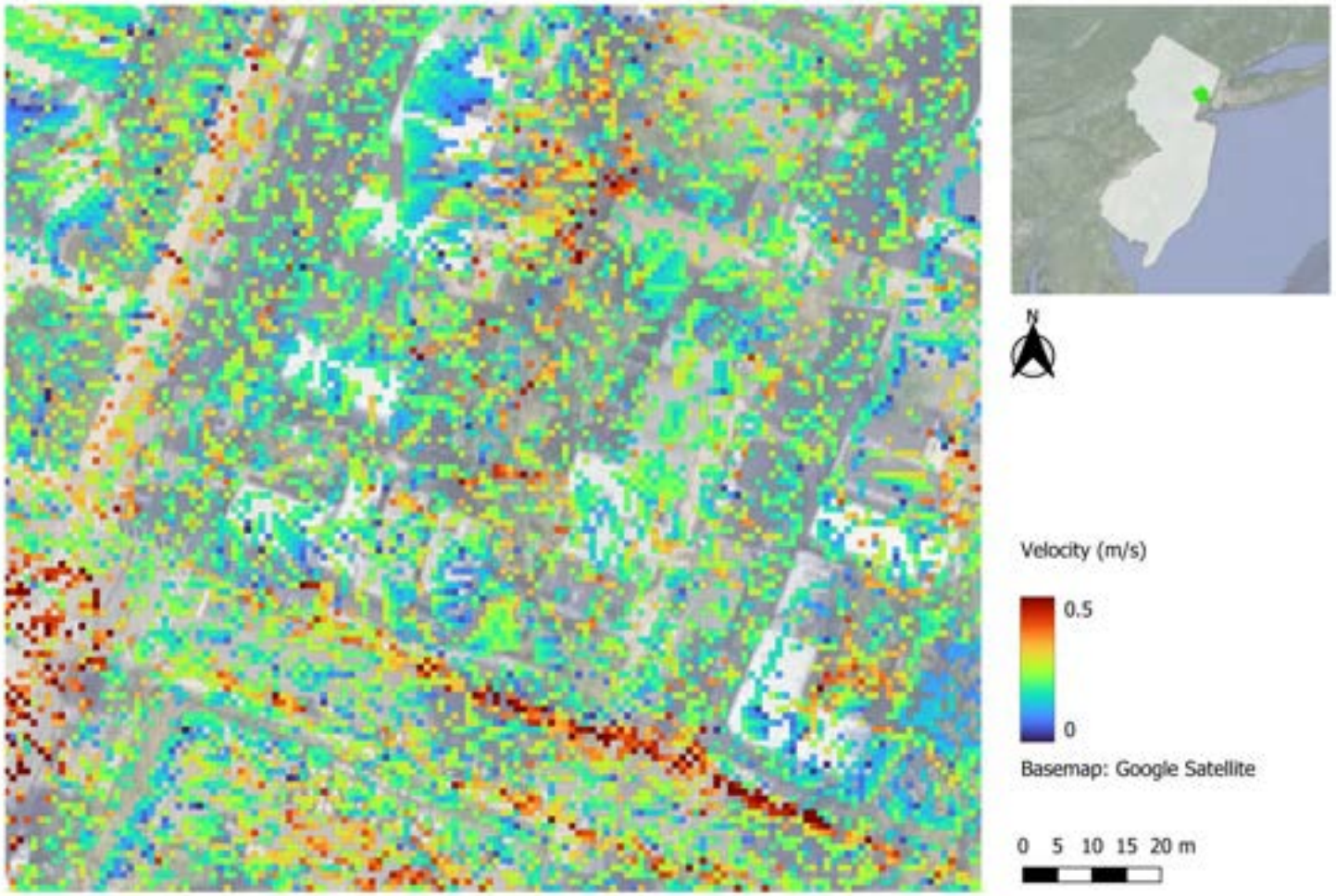

Figure 60 Calculated water velocity based on the empirical model at the Branck Brook Alliance site.

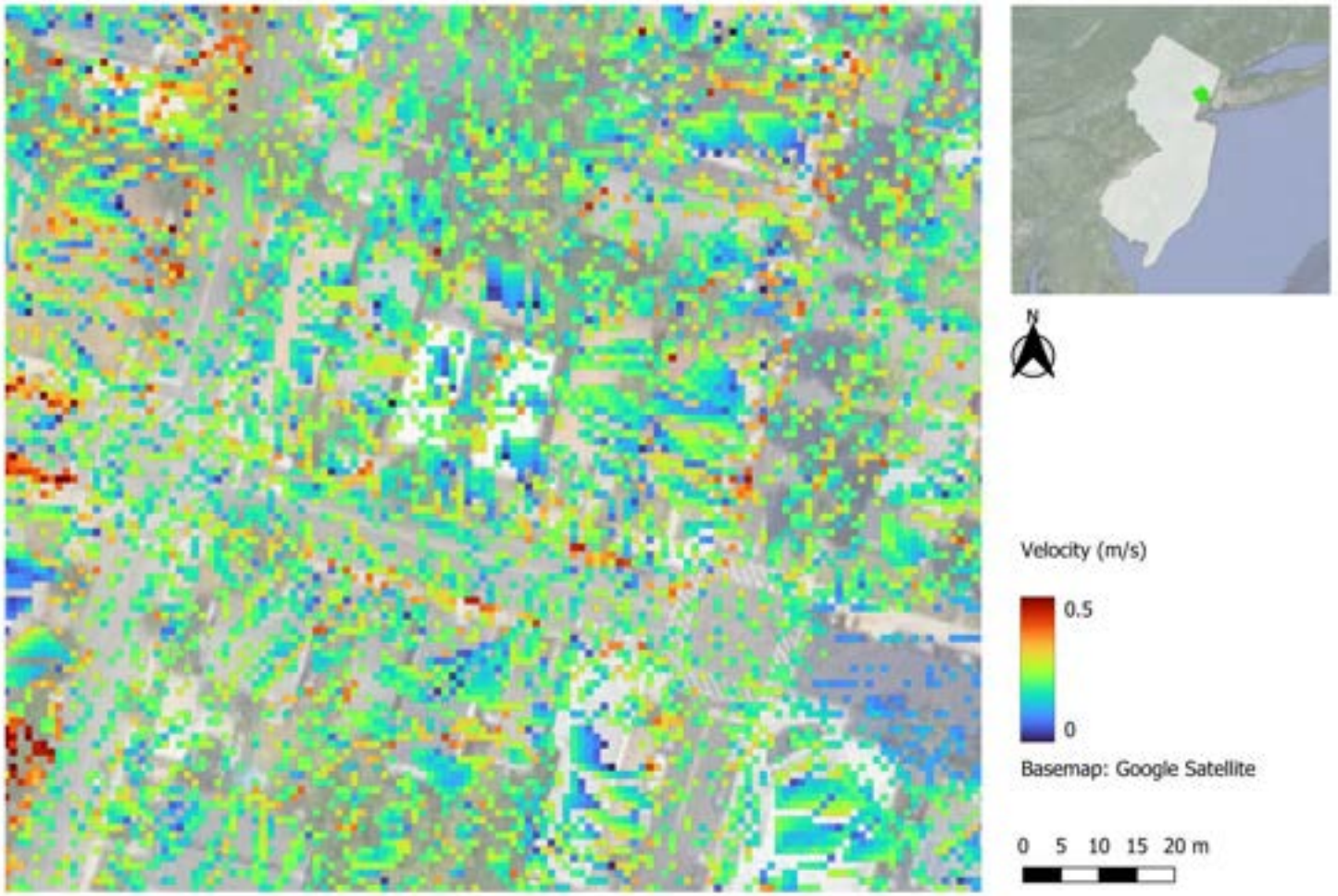

Figure 61 Calculated water velocity based on the empirical model at the Wanda Upshaw Meditation Garden site.

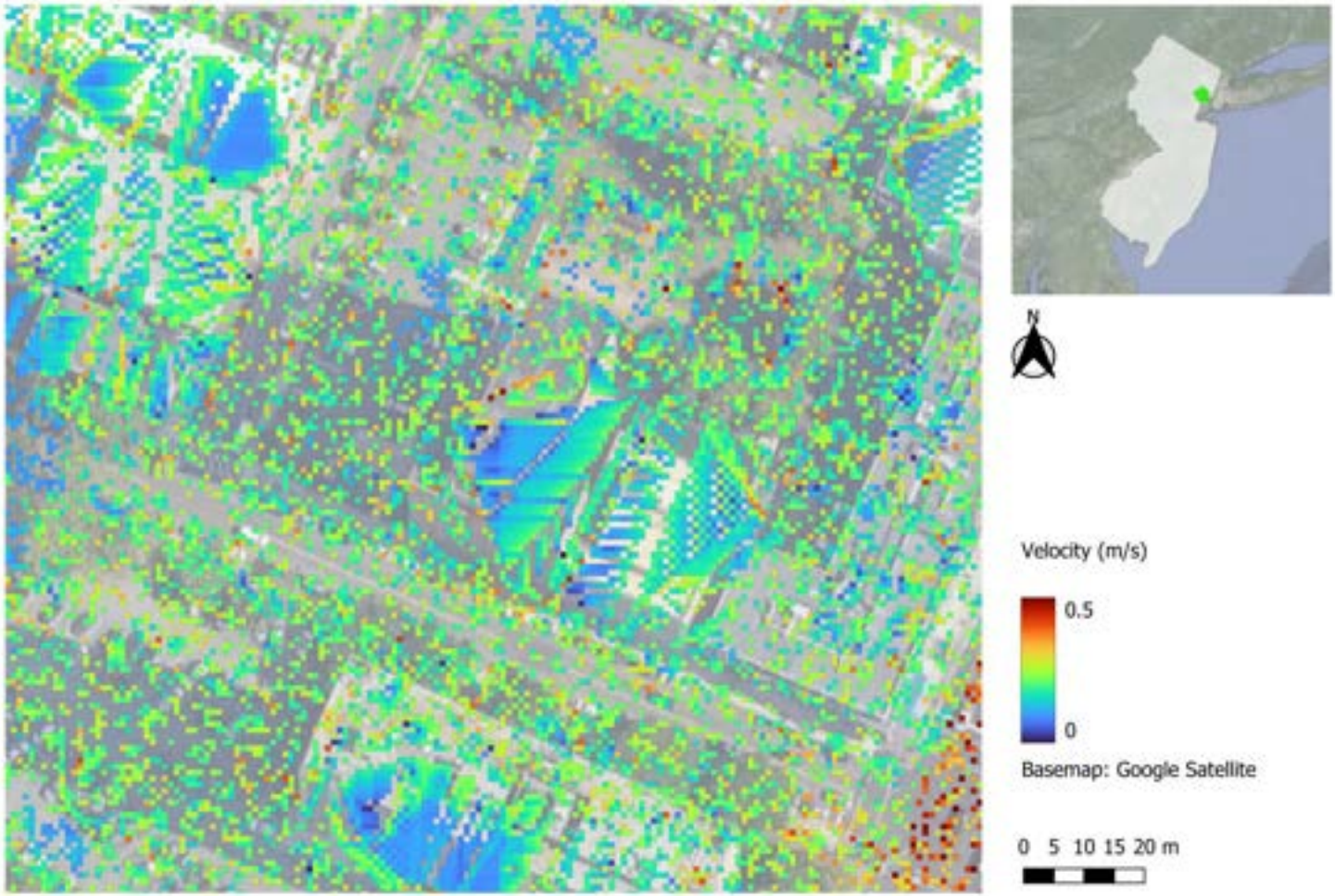

Figure 62 Calculated water velocity based on the empirical model at the Newark Educators Community Charter School site.

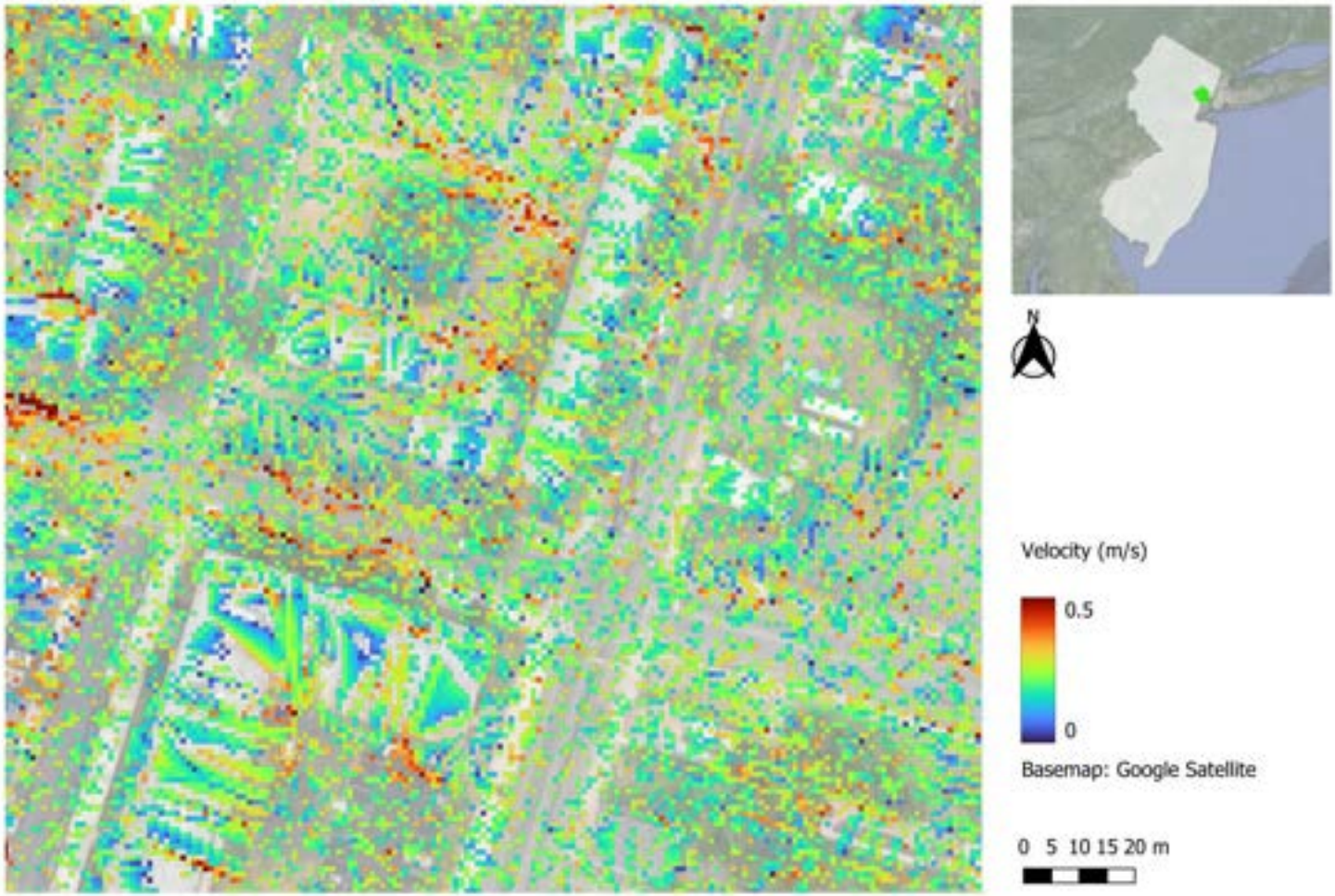

Figure 63 Calculated water velocity based on the empirical model at the Bergen Street Community Garden site.

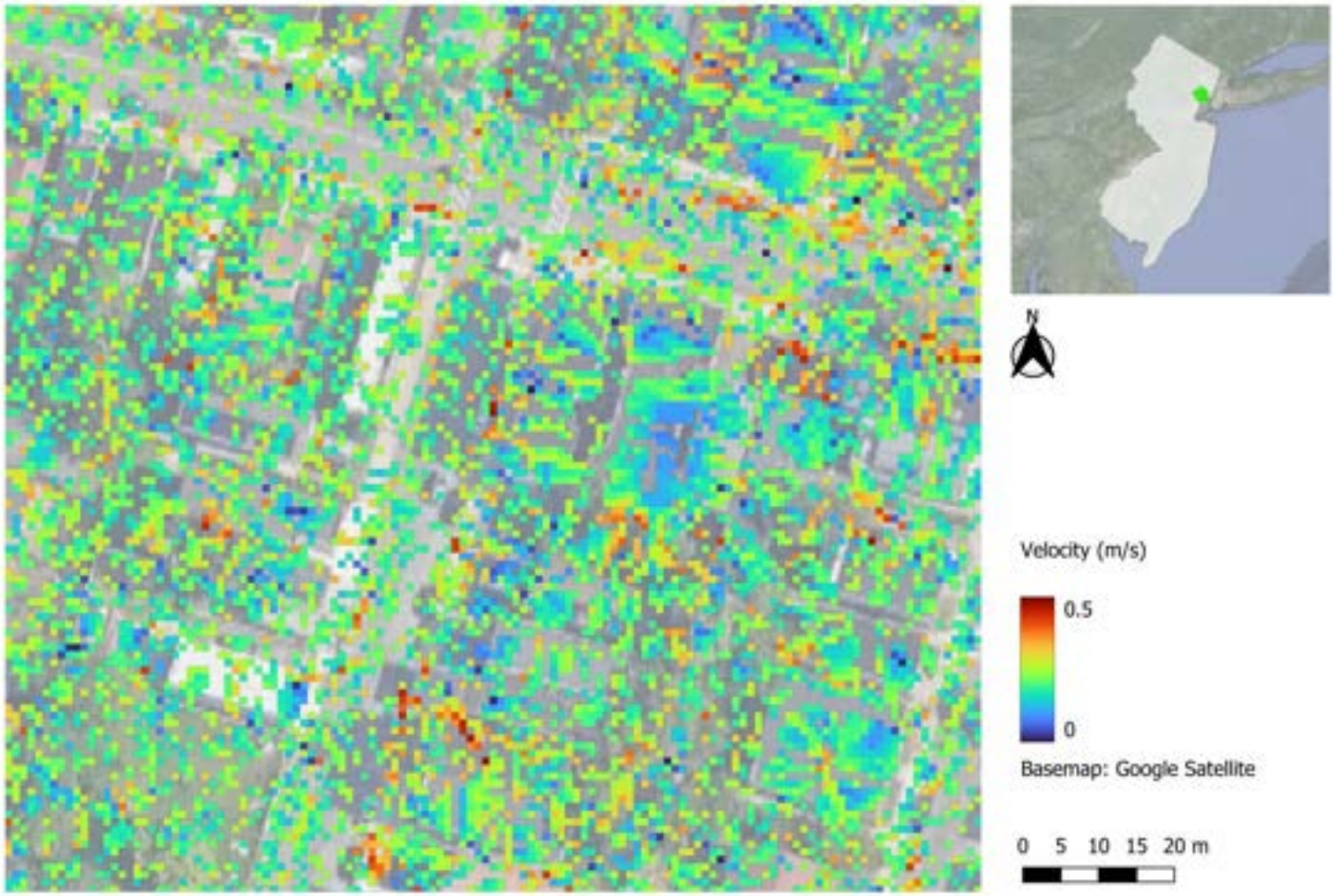

Figure 64 Calculated water velocity based on the empirical model at the 14th Avenue Community Garden site.

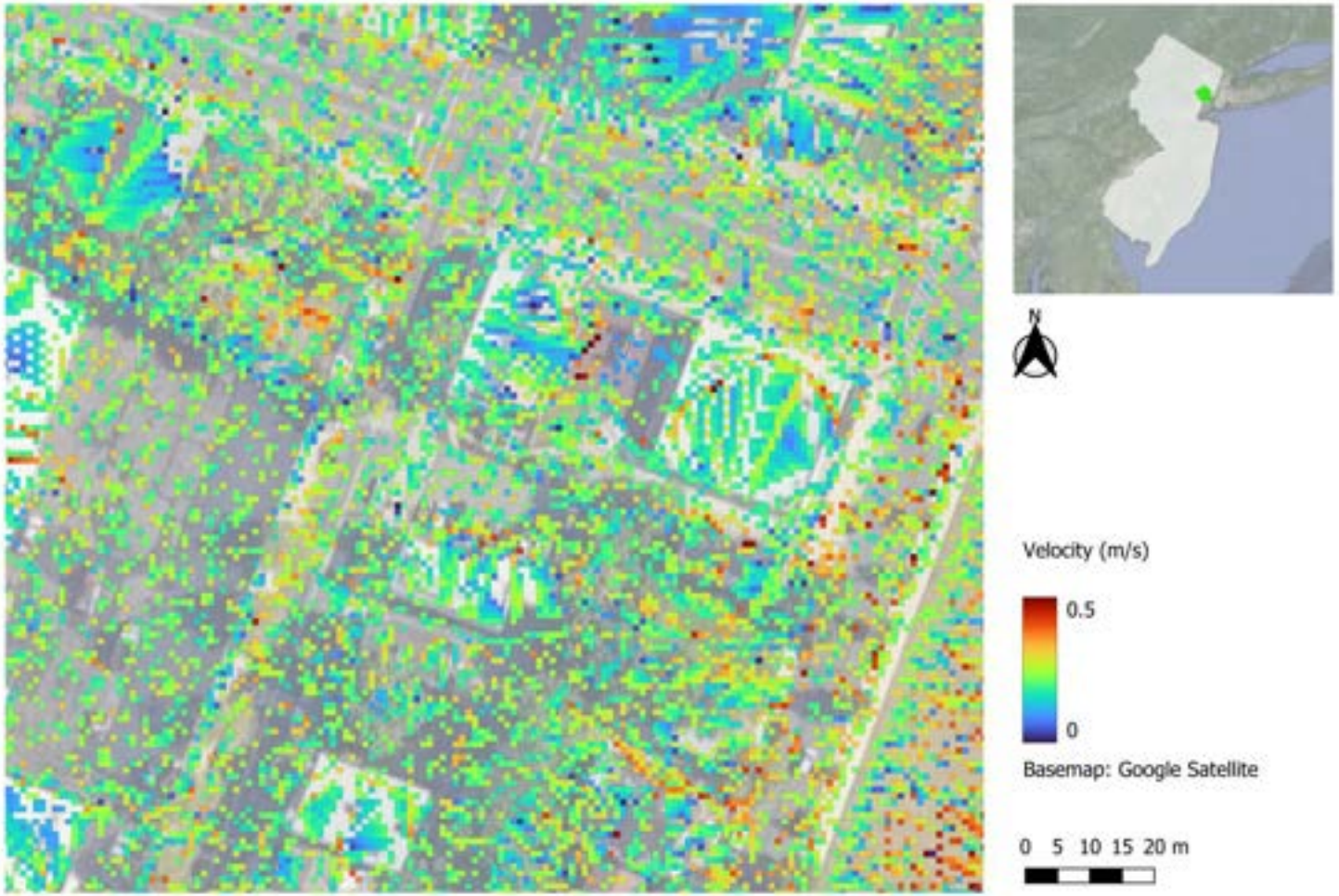

Figure 65 Calculated water velocity based on the empirical model at the Urban League of Essex County site.

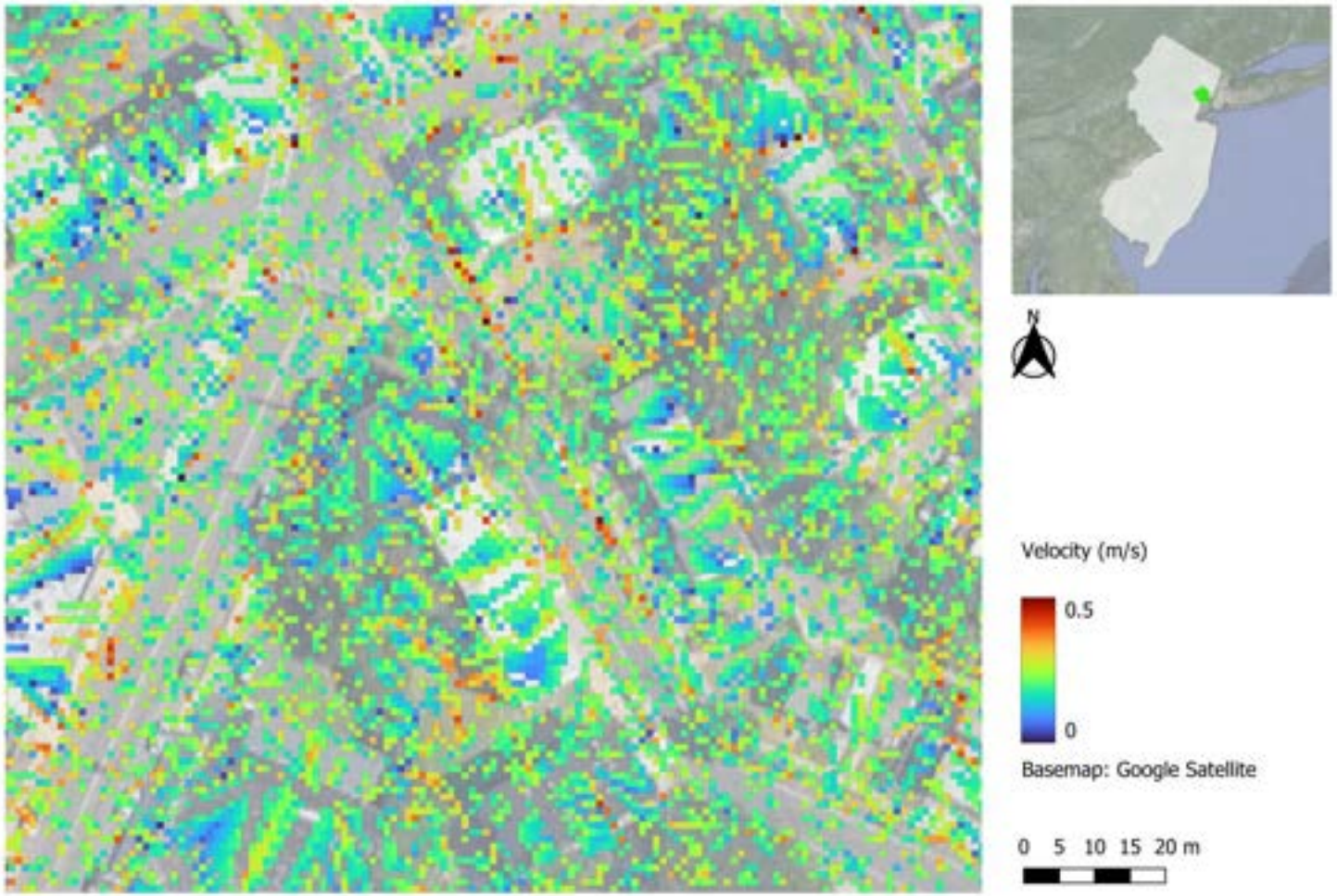

Figure 66 Calculated water velocity based on the empirical model at the Astor Street Community Garden site.

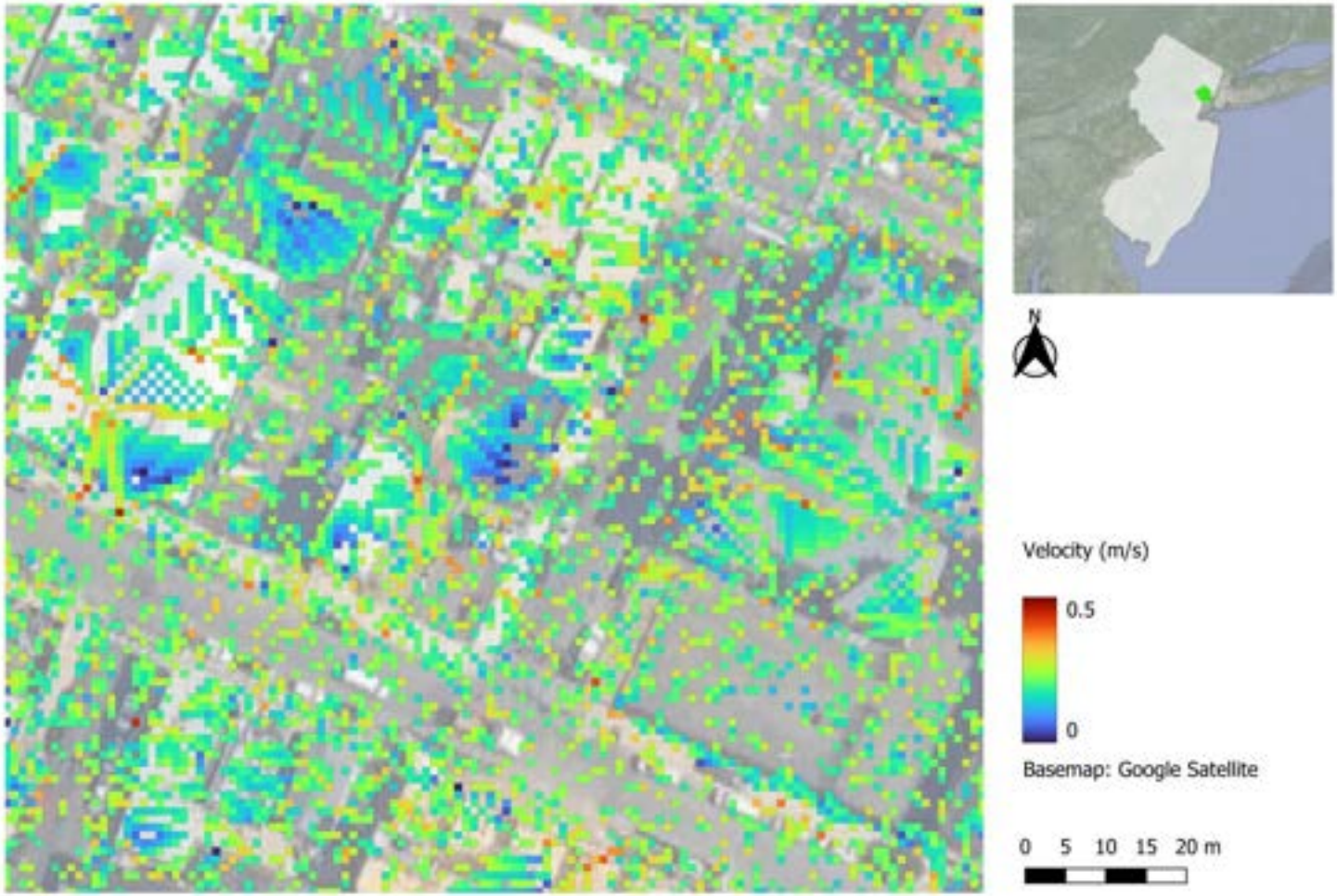

Figure 67 Calculated water velocity based on the empirical model at the South Street Academy site.

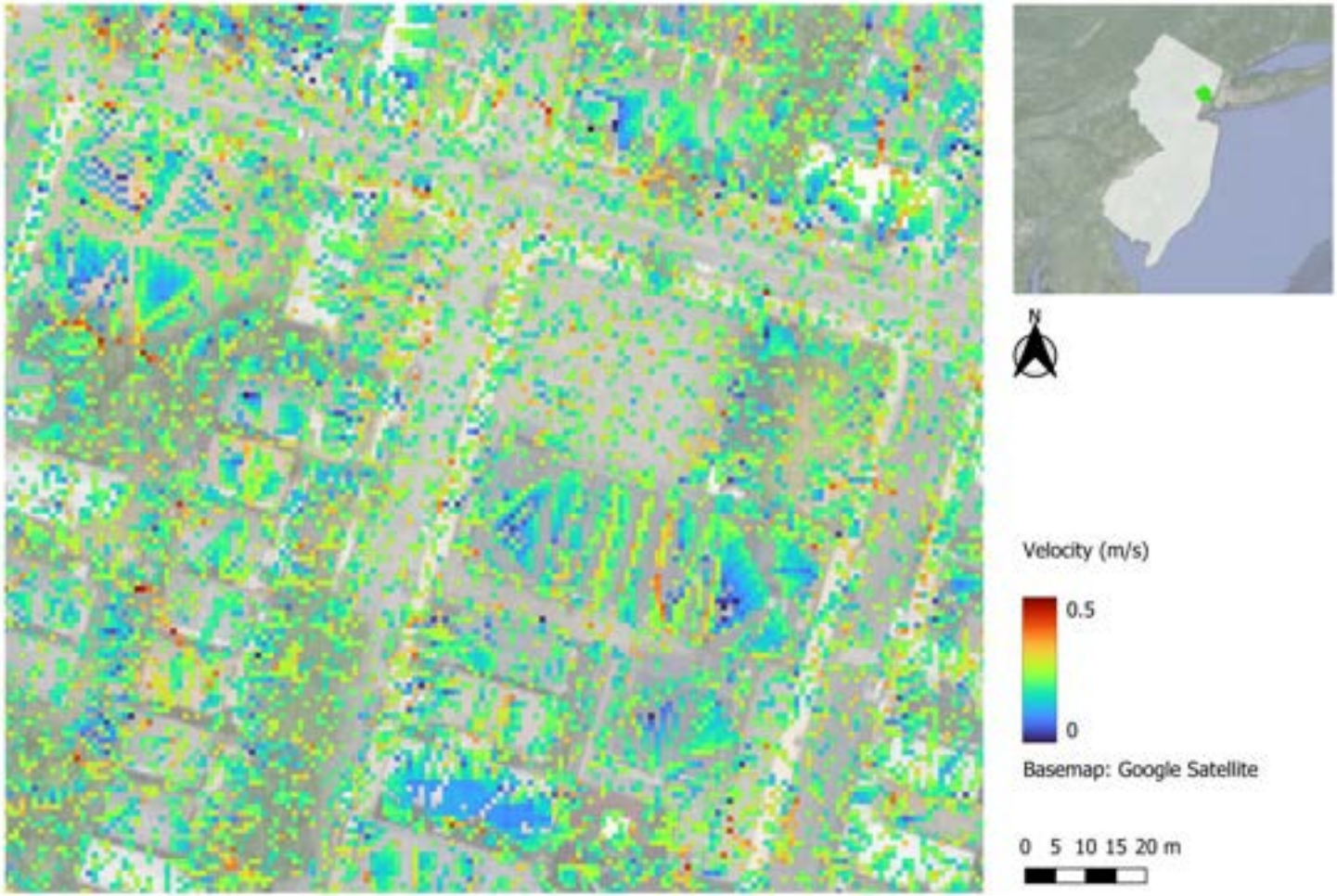

Figure 68 Calculated water velocity based on the empirical model at the St. Ann's Church site.

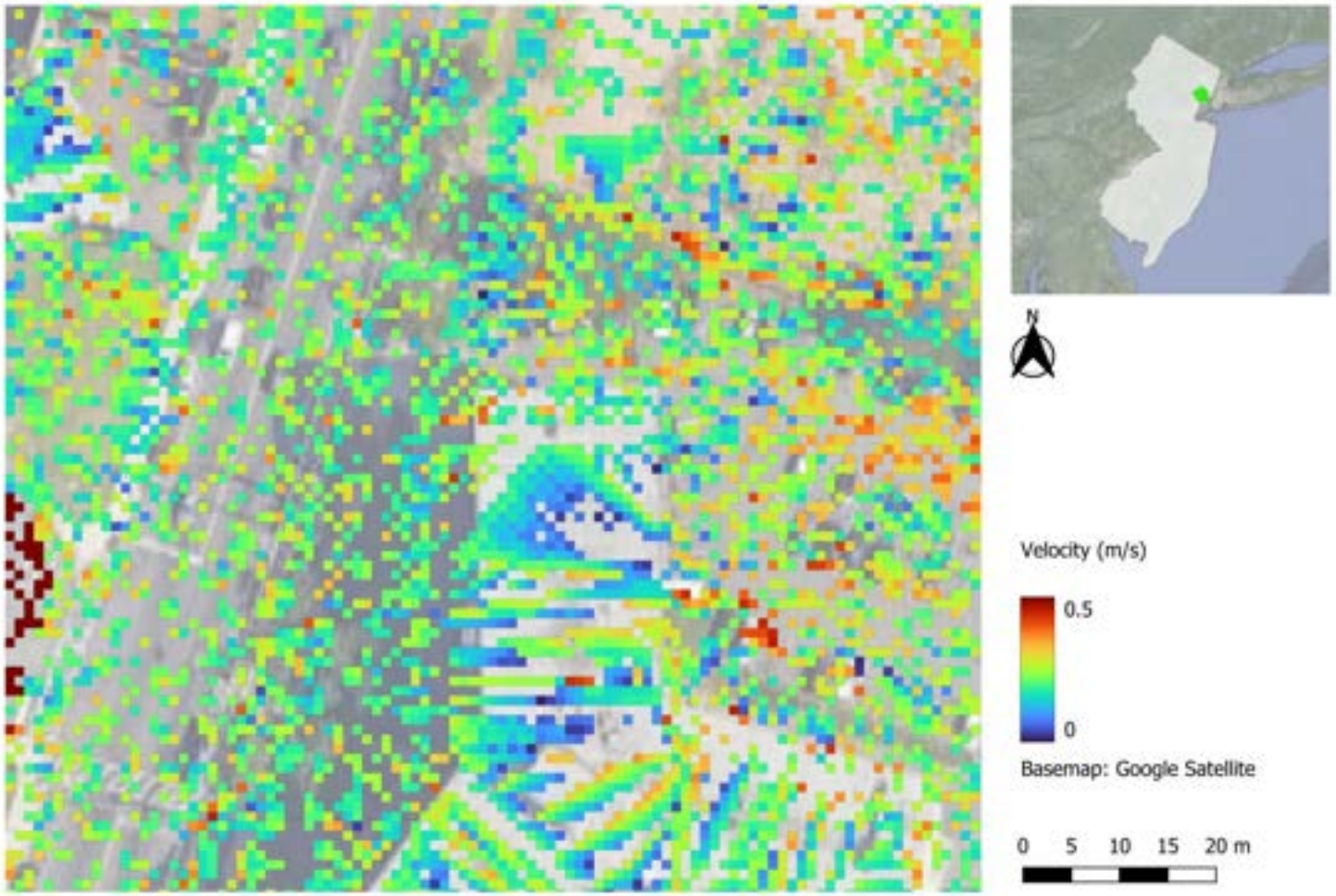

Figure 69 Calculated water velocity based on the empirical model at the James C. White Manor Senior Housing site.

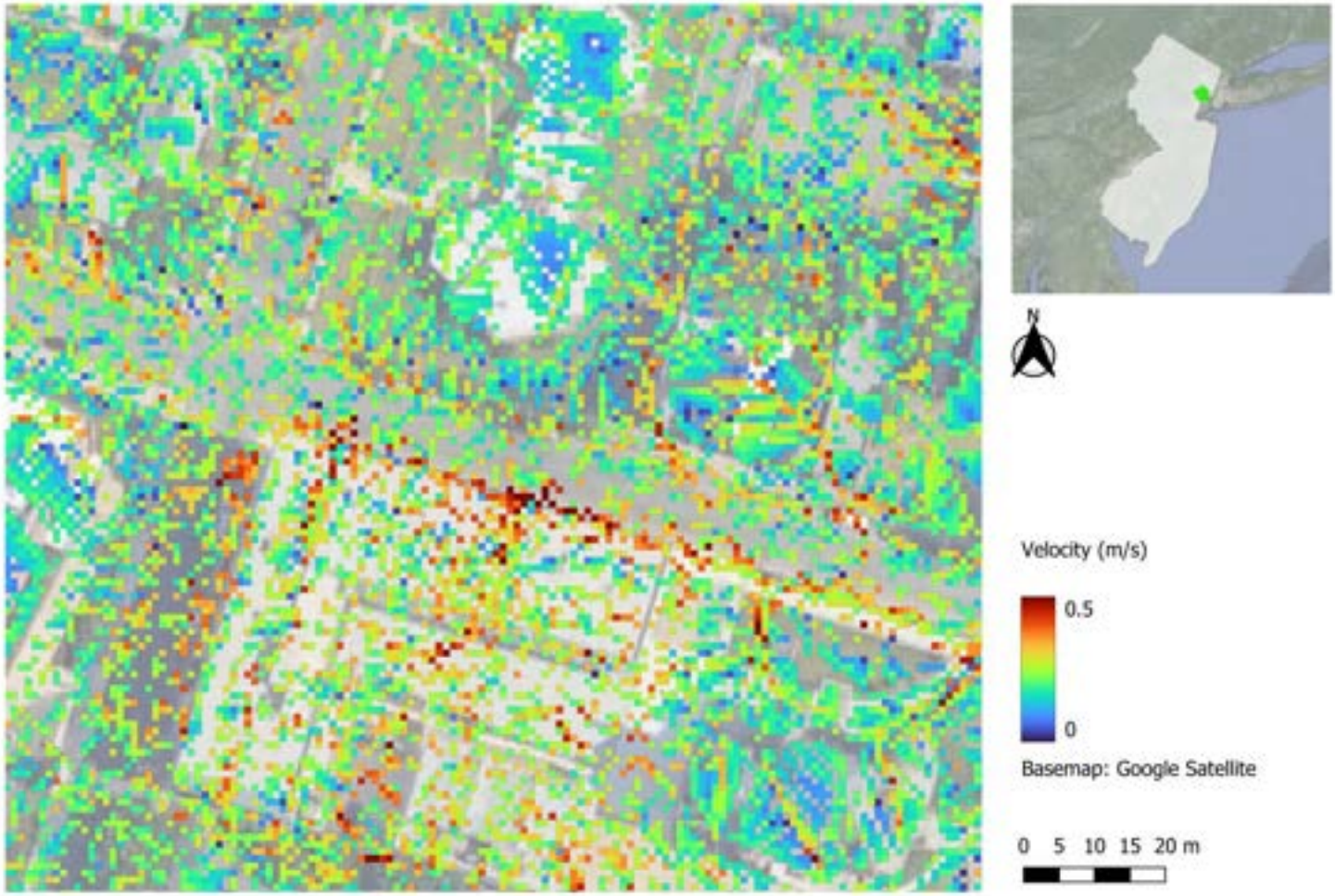

Figure 70 Calculated water velocity based on the empirical model at the Court Street Urban Farm site.

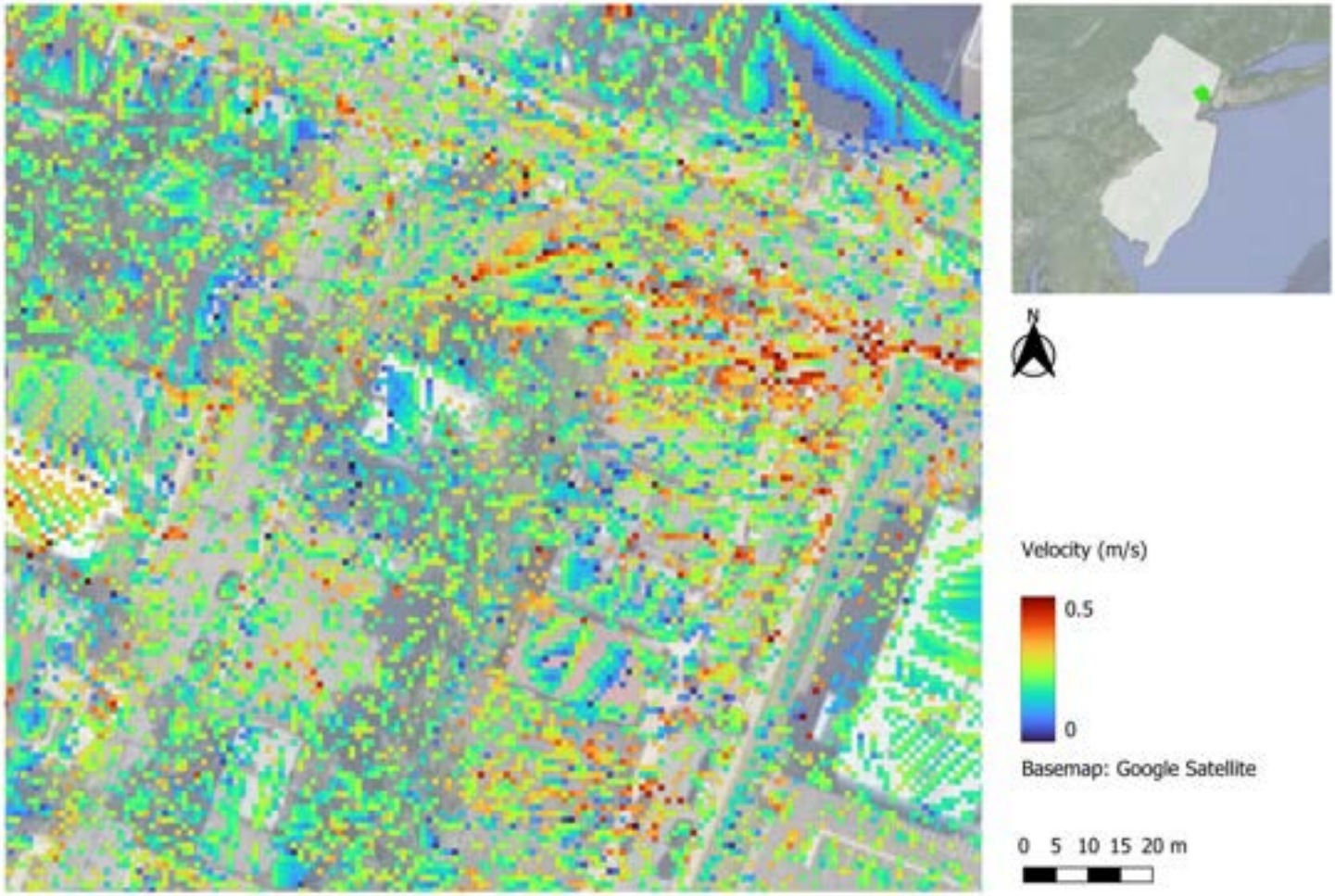

Figure 71 Calculated water velocity based on the empirical model at the Rutgers School of Health Professions site.

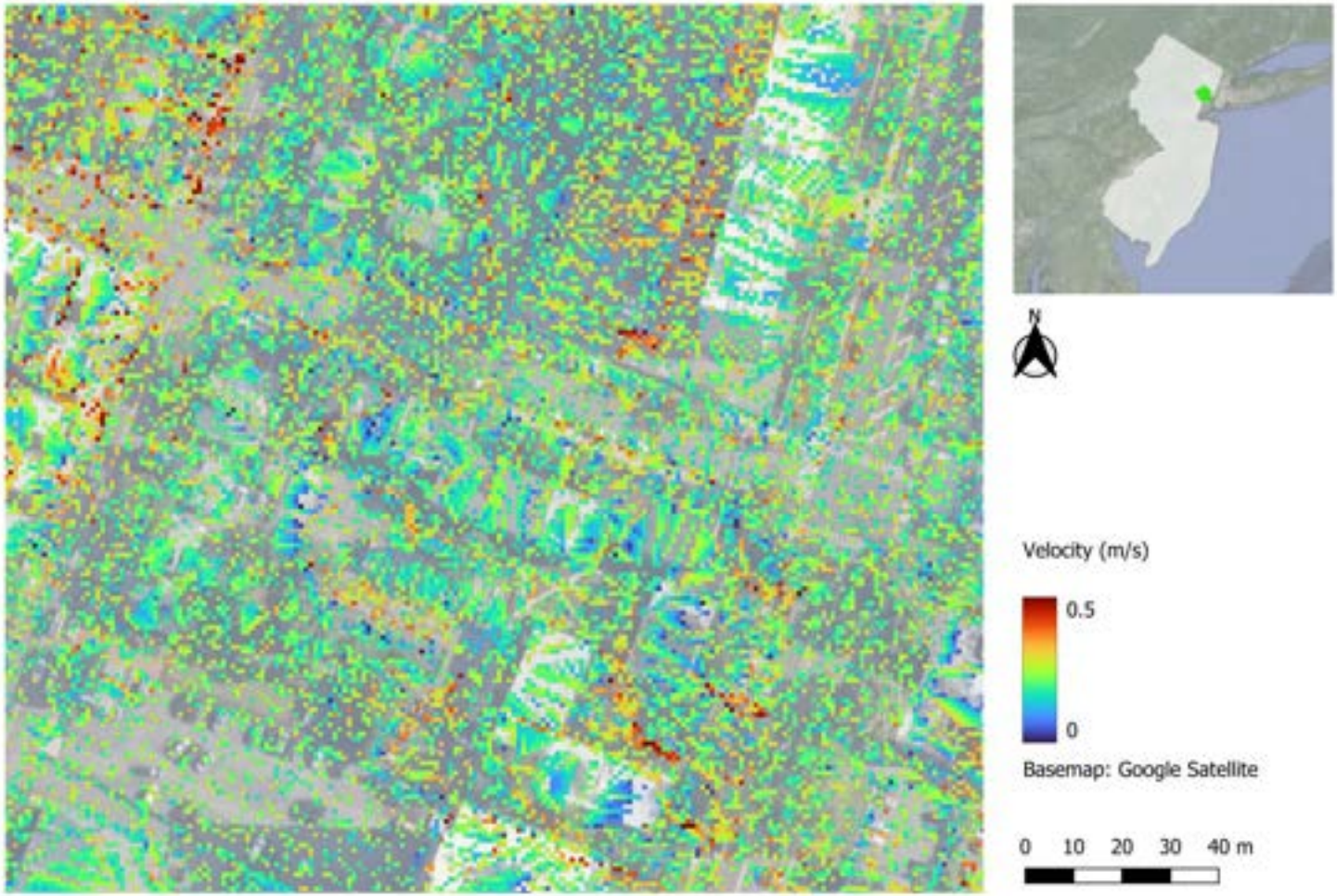

Figure 72 Calculated water velocity based on the empirical model at the Robert Treat Academy Charter School site.